NUREG/CR-4654

Radionuclide Transport as Vapor Through Unsaturated Fractured Rock

Prepared by R. T. Green, D. D. Evans

University of Arizona

Prepared for
U.S. Nuclear Regulatory
Commission

NUREG/CR-4654
RW

Radionuclide Transport as Vapor Through Unsaturated Fractured Rock

Manuscript Completed: August 1986
Date Published: July 1987

Prepared by
R. T. Green, D. D. Evans

T. J. Nicholson, NRC Project Manager

University of Arizona
Department of Hydrology and Water Resources
Tucson, AZ 85721

Prepared for
Division of Engineering
Office of Nuclear Regulatory Research
U.S. Nuclear Regulatory Commission
Washington, DC 20555
NRC FIN B7291
Under Contract No. NRC-04-81-224

ABSTRACT

The objective of this study is to identify and examine potential mechanisms of radionuclide transport as vapor at a high-level radioactive waste repository located in unsaturated fractured rock. Transport mechanisms and processes have been investigated near the repository and at larger distances.

Transport mechanisms potentially important at larger distances include ordinary diffusion, viscous flow and free convection. Ordinary diffusion includes self and binary diffusion, Knudsen flow and surface diffusion. Pressure flow and slip flow comprise viscous flow. Free convective flow results from a gas density contrast. Transport mechanisms or processes dominant near the repository include ordinary diffusion, viscous flow plus several mechanisms whose driving forces arise from the non-isothermal, radioactive nature of high-level waste. The additional mechanisms include forced diffusion, aerosol transport, thermal diffusion and thermophoresis.

Near a repository vapor transport mechanisms and processes can provide a significant means of transport from a failed canister to the geologic medium from which other processes can transport radionuclides to the accessible environment. These issues are believed to be important factors that must be addressed in the assessment of specific engineering designs and site selection of any proposed HLW repository.

TABLE OF CONTENTS

TABLE OF CONTENTS (Continued)

LIST OF FIGURES

LIST OF FIGURES (Continued)

LIST OF FIGURES (Continued)

LIST OF FIGURES (Continued)

LIST OF FIGURES (Continued)

LIST OF TABLES

LIST OF SYMBOLS

List of symbols used in text, number in paranthesis is either equation or page where cited or defined.

a = capillary tube radius (cm), (2.39)

a,b = empirical constants in equation (2.22)

a^* = (6.11)

a_c = two-dimensional attraction constant (2.57)

A = cross sectional area (cm^2), (2.32)

A_c = attenuation coefficient per atom or molecule (cm^2/molecule), (p. 60)

$A(e_o)$ = microscopic cross section of Compton effect (3.12)

$A(E)$ = microscopic cross section (3.10)

b = aperture thickness (cm), (p. 22)

b^* = (6.12)

B = momentum carried by gas molecules (2.35, 2.77)

B^* = momentum transfer (2.32)

C = circumferance (cm), (2.31)

C = total gas concentration (g/cm^3), (2.14)

c = constant for discrepancies in slip flow term (2.86)

c = constant (3.20)

c_i = gas concentration of i^{th} species (g/cm^3), (2.9)

c_f = final gas concentration (4.35c)

c_o = initial gas concentration (4.35c)

c_s = surface concentration (2.59)

c_v = heat capacity at constant volume (p. 124)

c^* = (6.13)

C_{Sorret} = Sorret coefficient (6.4)

Ci = Curies (p. 52)

d_{AB}, d_A, d_B = collision diameter (Å), (2.2)

d_m = molecular diameter (2.59)

D = coefficient of diffusion (3.2)

D_{AA} = self diffusion coefficient (cm^2/sec), (2.16)

D_{AB} = binary diffusion coefficient (cm^2/sec), (2.15)

D_a^t = thermal diffusion coefficient of gas (6.1)

D_k = Knudsen diffusion coefficient (cm^2/sec), (2.41)

D_p = photon diffusion coefficient (cm), (3.43)

D_r = theoretical drag on a bubble (4.30)

D_s = depth from heat source to surface (5.5)

D_s = surface diffusion coefficient (cm^2/sec), (2.58)

D_{so} = surface diffusion gas dependant constant (2.63)

D_T = diffusion coefficient in transition zone (cm^2/sec), (2.44)

D_1, D_2 = aspect ratios (5.8)

e = ionic charge (coulombs), (3.2)

E_{AB}^{r} = energy of molecular interaction (Ergs), (2.2)

$\hat{e}_x$, $\hat{e}_y$, $\hat{e}_z$ = unit vector principal directions in local coordinate system (3.10)

$\hat{e}'_x$, $\hat{e}'_y$, $\hat{e}'_z$ = unit vector principal directions in local coordinate system (3.10)

E = energy of photon (MeV), (3.10)

E' = energy of collision photon (MeV), (3.10)

E^* = energy of collision electron (MeV), (3.10)

E_a = surface barrier potential (2.62)

E_e = electric field (V/cm), (3.1)

Ei = exponential integral (2.49)

Eu = Eulers constant (2.45)

f_0 = diffuse reflection fraction--Knudsen flow (2.12)

f_1 = diffuse reflection fraction--slip flow (2.13)

F_b = rate of gas desorption by bubbling (4.8)

F_M = force caused by molecular resistance (6.24, 6.25)

F_q = rate of quiescent gas desorption (4.8)

F_T = force caused by thermal diffusion (6.21, 6.22, 6.23)

F_2 = fugacity constant (4.5)

$F(t)$ = unknown time variable (4.13)

$F(Z,t)$ = total rate of gas desorption (4.7)

g = acceleration of gravity (cm/sec^2), (2.66)

g_{AB} = initial relative speed between molecules A and B (cm/sec), (2.20)

G = mass flow of gas (g/sec), (2.37)

hr = hydraulic radius (cm), (2.1)

h = width of plate (cm), (2.36)

H = enthalpy (4.1)

H = heat capacity rate (5.7)

$H_{1,2}$ = Henry's constant (4.5)

I = electric current (amp), (3.9)

I_g = intensity of gamma radiation (ergs/cm^2·sec), (3.15)

I_g^o = initial intensity of gamma radiation (ergs/cm^2·sec), (3.16)

I_x = partial derivative of h with respect to x (Table 2.6)

j = electric current density (amp/cm^2), (3.9)

<j> = true value of electric current density (amp/cm^2), (3.53)

J_k = flux of gas by Knudsen flow (g·mole/cm^2·sec), (2.7, 2.38, 2.40)

J_o = flux of gas by ordinary diffusion (g·mole/cm^2·sec), (2.7)

J(r) = compton current density (3.10)

J_v = flux of gas by viscous flow (g·mole/cm^2·sec), (2.7)

J_{self} = flux of gas by self diffusion (g·mole/cm^2·sec), (2.7)

J_{sf} = flux of gas by slip flow (g·mole/cm^2·sec), (2.65)

J_s = flux of gas by surface diffusion (g·mole/cm^2·sec), (2.7)

J_f = flux of gas by forced diffusion (g·mole/cm^2·sec), (3.1)

J_b = flux of gas by binary diffusion (g·mole/cm^2·sec), (2.7)

J_p = flux of gas by pressure flow (g·mole/cm^2·sec), (2.65)

k = constant (2.25, 4.19)

k = intrinsic permeability (cm^2), (5.5)

k_h = effective horizontal permeability (5.21)

k_t = thermal diffusion ratio (6.2)

k_v = effective vertical permeability (5.16)

K = Boltzman constant ($1.38 \cdot 10^{-23}$ joules/°K), (Table 2.2, 3.2)

$K_h(e_s)$ = heat of adsorption function (2.57)

Kn = Knudsen number (p. 17)

$K_o(x)$ = zeroeth order modified Bessel function of the second kind (3.49)

l = length of parallel plate or capillary tube (figure 2.9)

L = length of capillary tube (2.48)

L = diffusion length (cm), (3.43)

m = mass of a molecule (g), (2.11)

M = molecular weight of gas (g/mole), (2.8)

M = ion mobility (cm^2/V·sec), (3.1)

n_i = number density of ions (ions/cm^3), (3.1)

n = number of impacts/cm^2·sec (2.23)

n = kinematic viscosity of gas (2.10)

N = gas molecule density (molecules/cm^3), (2.23)

N_s = number of scatterers per unit volume (3.13)

N_c = total number of collisions per unit length (3.50)

p_i = partial pressure of i^{th} gas (dynes/cm), (2.9)

p_D = dimensionless pressure (5.11)

P^* = vapor pressure (4.1)

P = porosity (5.14)

P = total gas pressure (dynes/cm), (2.8)

ΔP = pressure between capillary water and atmosphere (dynes/cm), (2.1)

P_a = atmospheric pressure (dynes/cm), (4.24)

P_i^c = critical pressure of gas i (dynes/cm), (2.22)

$P_g(t)$ = pressure of ideal gas in bubble (4.25d)

Pr = Prandlt number (5.6)

$P(x)$ = probability of x (3.17)

Q = volume of gas througth area A per sec (2.34)

$Q_c(a/\lambda)$ = (2.45)

$Q_p(b/\lambda)$ = (2.52)

r = radial distance between molecules A and B (cm), (2.2)

r = radial distance (cm), (4.11)

$r_g(Z,t)$ = rate of gas production by chemical reaction (4.7)

r_i = thickness ratio of layer i to overall thickness (5.18)

r_y = radial component of position vector (3.39)

R = gas constant ($cm^3 \cdot atm/deg \cdot mole$), (2.8)

R = radius of bubble (cm), (4.14)

Ra = Rayleigh number (5.5)

Ra_{cr} = critical Rayleigh number (p. 125)

Ra^L = Rayleigh number for a layered system (5.15)

Ra^L_{cr} = critical Rayleigh number for a layered system (5.18)

R_{eff} = effective range of electron (g/cm^2), (3.10)

R_o = initial bubble size (4.19b)

$\dot{R}$ = radial growth of bubble at bubble surface (cm/sec), (4.14)

s = distance of travel of a photon (cm), (3.15)

s = surface tension (2.1), (4.26)

S = photon direction vector (3.38)

S_p = strength of source in terms of photons/sec/unit length of line source (3.43)

S_s = viscous shearing stress (2.75)

S_{rr}, etc. = spherical components of the stress field (4.25)

$S^{(A)}$, $S^{(B)}$ = (6.7), (6.8)

t = time (sec), (2.66)

t = mean life of a particle between two walls (sec), (4.33)

T = temperature (°K), (2.8)

$\bar{T}$ = vector transformation (3.24)

T_i^c = critical temperature of gas i (°K), (2.22)

t_d = exponential decay time constant (4.35c)

t_* = dimensionless time (5.12)

T_t = travel time between adsorption sites during surface diffusion (2.61)

T_o = property of solid surface in surface diffusion (2.62)

u_o = slip flow velocity (cm/sec), (2.74)

$U^{(1)}$, $U^{(2)}$, $U^{(3)}$ = (6.16), (6.17), (6.18)

v = gas molecule velocity (cm/sec), (2.24)

v = radial velocity of the liquid (cm/sec) (4.11)

$\bar{v}$ = mean gas velocity of single gas molecule irrespective of direction (cm/sec), (2.11)

v_d = drift velocity (cm/sec), (2.28), (3.7)

v_i = dimensionless velocity (5.1)

v_t = component of molecular velocity of translation parallel to wall (cm/sec), (p. 28)

v_p = particle velocity caused by thermal gradient (cm/sec), (6.26), (6.27)

V_{AB} = reduced initial relative speed between molecules A and B (2.20)

V = volts (p. 57)

V = volume (4.1)

V = volume of anulus per unit length (3.51)

$V(t')$ = volume of the liquid (4.7)

x_{eff} = effective thermal conductivity (5.14)

x_i = mole fraction of the i^{th} species (3.6)

x_h = effective horizontal thermal conductivity (5.22)

x_v = effective vertical thermal conductivity (5.17)

X_i = dimensionless distance (5.13)

X_λ = (6.14)

X_a = transtional part of thermal conductivity of gas (6.21)

Y_λ = (6.15)

Z = gas supersaturation (4.7)

α = most probable gas molecule speed (2.24)

α = contact angle between the solid and water (2.1)

α = thermal diffusivity (5.9)

α_t = thermal diffusivity factor (6.3)

β = coefficient of volumetric thermal expansion (5.5)

β = frequency of a photon (3.41)

β_o = dimensionless reflection factor in Knudsen flow (2.12)

β_p = measure of proportionality of intrinsic permeability in layered system (5.18)

β_t = tortuosity (2.96)

β_1 = dimensionless reflection factor in slip flow (2.13)

Δ = angle at which molecules are deflected (2.19)

Δ_{ij} = Kronecker delta (5.2)

e = error between approxiamtion and true value of current density (3.53)

e_{AB} = maximum attractive energy between molecules A and B (2.2)

θ = dimensionless temperature (5.3)

θ_e = angle of deflection between thr trajectory of the incident photon and collision photon (3.12)

θ_d = drained porosity (2.96)

θ_i = dipolar angle (2.5)

θ_o^e = azmuthal angle of electron in local coordinate system (3.41)

θ_s = fraction of surface coverage (2.57)

λ = mean free path of a molecule (cm), (2.10)

λ_A = thermal conductivity of gas A (6.9)

λ_{AB} = thermal conductivity of binary gas (6.10)

λ_p = measure of proportionality of intrinsic permeability in layered system (5.18)

λ_s = mean free path along the surface (2.59)

λ_s' = distance between adsorption sites during surface diffusion (cm), (2.61)

μ = moment of a single molecule dipole (2.5)

μ = total attenuation coefficient (3.45)

μ = absolute viscosity (g/cm·sec), (2.66)

μ = attenuation coefficient attributed to Compton scattering (cm^{-1}), (3.16)

μ = macroscopic cross-section (cm^2/g), (3.13)

μ = gas viscosity (2.65)

μ' = liquid viscosity (4.20)

$\bar{\mu}$ = average cosine of the scattering angle (3.44)

μ_a = absorbing attenuation coefficient (cm^{-1}), (3.45)

μ_{AB} = reduced mass (2.21)

μ_{mix} = viscosity of gas mixture (2.71)

μ_o = total linear attenuation coefficient (cm^{-1}), (3.15)

μ_s = scattering attenuation coefficient (cm^{-1}), (3.45)

μ_{tr} = transport attenuation coefficient (cm^{-1}), (3.44)

ρ = random variable uniform over [0,1], (3.18)

ρ = gas density (g/cm^3), (2.8)

ρ = electrical resistivity (ohms·cm), (3.8)

ρ_l = liquid density (g/cm^3), (4.14)

ρ_r = reduced density (4.15)

Σ_d = standard deviation (3.53)

$\phi_A - \phi_B$ = angle of translation between molecules A and B (2.5)

ϕ_e = gamma flux per unit solid angle per unit area per unit energy (3.10)

ϕ_e = photon flux per unit energy (3.43)

ϕ_{ij} = (2.73)

ϕ_o = azmuthal angle in x-z plane (p. 66)

ϕ_o^e = deflection angle of electron in local coordinate system (3.40)

ϕ_2 = dissolved gas activity constant (4.5)

$\phi(r)$ = Lennard-Jones potential energy function (Figure 2.2)

$\hat{\Omega}'$ = collision photon vector defined in local coordinate system (3.35)

$\hat{\Omega}$ = collision photon vector defined in global coordinate system (3.10)

$\hat{\Omega}_{Dab}$ = collision integral (2.19)

$\hat{\Omega}_s$ = scattering cross section (barns), (3.12)

$\hat{\Omega}^*$ = trajectory of electron (3.10)

$\hat{\Omega}_x'$, $\hat{\Omega}_y'$, $\hat{\Omega}_z'$ = cartesian components to photn unit direction vector in local system (3.33)

$\hat{\Omega}_x$, $\hat{\Omega}_y$, $\hat{\Omega}_z$ = cartesian components to photn unit direction vector in global system (3.33)

GLOSSARY OF TERMS
(As used in this report)

Attenuation coefficient: Equal to the macroscopic cross section, used in reference to photon transport.

Aerosol transport: The movement of aerosol particles as vapor.

Binary diffusion: The ordinary diffusion of two fluids (gases or liquids) through each other.

Chapman-Enskog theory: The same as rigorous kinetic theory.

Compton current: The electric current caused by the return flow of electrons moving in response to the preferential movement of Compton scattered electrons.

Compton scattering: The collision of a gamma ray and a particle which results in a Compton scattered electron and a collision induced photon of lower energy.

Couette flow: Flow of a Newtonian fluid through a capillary tube.

Countercurrent: Coupled liquid-film and gas movement induced by a heat source. A liquid-film moves towards the heat source, vaporizing as the vapor density decreases. The vapor moves away from the heat source, until it condenses in regions where the vapor density is high.

Diffuse reflection: Gas molecule are reflected at no preferential angle.

Dual porosity system: A medium with two inherently different types of pore spaces, i.e., matrix porosity and fracture pores.

Electrophoresis: The movement of ionized particles suspended in a fluid, induced by an electric field.

Forced diffusion: Diffusion in response to an external force, e.g., an external electric force.

Free convection: The movement of a fluid (gas or liquid) in response to a gas density difference in the absence of external hydraulic forces.

Gaseous transport: The transport in the gas phase.

Henrys law: For a slightly soluble gas which dissolves in a finite mass of liquid at a given temperature, the concentration is very nearly directly proportional to the partial pressure of that gas.

Ion drift velocity: The mean drift velocities of ions along the electric field lines.

Kinetic theory: The interaction between particles examined at molecular scales.

Knudsen number: The ratio of the mean free path length of a gas molecule to the aperture of the space through which the gas moves.

Knudsen flow: Gas movement resulting from collisions between gas molecules and solid surfaces, such as pore walls.

Lennard-Jones parameters: Parameters used in an empirical formula which relates the potential energy between two molecules.

Macroscopic cross section: A measure of the probability per unit volume that a collision between a specific photon and a particle will result.

Mean free path length: The average distance between consecutive molecule-molecule collisions.

Mean molecular gas velocity: The mean gas velocity of gas molecules irrespective of direction.

Microscopic cross section: A measure of the probability per atom or molecule that a collision between a specific photon and a particle will result.

Ordinary diffusion: Diffusion induced by a concentration gradient.

Photon transport: The mass movement of photons.

Poiseuille flow : Flow of a Newtonian fluid between two parallel plates.

Pressure flow: Fluid movement induced by a gradient in total pressure.

Rayleigh number: The dimensionless ratio of the buoyancy force to the viscous retardation force.

Reprocessed fuel: Spent fuel assemblies from which either the uranium and/or plutonium has been removed and reprocessed.

Rigorous kinetic theory: Kinetic theory which accounts for potential energy transfer between two molecules.

Self diffusion: Fluid movement resulting from collisions between like molecules.

Simplified kinetic theory: Kinetic theory in which elastic properties and interactions are ignored.

Slip flow: Flow induced by a total pressure gradient at the fracture surface-gas interface which occurs when the Knudsen number is approximately unity.

Sorret coefficient: Used to relate the thermal diffusion factor to gas concentrations in a binary system.

Specular reflection: The collision of a gas molecule with a surface where the angle of incidence equals the angle of reflection and where the kinetic energy of the incident gas molecule is equal to the kinetic energy of the reflected gas molecule. Also referred to as mirror-like reflection.

Spent fuel: Intact nuclear fuel assemblies from either pressurized or boiling water nuclear reactors.

Stockmayer potential: The potential energy difference between two polar molecules.

Surface diffusion: Diffusion of an adsorbable gas in the presence of a concentration gradient along a surface covered with a few monolayers of an adsorbant.

Thermal diffusion: Thermally-induced movement of gas molecules, generally the movement of larger particles (as large as micrometer size particles) through angstom size gas molecules.

Thermophoresis: The movement of fluid molecules with variable mean velocities impinging on larger size particles from opposite sides.

Vapor: Gases and diffused aerosols suspended in air.

Vapor transport: The combined transport process of both gaseous and aerosol transport.

Viscous flow: Laminar or turbulent flow resulting from a total pressure gradient.

ACKNOWLEDGEMENTS

We wish to acknowledge the help of Dr. W. L. Filippone of the Department of Nuclear and Energy Engineering for his assistance with Forced Diffusion, contributions to this report from Dr. K. G. Vemulapalli of the Chemistry Department on the theory of solubility, and to J. W. Andrews, D. E. Earp, M. Engle and especially R. Seidemann of the Department of Hydrology and Water Resources for techical and manuscript preparation assistance -- all of the University of Arizona. We also like to thank Mr. J. Massman of Hart, Crowser & Assoc., Mr. E. Weeks of the U.S.G.S and Dr. K. Pruess of Lawerence Berkeley Laboratories for the help they supplied through personal conversations.

EXECUTIVE SUMMARY

Radionuclide Transport as Vapor through Unsaturated Rock

Radionuclide transport as vapor through unsaturated fractured rock has become a prominent technical issue. Interest in vapor transport has evolved with the prospect of locating a high-level waste (HLW) repository in the unsaturated zone becoming a credible alternative to long term disposal of high-level waste. The objective of this study is to identify and evaluate potential mechanisms of radionuclide transport as vapor in unsaturated fractured rock.

The issues brought forth and discussed in this study are believed to be important factors that must be addressed in the assessment of the specific engineering design (vapor transport mechanisms acting near a repository) and site selection (vapor transport over large distances) of any proposed HLW repository.

Vapor transport mechanisms and processes near a repository, either individually or coupled with other transport mechanisms, can provide a significant means of transport from a failed canister to the geologic medium and possibly as far as the zone of higher saturation enveloping the canister or repository region. From the point where vapor transport near the repository ceases importance, other transport mechanisms--both in the vapor phase or in the liquid phase--can transport contaminants outward to the accessible environment. Although the distance may be as short as several centimeters, mass flux by vapor transport mechanisms and processes dominant near a repository could be an important--if not the most important--means of transport across this gap during specific periods of time after canister emplacement.

Transport mechanisms and processes are investigated near a repository and at larger distances. In general, transport mechanisms important near a repository are influenced by the nature of the high-level waste and design of the waste package while those transport mechanisms important at larger distances are influenced by the geologic medium.

Characterization of the geologic medium and adequate gas flow modeling is necessary to ascertain the importance of radionuclide transport as vapor at large distances from a repository. Transport mechanisms or processes potentially important at larger distances include ordinary diffusion, viscous flow and free convection. Ordinary diffusion includes any diffusion process driven by a concentration gradient. These are self and binary diffusion, Knudsen flow and surface diffusion.

Pressure flow and slip flow comprise viscous flow. The driving force of viscous flow is the total gas pressure gradient. The movement of gas in response to a gas density difference in the absence of external hydraulic forces is free convection.

Free convective flow is possible in fractured rock overlying a sufficiently large heat source. A HLW repository of sufficiently large lateral extent can create an artifical high temperature layer causing a density contrast in the gas which permeates the interconnected air space of the rock. The density contrast in the gas can result in free convection cells. The Rayleigh number, which is a dimensionless parameter measuring the ratio of buoyancy forces relative to viscous resistance, is a useful indicator as to whether convection cells will occur. The Rayleigh number representing each scenario was calculated based on reasonable and conservative rock and gas properties and in each case the Rayleigh number was significantly less than the critical Rayleigh number of $4\pi^2$. Since all Rayleigh numbers were at least two orders of magnitude less than the critical Rayleigh number, free convection of gas in the fractured rock overlying a repository is not expected to occur. Further analysis, however, is required to insure that this preliminary conclusion is also valid for the conservative case where a non-uniform heat source and edge effects are considered.

Transport mechanisms important near a repository include ordinary diffusion, viscous flow plus several mechanisms whose driving forces arise from the non-isothermal, radioactive nature of high-level waste. These mechanisms include forced diffusion of ionized vapor particles, aerosol transport, thermal diffusion and thermophoresis.

One of these additional driving forces near the repository is one resulting from an electric field. Ionized particles will move in response to an electric field if the intensity of the electric field is sufficiently large and the particles are relatively mobile.

Gamma ray emission by high-level waste can create an electric field by Compton scattering. Gamma rays of a specific range in energy (0.03 to 10.0 MeV) result in Compton scattering upon collision with particles located along their pathway. A photon of lower energy and an electron are scattered during the collision. The collision causes a preferential outward movement of electrons resulting in a charge displacement. A return flow of electrons results to counter this displacement thus inducing an electric field. The resulting electric field can cause movement of any ionized mobile particle. This particle or gas molecule movement is referred to as forced diffusion.

Two limiting cases were investigated for their potential of forced diffusion: 1) a HLW canister located in a rock mass and 2) a HLW canister located in air. The two cases are thought to approximate the range of conditions at a HLW canister. Significantly large air spaces may occur near the surface of a HLW canister as a result of several different effects (i.e., large fractures, open boreholes, canister cladding failure, etc.) hence, the justification for the second case. Although negligible for the rock case, the electric field intensity and ion drift velocity were significant when calculated for the air case (50 V/cm and 100 cm/sec, respectively, within 10 cm of the canister surface and 300 years after emplacement).

Radionuclide transport as an aerosol is a potentially important mechanism near a repository. Radionuclides in high-level waste with a significant vapor phase include ^{3}H, ^{14}C, ^{85}Kr and ^{129}I. Only these radionuclides are expected as gases. Aerosol particles, however, can contain any soluble radionuclide present in the solution from whence the aerosol is produced. The formation of a heat pipe proximal to a HLW canister can provide an opportunity for aerosol production. The liquid film on a fracture surface moves toward the source of heat (waste canister) in response to differences in matric potential and surface forces, is vaporized at higher temperatures then moves away from the heat source until it condenses at lower temperatures. The decrease in gas solubiltiy in the liquid film as temperature rises in the moving liquid may cause bubbling which in turn introduces aerosol droplets into the airspace overlying the liquid film.

Aerosol generation, however, requires specific conditions to be present at the canister. Sufficiently thick liquid films in conjunction with sufficiently large air spaces must be available for bubble growth and rupturing to occur. Fractures of less than several hundred micrometers are too narrow for the formation of bubbles by this process and thus can not provide a setting for aerosol production. Additionally, temperature increase in the liquid film must occur rapidly so that gas desorption will result in gas desorption by bubbling rather than quiescently.

In the situation where bubbling occurs and an aerosol is produced, airborne particles will move in response to any driving force acting on the airspace. Typical driving forces include pressure and concentration gradients. Other driving forces, however, may be present. For example, ionized aerosol particles will respond to an external electric field resulting from Compton scattering or any other cause.

Airborne ionized particles will repel any similarly charged surfaces and move toward areas of opposite charge. The return flow of electrons which move in response to forced diffusion will seek the path of least resistance, one probable pathway being the liquid film on fracture surfaces, thereby negatively charging fracture surfaces. The significance of this process is that negatively particles will, on the average, remain airborne longer and thus travel farther than positively or neutrally charged particles in the presence of forced diffusion. Positively charged particles will move quickly to the negatively charged surfaces and resorb without traveling a significant distance. In this respect, the electric field may aid the containment of contaminants.

High temperatures can occur at waste canisters during decay of high-level waste, thus, creating significant thermal gradients. Movement of gas molecules or particles in response to a thermal gradient is another potential mechanism near a repository. The transport mechanism resulting from thermal gradients is generally referred to as thermal diffusion when gas molecules are concerned and as thermophoresis when larger sized particles are of interest. Although different theoretical arguments are used to explain each mechanism, the resulting flux by either mechanism is not significant unless widely varying sized molecules or particles are present.

Several radionuclide transport mechanisms and processes have been individually introduced and investigated. Additional transport mechanisms however, may exist which do not fit into any of the earlier mentioned categories. These additional transport mechanisms or processes include any other process or coupled process not yet discussed which may occur at possible repository conditions. Furthermore, the significance of an individual transport mechanism may be augmented by forces other than the major driving force of the transport mechanism. An example is electrophoresis--movement of ionized particles suspended in a fluid induced by an imposed electric field.

Electrophoresis could occur in the liquid film on a fracture surface. This mechanism is analogous to forced diffusion of ionized particles suspended in air. The scenario is complicated because any additional pathway for returning electrons (such as liquid films or fracture surfaces) short-circuits the electric current and reduces the intensity of the electric field by an undetermined amount. Since the electric field intensity for this case is unknown, the magnitude of electrophoresis can not be predicted. Electrophoresis if important, however, will be a phenomenon found acting near a repository because Compton scattering occurs only in this area.

Surface diffusion may also be affected by gradients other than concentration. In general, the importance of surface diffusion becomes appreciable when gas sorbed on a solid surface is limited to a few layers. The driving force of surface diffusion is a gradient in concentration of the sorbed gas. However, the driving force of particles or molecules along the surface can be augmented or impeded by the presence of other gradients. Gradients in temperature or electric potential need to be coupled with surface diffusion to ascertain the complete significance of the surface flow of contaminants.

In conclusion, radionuclide transport as vapor through unsaturated rock may be the result of several complex coupled processes. The magnitude of transport can not be quantified without specific knowledge of the waste form, the engineered barrier design, and the overall repository design as well as the hydrogeologic characteristics on the surrounding geologic media. The various physical transport processes will be greatly influenced by the developed temperature gradient in the immediate vincity of the repository and by the water redistribution due to the imposed thermal gradients. The significance of radionuclide transport should be throughly examined as a site characterization component and as the engineered design is formulated.

1. INTRODUCTION

Unsaturated fractured rock media are being investigated as potential sites for high-level waste (HLW) repositories by the Department of Energy and its contractors. The transport mechanisms for contaminants from a HLW repository located in unsaturated rock to the accessible environment are complex and not entirely understood. The principal pathway is considered to be downward to a regional water table and then to the accessible environment. Transport of contaminants as vapor is an additional mechanism whose contribution to the overall transport process needs to be established (Winograd, 1981; Roseboom, 1983 and Wollenberg et al, 1983). Factors that may add to the complexity of the vapor transport phenomenon include both the nature of the medium (i.e., fracture characteristics, porosity and anthropogenic alteration to the geologic media) and of the contaminants (i.e., sorptivity, solubility and radioactivity).

The objective of this study is to identify the mechanisms and processes of transport of radionuclides as vapor which can contribute to the overall transport process and the conditions at which these mechanisms and processes are potentially important. Each transport mechanism is evaluated in terms of what conditions would permit the mechanism to be significant. The mechanism is then dismissed or identified, when possible, as a potential contributor to the transport of radionuclides in unsaturated fractured rock.

The potential of radionuclide transport as vapor is investigated by first identifying radionuclides which can be transported as vapor. The physical setting of a repository located in unsaturated fractured rock is described with regards to its effect on transport as vapor. Several physical mechanisms and processes related to vapor transport are identified. Two inherently different transport processes identified are transport as a gas and transport as an aerosol. Both processes are referred to here as vapor transport.

Gas will move through a medium in response to several different driving forces. Concentration and pressure gradients result in the driving forces observed in typical subsurface movement of either gas or liquid. The governing equations which describe gas flow resulting from gradients in concentration or pressure are developed for a variety of possible physical settings and geometries which may exist at a HLW repository located in unsaturated fractured rock.

Several transport mechanisms have been identified which may be important near high-level waste even though they are rarely observed in nature. As will be discussed, identification of the potential of radionuclide transport as an aerosol brings to light the possibility of transport of any radionuclide present as a solute in liquid film on a fracture surface in the immediate vicinity of a HLW canister. Any radionuclide introduced into the geologic environment from a failed canister may be transported as vapor if it is a solute in rock water when this transport mechanism is present.

Gamma ray emitting radionuclides can create substantial electric fields by Compton scattering. Electric fields may affect the transport of contaminants by forced diffusion or some other process. Many radionuclides present in spent fuel are gamma ray emitters.

Large scale free gas convection may occur as a consequence of the expected high temperatures at a HLW repository. The governing equations are identified and several simplified scenarios are investigated.

1.1 Radionuclide Species

The nature of radionuclides placed in a HLW repository is an important factor that needs consideration when characterizing vapor transport of radionuclides. The composition of nuclear wastes to be placed in HLW repositories is varied and depends on reactor operation and the nuclear fuel cycle. Light water reactors (LWR) are the most common commercial nuclear reactors in the United States and, therefore, the most common source of high-level waste. Three nuclear fuel cycles for fuel removed from a LWR have been studied for their impact on commercial high-level waste management (Wang et al., 1983). 1) Spent fuel (SF) containing both uranium and plutonium as waste components is disposed directly after removal from the reactor. LWR spent fuel consists of fuel assemblies from either pressurized water reactors (PWR) or from boiling water reactors (BWR). 2) High-level waste resulting from the uranium-only recycle is spent fuel reprocessed by removal of most of the uranium and plutonium. Only uranium is recycled and trace amounts of uranium and plutonium remain in the reprocessed high-level waste. 3) The third process is referred to as total recycle and is one in which both uranium and plutonium are removed and reprocessed. The levels of trace amounts of uranium and plutonium remaining in high-level waste are higher in total recycle than in uranium-only recycle. Reprocessing will not remove fission products except for all the tritium, the noble gases (He, Kr and Xe) and 99.9% of the volatile elements (I and Br) (Wang et al., 1983).

Heat emmitted by spent fuel is generated by two main components, fission products and the transuranic actinides (Wang et al., 1983). During the first few hundred years after removal of nuclear fuel from a reactor, the principal contributors to heat generation are fission products such as strontium-90 and cesium-137. The amount of heat generation by fission products is largely independent of the fuel cycle. Subsequent to high activity by fission products, transuranic actinides and their daughters become the major contributors to heat generation. Transuranic actinides are relatively long-lived and include elements such as plutonium, americium and curium. The quantity of transuranic actinides contained in high-level waste also varies greatly with the choice of fuel cycle. Removal of plutonium will cause significant decreases in the heat generating capability of high-level waste.

Radionuclides with a significant vapor phase are not present in reprocessed fuel, hence, gaseous transport of radionuclides will not occur for this case. However, nuclear fuel reprocessing facilities for high-level waste from commercial nuclear reactors are not available in the United States. There are no plans for construction of a reprocessing facility in the near future. Therefore, HLW repository design should consider the consequences resulting from the burial of spent fuel complete with all fission products and transuranic actinides.

Radionuclides which exist as compounds with a significant gas phase are ^{3}H, ^{14}C, ^{85}Kr and ^{129}I. The respective half-lives for the gases are 12.26 yrs, 5730 yrs, 10.76 yrs and 1.7×10^{7} (CRC Handbook of Chemistry Physics, 1974). Carbon dioxide, CO_2, and methane, CH_4 are gases that pose a potential hazard because of their possible ^{14}C content. Of the volatile radionuclides, ^{129}I appears to have the greatest potential as a hazard because of its toxicity and long half-life.

Radionuclides that are of interest to the study of vapor transport, therefore, include the volatile species when gaseous transport mechanisms are considered and all radionuclides--including more serious contaminants such as the transuranic actinides--when transport as aerosol is present. The particular inventory of radionuclides from a SF canister is derived from the results of SANDIA-ORIGEN (Sutherland and Bennett, 1979). The particular species and the chemical compound of species that will be introduced into the geologic environment from a failed HLW canister will depend upon the chemistry of the geologic medium, the rock water and the radioactive waste. The complex chemical interactions between these three and the chemical profile of a HLW repository are not entirely understood and are only considered in general terms in this study.

1.2 Description of Physical Setting

Different physical processes can contribute to vapor transport of radionuclides. Each particular transport mechanism requires specific conditions to be present before the mechanism can significantly contribute to the overall transport process. Vapor transport of radionuclides, therefore, has to be examined for each physical setting where any of the contributing transport mechanisms may be important. Preliminary investigations of vapor transport indicate that some transport mechanisms may be important in a zone near the repository while others may be important at a larger distance. Factors influencing transport mechanisms near the repository include radiation and heat generation from high-level waste. The significance of vapor transport in the zone near the repository may be to transport radionuclides from the canister source to liquid in the matrix and in the fractures a short distance away. Although the distance of transport may be as short as several centimeters, transport as vapor may be significant because it can supply a major transport link from the canister to zones of increased saturation at some distance (Figure 1.1). The importance of this transport link is increased because high temperatures at HLW canisters can dry the rock proximal to the waste package, restricting transport as liquid in the zone near the repository. The zone near the repository is defined as distances up to centimeters to meters from the canister. Radionuclides in the zone near the repository are largely influenced by the engineering design of the canister and the nature of the waste.

In contrast are transport mechanisms which are important over large distances. Large distances are assumed to be tens of meters to hundreds of meters. Transport mechanisms important over large distances are, in general, influenced more by the geologic medium than the nature of high-level waste buried at the repository. One notable exception is heat generated by radioactive decay at the canisters. Burial of a sufficient number of canisters along a single plane in the subsurface can have a thermal effect at large distances for a repository that extends over hundreds or thousands of square meters.

Neither the specific repository site nor the engineering design of the repository and canister have been determined. Several criteria--social, political and technical--will be examined before an acceptable repository site is chosen. The engineering design of the repository and canister depends on research of expected transport mechanisms. The design of waste canisters is very important in terms of the expected

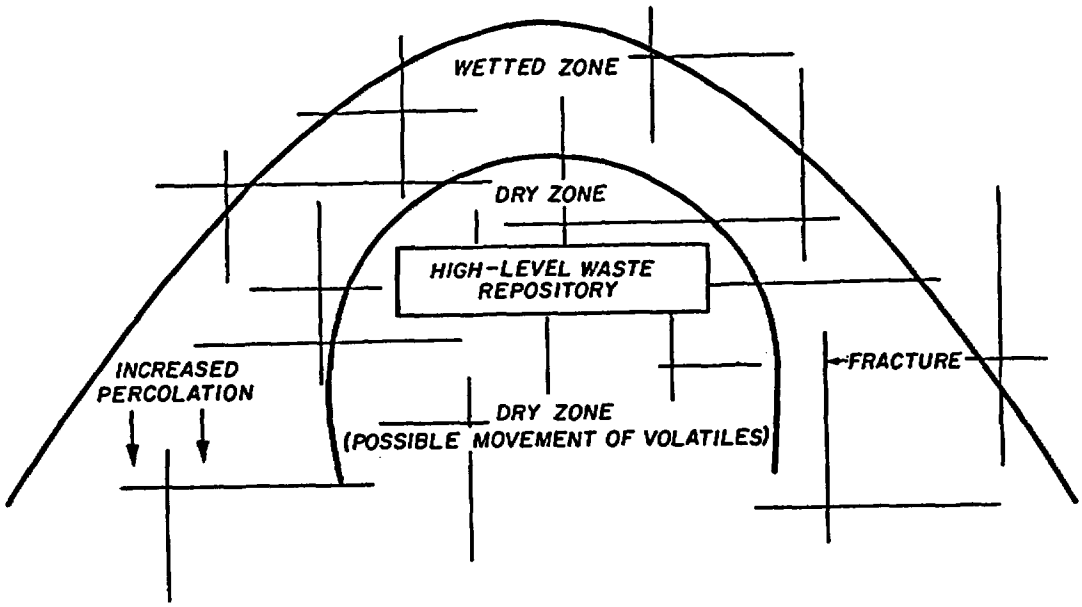

Figure 1.1. Schematic of high-level waste repository located in fractured media illustrating thermally induced zone of lower saturation enveloped by zone of higher saturation.

magnitude of the source of radionuclides and the generation of heat and radiation at the time of emplacement and how the source varies with time after emplacement. The canister cladding, number of fuel assemblies per canister and backfill material are not yet specified.

Until the engineering design of the repository, exact inventory of high-level waste and repository site are specified, the contaminant source must be treated as a variable. Without a specified source, vapor transport mechanisms are investigated relative to other transport mechanisms when possible. Otherwise, they are investigated in general terms only.

The unique problem of HLW disposal in unsaturated fractured rock raises the question of the importance of radionuclide transport as vapor. This question, as posed in light of the aforementioned discussion, requires examination at several scales of length and at different physical settings. Each aspect will be investigated separately.

2. GAS MOVEMENT IN A FRACTURED MEDIUM

2.1 Introduction

The movement of gas in an unsaturated, non-isothermal, fractured medium which is located in the presence of a radioactive source can take place as a result of several different driving forces. The driving forces present in the aforementioned setting include those resulting from: 1) a concentration or partial pressure gradient; 2) a total pressure gradient; 3) a liquid or surface concentration gradient; 4) an external electrical field and 5) a thermal gradient. Each particular driving force results in an associated transport mechanism. A concentration gradient can cause ordinary diffusion. Ordinary (or concentration) diffusion includes Knudsen flow, self-diffusion, binary diffusion and surface flow. A gradient in the total pressure can result in viscous flow which includes Poiseuille (or Couette) and slip flow. An electric field can result in forced diffusion. And finally, a thermal gradient can cause a mechanism called thermal diffusion.

A review of the equations governing gas movement in a fractured medium is presented here. The physics and mathematical formulation of each flow mechanism will be discussed individually and independently from each other. A binary gas system will be assumed when a single gas system does not adequately represent a physical process.

The representation of gas movement through non-isothermal fractured media entails an examination of the problem through several possible perspectives. Similar to the examination of the transport mechanisms of saturated flow in fractured media, there is an enigma in deciding the appropriate course necessary to adequately represent the physical mechanisms which govern non-isothermal gas movement through fractured media. The major factors which dictate which approaches are feasible are the scale of the problem of interest and the availability of the technology required to apply the selected approach.

2.1.1 Scale of Investigation

Representation of gas movement through fractured, consolidated media is a perplexing and difficult endeavor. At one extreme, consolidated unfractured rock matrix has low permeability which may be assumed to be treated as a continuum. At the other extreme is a set or several sets of fracture systems superimposed on rock matrix of low permeability.

When the orientation, spacing, aperture, and lateral extent of the fractures are regular in their nature and adequately defined, the medium can be treated as an equivalent porous medium (EPM). A dual porosity system such as this can generally be considered a continuum with a sufficiently large representative elemental volume (REV) and therefore treated with methodologies developed for porous media.

A major dilemma arises when the medium cannot be represented by a reasonably sized REV. This dual porosity system can not be treated as a continuum and methodologies designed for porous media are, in general, inadequate.

Application of the REV concept to vapor transport raises additional problems. The size of the REV required to represent a system is dependent upon the particular properties of interest of the system. As an example, a REV may be considered homogeneous in terms of gas porosity but highly heterogeneous with respect to gas permeability. The non-isothermal effect of high-level waste at the repository and the additional pathways present in the disturbed zone are two major contributions to the heterogeneity of the system. As a result, a particular transport mechanism may have to be investigated with a REV of one size while another transport mechanism will require a REV of a different size.

Vapor transport is investigated at two levels 1) in a zone near the repository with a single fracture characterized by a parallel plate model and 2γ at larger distance in which the system is treated as a continuum thus permitting an analysis using porous media methodologies. The pore structure of a rock matrix may be better represented with a capillary tube model than the parallel plate model used for fractures. The use of a capillary tube model will make the rock matrix analysis analogous to continuum models used for porous media. Thus, mathematical formulation for the various flow mechanisms are presented in both geometries, capillary and parallel plate, when appropriate.

Gas movement can occur as gas dissolved in a fluid, however, only vapor transport as vapor flow through the air spaces in the system is considered here. The degree of saturation in fractured rock has a significant effect upon vapor transport. As a system drys out, the degree of gas porosity increases while the remaining liquid water exists at a larger negative pressure. Fractures and pore spaces saturate according to the expression

$$(2.1) \quad \Delta P = 2\, s \cos \alpha / h_r$$

where h_r is the hydraulic radius, s is surface tension of the water, α is the angle of contact between the solid and water and ΔP is the pressure difference between the capillary water and the atmosphere. Therefore, the amount of airspace available for vapor flow is highly dependent upon the negative pressure of the system. Assuming a contact angle of 0^o and a surface tension of 72.7 dynes/cm yields the following effective radii for the respective negative pressures (see Table 2.1).

Table 2.1 Values of hydraulic radius (cm) and pressure (bars) when assuming a contact angle of 0^o and a surface tension of 72.7 dynes/cm.

hydraulic radius (cm)	1	10^{-1}	10^{-2}	10^{-4}	10^{-6}
pressure (bars)	1.45E-4	1.45E-3	1.45E-2	1.45	1.45E2

Vapor phase transport will be greatly diminished at small negative pressures because most voids in a medium will be saturated. It is possible that voids in the rock matrix of a dual porosity system can be saturated while under the same pressure, fractures will be unsaturated except for liquid film retained on solid surfaces by surface tension. Additionally, flow mechanisms that affect vapor phase transport in the rock matrix are not necessarily the same mechanisms that govern vapor phase flow in rock fractures.

2.1.2 Theoretical Basis of Gas Movement

A theoretical discussion of the physics of gas movement generally employs kinetic theory in the formulation of the governing equations. Kinetic theory can be used in a simplified manner or, in some cases, rigorously. Rigorous kinetic theory of monatomic gases and mixtures is referred to as the Chapman-Enskog theory. In contrast is simplified theory of dilute gases based on entirely different assumptions. Both theories are useful to investigate the physics of gas flow (Hirschfelder et al., 1954).

A major difference between rigorous kinetic theory and simplified kinetic theory is that molecules are assumed to collide in a manner not unlike billiard balls in the latter theory, while interrelated movement of two molecules is accounted for by a potential function as described in the rigorous approach of Chapman-Enskog theory (Figure 2.1).

The following assumptions couched in simplified kinetic theory create an unrealistic model but good results are nevertheless produced. These assumptions are (Hirschfelder et al., 1954)

i) all molecules are rigid, non-attracting spheres of diameter d.
ii) all molecules travel at the arithmetic mean velocity v.
iii) all molecules travel parallel to one of the three cartesian axes.

More realistic but more involved assumptions are required when applying the rigorous theory of gases. In essence, Chapman-Enskog theory is based on a distribution function that represents the location of the molecules of a particular species which lie in a unit volume about a particular point. The distribution function is a solution of an integral-differential equation known as the Boltzman equation. The Boltzman equation is valid at pressures sufficiently low that collisions involving more than two molecules can be effectively neglected. Additionally, the free mean path is small relative to the dimensions of the aperture of the space through which the gas flows. Consequently, rigorous kinetic theory is not applicable when investigating slip flow or Knudsen flow.

Complex interactive forces between two molecules are not neglected by Chapman-Enskog theory as in simplified kinetic theory. When applying rigorous kinetic theory, intermolecular forces and differences in size between molecules are considered. The Lennard-Jones function is empirically derived but provides a reasonable approximation of the forces between two non-polar molecules. The potential energy of interaction between a molecule of gas A an a molecule of gas B is defined (Chapman and Cowling, 1970)

$$(2.2)\quad E_{AB}(r) = 4e_{AB}[(d_{AB}/r)^{12} - (d_{AB}/r)^{6}]$$

where $E_{AB}(r)$ is the energy of molecular interaction (ergs), d_{AB} is the collision diameter (Å) between molecules A and B, e_{AB} is the maximum attractive energy between the two molecules and r is the radial

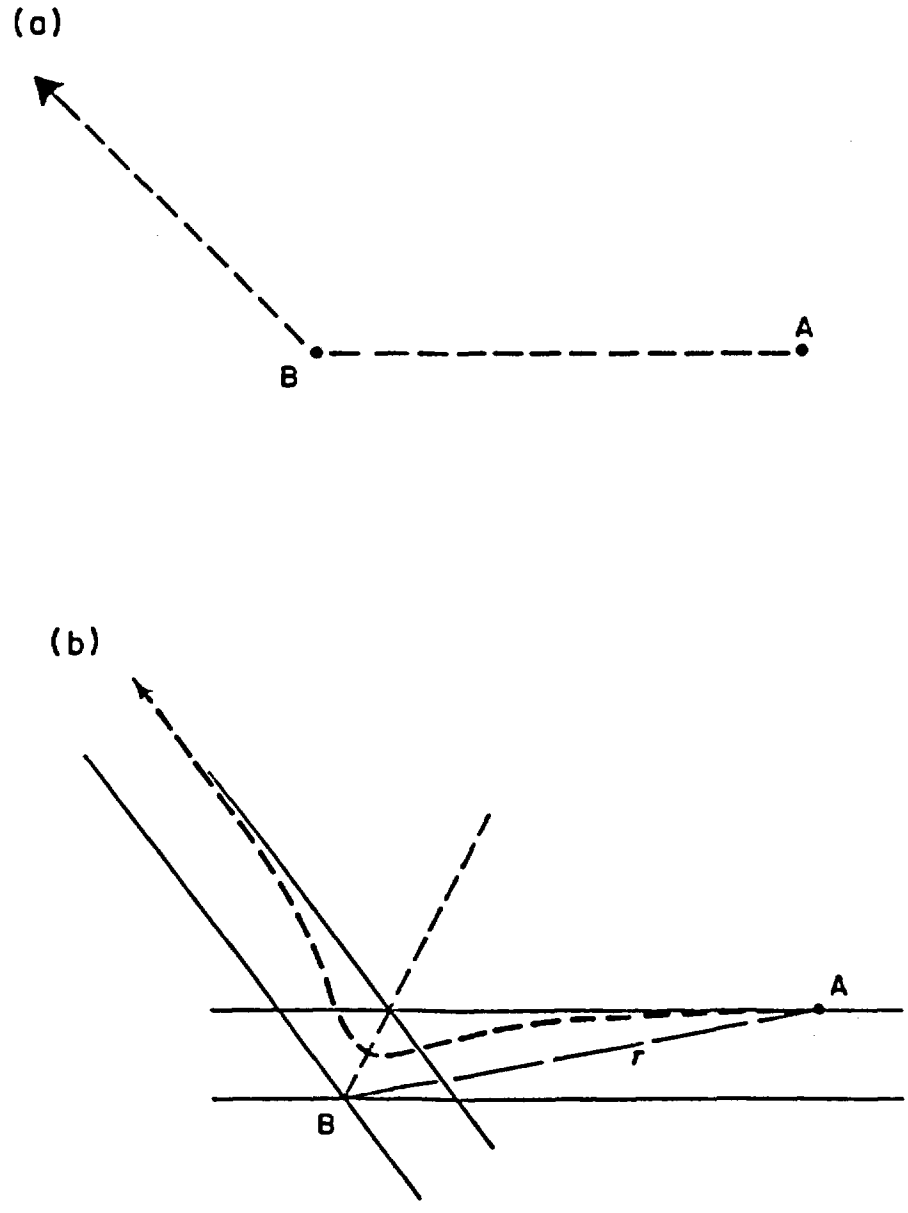

Figure 2.1. Representation of molecule-molecule interaction according to a) simplified kinetic theory and b) rigorous kinetic theory. Molecule A travels toward molecule B along trajectory (dotted line) (adapted from Hirschfelder et al., 1954). Reprinted by permisssion of John Wiley & Sons, Inc., © (See page 15).

distance separating molecules A and B. The system defined by Equation (2.2) is referred to as the 12,6 model. The parameter d_{AB} equals r and e is the maximum force of attraction when E is zero. Values for the force constants e and d are dependent upon the particular gases and are determined empirically. The composite terms e_{AB} and d_{AB} are defined by

$$e_{AB} = (e_A\ e_B)^{1/2} \tag{2.3}$$

and

$$d_{AB} = (d_A + d_B)/2 \tag{2.4}$$

Values of d_i and e_i for like molecules of several gases of interest to this study are listed in Table 2.2 (Hirschfelder et al., 1954, and Bird et al., 1960). The force constant e is normalized with respect to Boltzmans constant, K.

Table 2.2 Values of the Lennard-Jones parameters, d and e/K for selected gases (after Hirschfelder et al., 1954, and Bird et al., 1960).

Gas	Molecular Weight	Lennard-Jones Parameters d(Å)	e/K(°K)
H_2	2.016	2.915	38.0
Kr	83.80	3.498	225.0
Air	28.97	3.617	97.0
N_2	28.02	3.681	91.5
O_2	32.00	3.433	113.0
CO_2	44.01	3.996	190.0
I_2	253.82	4.982	550.0
CH_4	16.04	3.822	137.0

The empirical relationships stated in Equations (2.3) and (2.4) are assumed valid for a nonpolar, nonreactive binary gas. These two empirical relationships allow accurate determination (within 10%) of d_{AB} and e_{AB} based on experimentally determined values of the intermolecular forces d_A, d_B, e_A and e_B of pure gases (Bird et al., 1960).

The r^{-12} part of Equation (2.2) accounts for the repulsive forces between the molecules and the r^{-6} part accounts for attraction. Figure 2.2 is a plot of the Lennard-Jones potential energy function as it varies with the distance between molecules. As is illustrated, replusion increases dramatically as two molecules become increasingly close, however, the two molecules are attracted toward each other at greater separations.

The Stockmayer potential is generally used to calculate the potential between polar molecules. The Stockmayer potential differs from the Lennard-Jones potential by an additional term which accounts for the angular dependence of the dipole-dipole interaction. This potential is defined (Hirschfelder et al., 1954)

$$(2.5) \quad E(e_A,e_B,\phi_A-\phi_B) = 4e[(d_{AB}/r)^{12} - (d_{AB}/r)^6] - [(\mu_A\mu_B)/r^3]\, g(e_A,e_B,\phi_A-\phi_B)$$

where μ is the moment of a single molecule dipole and $g(e_A,e_B,\phi_A-\phi_B)$ is defined

$$(2.6) \quad g(e_A,e_B\phi_A-\phi_B) = 2\cos e_A \cos e_B - \sin e_A \sin e_B \cos(\phi_A - \phi_B)$$

where e_i is the dipolar angle and $\phi_A - \phi_B$ is the angle of translation between the two molecules (Figure 2.3). Lennard-Jones and Stockmayer potentials can be used to determine gas diffusion coefficients in the rigorous gas theory approach.

2.2 Ordinary Diffusion

Movement of gas through air resulting from a concentration gradient is attributed to Brownian motion of the gas molecules. This transport mechanism is referred to as ordinary (or concentration) diffusion. Gas molecules can collide with other gas molecules, with walls retaining the gas or with molecules forming a layer on the retaining pore walls. Gas movement caused by collisions between gas molecules and pore walls is referred to as Knudsen flow, J_k, movement resulting from collisions between like molecules is referred to as self diffusion, J_{self}, and movement of gas by diffusion along the layer of molecules adsorbed onto the surface of the retaining pore wall is called surface diffusion, J_s, in response to their respective concentration gradients is binary

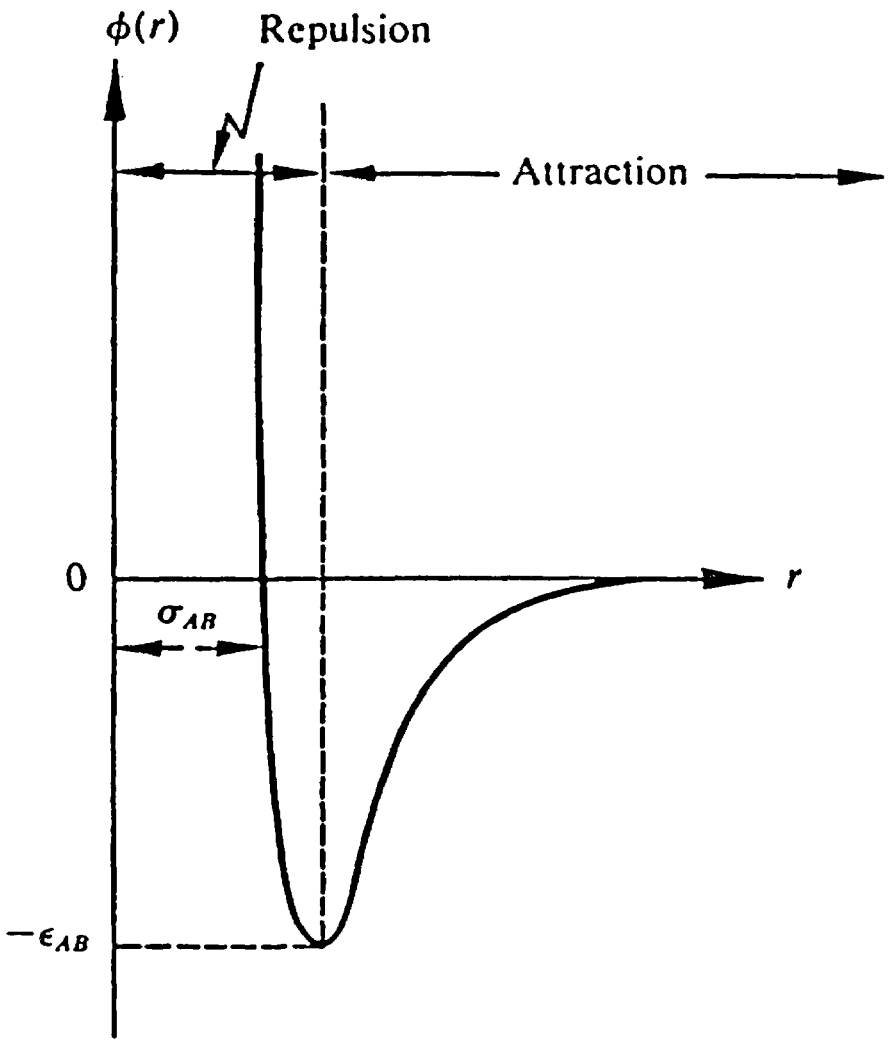

Figure 2.2. Leonard-Jones potential energy function $\phi(r)$ as a function of the distance r between molecules (from Geankoplis, C. J., " Mass Transport Phenomena," Columbus: Ohio State Univ., 1972. With permission. ©

Figure: Fig. 1.3-1 on p. 27, Fig. 1.5-3 on p. 49, and Table I-M on pp. 1126-1127 of Hirschfelder, J.O., C.F. Curtis, and R.B. Bird, 1954, Molecular Theory of Gases and Liquids. Reprinted by permission of John Wiley & Sons, Inc.©

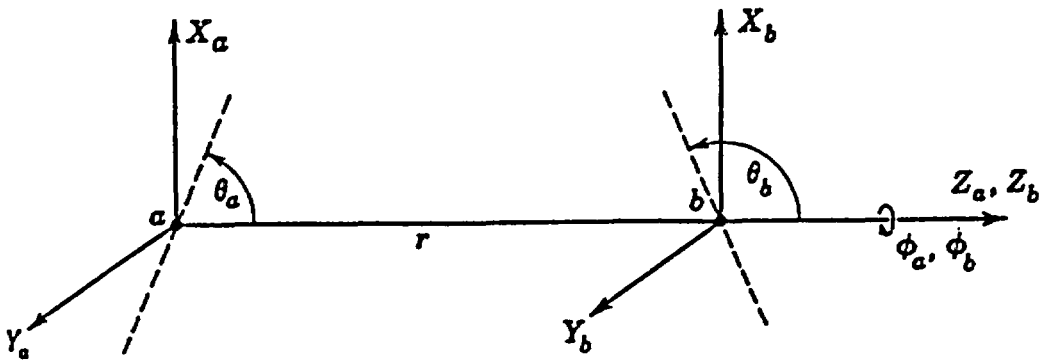

Figure 2.3. Points a and b represent the centers of two molecules. The dotted lines through a and b indicate the axiis of the dipoles. θ_a, θ_b, ϕ_a, ϕ_b define the orientations of the two molecules (from Hirschfelder et al., 1954).

diffusion, J_b. The direction of flux of two separate gases can either occur in the same direction or in opposite directions.

The total flux resulting from these different transport mechanisms, J_o, can be written

(2.7) $$J_o = J_k + J_{self} + J_b + J_s$$

These four transport mechanisms are grouped together because the driving force of each mechanism is a concentration (or partial pressure) gradient. If more than one gas is present in significant quantities, self diffusion is not present and only the binary term contributes to total diffusion flux. Flux resulting from self-diffusion is represented in J_b in a binary gas system.

Rigorous kinetic theory is employed in formulating accurate expressions for self and binary diffusion. All other expressions needed to define ordinary diffusion under various conditions are developed using simplified kinetic theory.

The ideal gas law is predicated on simplified kinetic theory. An ideal or perfect gas is defined as a gas in which molecules, of negligible size, exert no forces on each other except contact forces at the instant of impact (Present, 1958). The ideal gas law can be stated

(2-8) $$\rho R T = P M$$

where

ρ = density (gm/cm^3)
R = gas constant (cm^3-atm/deg-mole)
T = temperature (°K)
P = pressure (dynes/cm)
M = molecular weight (gm/mole)

Because the assumption of an ideal gas law is based on simplified kinetic theory of gases, it is not strictly applicable when the rigorous theory of gases is employed.

In general, the ideal gas law is valid for gases under moderate pressures (about 1 bar), a pressure which is to be expected at a HLW repository located in the unsaturated zone except at early times proximal to a HLW canister (Pruess and Wang, 1984). Therefore, employing the ideal gas law will not significantly compromise the validity of the following mathematical arguments used to define gas flow mechanisms near a HLW repository.

As stated, the driving force of the various transport mechanisms which contribute to ordinary diffusion is the gas concentration gradient dc_i/dx. For a gas, the concentration gradient can be expressed in terms of the partial pressure using the ideal gas law

(2.9) $$dc_i/dx = 1/RT \, dp_i/dx$$

where c_i is the concentration and p_i is the partial pressure of a particular species. Therefore, each transport mechanism with a driving force resulting from a concentration gradient can be alternatively expressed in terms of a partial pressure gradient.

Two important concepts used during simplified kinetic theory arguments are the mean free path length and the mean molecular gas velocity. The average distance between molecule-molecule collisions is referred to as the mean free path length, λ, or Maxwellian free space mean path. Mean free path length is defined (Present, 1958)

$$\lambda = 3\,\eta/(\rho\,\bar{v}) \tag{2.10}$$

where η is the kinematic viscosity of the gas. The term $\bar{v}$ is the mean gas velocity of gas molecules irrespective of direction. Mean gas velocity can be determined by the expression (Kennard, 1938)

$$\bar{v} = (8\,K\,T/\pi\,m)^{1/2} \tag{2.11}$$

where m is the mass of a gas molecule.

Of integral importance to the investigation of gas flow is the ratio of the mean free path length to the distance between pore walls, b. This ratio is referred to as the Knudsen number, Kn. The relative importance of molecule-molecule collisions to molecule-wall collisions is indicated in the Knudsen number. The frequency of molecule-molecule collisions exceeds the frequency of molecule-wall collisions when the distance separating pore walls is greater than the average distance between molecule-molecule collisions. Table 2.3 (from Kennard, 1938) lists for several gases the mean free path, viscosity, molecular weight and molecular diameter as defined in simplified kinetic theory, all at one bar pressure and 15°C.

Pure Knudsen flow represents the limit as the Knudsen number ratio tends toward infinity. When $\lambda \gg b$, gas molecules will have greater occasion to collide with the pore walls rather than colliding with other gas molecules. When the Knudsen number decreases to about unity ($\lambda/b \doteq 1$), either slip flow, which is a component of viscous flow, or self-diffusion becomes prominent.

The behavior of a gas molecule upon collision with a surface and its trajectory subsequent to the interaction has an important effect upon the flow of gas when the Knudsen number is large (i.e. low pressure and/or small apertures). A gas molecule can be reflected off of a surface in one of two ways. Specular reflection (or mirror-like reflection) defines a collision in which the angle of incidence of the gas molecule is equal to the angle of reflection and where the kinetic energy of the incident gas molecule is equal to the kinetic energy of the reflected gas molecule. The average forward tangential momentum of the incident molecule is therefore preserved during specular reflection.

The other possible manner of reflection is diffuse reflection. Diffusely reflected gas molecules attain thermal equilibrium with the reflecting surface upon interaction with the wall and the angle of

Table 2.3 Some Molecular Data of gases.

	M	n	λ	d
H_2	2.016	871	11.77	2.74
Helium	4.002	1943	18.62	2.18
CH_4(methane)	16.03	1077	5.16	4.14
NH_3	17.03	970	4.51	4.43
H_2O	18.02	926	4.18	4.60
N_2	28.02	1734	6.28	3.75
C_2H_4(ethylene)	28.03	998	3.61	4.95
C_2H_6(ethane)	30.05	900	3.15	5.30
O_2	32.00	2003	6.79	3.61
HCL	36.46	1397	4.44	4.46
Argon	39.94	2196	6.66	3.64
CO_2	44.00	1448	4.19	4.59
Krypton	82.9	2431	5.12	4.16
Xenon	130.2	2236	3.76	4.85
Air	28.96	1796	6.40	3.72

M = molecular weight (g/mole)
n = viscosity (10^{-7} dyne·sec/cm^7)
λ = mean free path (10^{-6}cm)
d = diameter (10^{-8}cm)

reflection obeys the cosine law (Lassettre, 1956). The cosine law states that a reflecting particle is equally likely of passing through a particular solid angle as it is of passing through any other equally large solid angle. Diffuse reflection can be thought of as a gas molecule momentarily adsorbed onto the surface it strikes (about 10^{-12} - 10^{-13} seconds is required for equilibrium) then evaporating soon thereafter with an independently determined new direction (Langmuir, 1916).

A dimensionless reflection factor, β_0

(2.12) $$\beta_0 = (2 - f_0)/f_0$$

is often used to weight the equations which govern the flow of gas molecules during Knudsen flow for variations in the type of reflection by the gas molecules. The variable f_0 is defined as the fraction of molecules which undergo diffuse reflection. Likewise $1 - f_0$ is the fraction of those molecules which are specularly reflected during free molecular flow.

An additional dimensionless factor β_1 is defined to account for possible specular reflection during slip flow. This second factor is defined (Carman, 1956)

$$\beta_1 = 3\pi/16\ (2 - f_1)/f_1 \tag{2.13}$$

The fractions f_1 and $1 - f_1$ have similar definitions for slip flow as do the fractions f_0 and $1 - f_0$ for Knudsen flow.

If the reflections of all gas molecules are diffuse, f (either f_0 or f_1) is unity and both dimensionless factors degenerate to a minimum. However, if f has a value other than unity, then a certain amount of specular reflection is represented in each factor. The variable f need not have the same value in both Knudsen flow and slip flow.

Maxwell concluded that gas molecule reflection is composed of nearly equal portions of diffuse and specular reflection (i.e., f = 0.5). However, Knudsen conducted experiments which lead him to believe that all gas molecules were diffusely reflected during free moleculer flow (Carman, 1956). Experimental data indicate that there is some preservation of momentum by gas molecules after colliding with a solid surface and subsequent analysis of Knudsen's data (Hiby and Pahl, 1952) has revealed that the value of f_0 is approximately 0.98, suggesting that some specular reflection does occur during Knudsen flow.

The value of f_1 for slip flow, however, varies with different gas-surface systems and has observed values that range from 0.79 to 1.0. All molecules undergo diffuse reflection during slip flow on roughened surfaces such as old shellac, silver oxide and machined brass and for this case β_1 has the minimum value of 0.59 (Carman, 1956). Given this observed characteristic, the naturally rough texture of fracture surfaces would exhibit entirely diffuse reflection and β_0 would be unity, while β_1 would equal 0.59. Thin liquid films on fracture surfaces will also affect reflection although the effect is not known.

Observed molecular flow rates, however, are generally less than those predicted by purely diffuse reflection (Massignon, 1979). A Monte Carlo

simulation of free molecular flow (DeMarcus, 1959) suggests that a diffuse reflection factor of 0.8 is neccesary for all gas molecule-wall interactions to agree with an observed free molecular flow rate 30% below the predicted flow rate. A more elaborate theory than the one described may be required to agree with observed data. Among the more elaborate theories is backward scattering of reflected gas molecules as defined by Lambert's law of preferential absorption of molecules on a solid surface (Massignon, 1979).

2.2.1 Self and Binary Diffusion

The flow of a single gas by self diffusion or two gases by binary diffusion occurs in response to a concentration gradient when the Knudsen number is small. Ficks first law relates the mass flux by self-diffusion, J_{self} or by binary diffusion, J_b of a diffusing substance which passes across a unit cross sectional area to the concentration gradient by the expression

$$(2.14) \qquad J_b = - D_{AB} \nabla C$$

where C is the total concentration of species A and D_{AB} is the coefficient of diffusivity of species A diffusing through B. The diffusion coefficient appears as D_{AA} and the flux as J_{self} in self diffusion. Ficks law was originally obtained empirically but has since been derived using kinetic theory and several important assumptions (Geankoplis, 1972).

Values for the diffusion coefficient vary with the type of flow mechanism and with the physical conditions of the system (i.e., temperature and pressure). Methodologies used to determine the values of the diffusion coefficient vary with the basic approach employed, either empirical or analytical, and the level of sophistication of each approach.

Experimentally calculated diffusion coefficients are derived from a number of different procedures. Geankoplis (1972) discusses several of the more popular techniques used. Experimental determination of the diffusion coefficients of a gas is usually accomplished by measuring the movement of a radioactive isotope of the diffusing gas even though the physical properties of the radioactive isotope may differ from the average properties of the gas. Although experimentally determined values for diffusion coefficients are available for a variety of gases at different temperatures and pressures, values for additional gases

under different conditions are not available and must be measured or predicted theoretically.

The diffusion coefficient can be theoretically determined using either simplified or rigorous kinetic theory. The nature of diffusion often dictates which methodology is employed.

Diffusion of one gas into another gas can be calculated using simplified kinetic theory with the expression (Present, 1958; Bird et al., 1960)

$$(2.15) \qquad D_{AB} = 1/3 \; \bar{v} \; \lambda$$

Evaluating this expression using the ideal gas law and the definitions of mean free path length and mean gas velocity yields

$$(2.16) \qquad D_{AA^*} = 2/3 \; (K^3/\pi^3 m_A)^{1/2} \; T^{2/3}/P d_A^2$$

where both gas A and A^* are comprised of rigid spheres of identical mass and diameter. The terms d_A and m_A are the diameter and mass of the gas molecules. P is the total pressure. The diffusion coefficient of two rigid spheres of unequal diameter and mass becomes

$$(2.17) \qquad D_{AB} = 2/3(K^3/\pi^3)^{1/2}(1/2m_A + 1/2m_B)^{1/2} \; T^{3/2}/$$

$$P[(d_A + d_B)/2]^2$$

Although values calculated by Equations (2.16) and (2.17) are generally good, more accurate results can be determined by employing rigorous kinetic theory. Chapman-Enskog theory allows the calculation of the diffusion coefficient for low density gases using

$$(2.18) \qquad D_{AB} = 0.0018583 \; [T^3(1/M_A + 1/M_B)]^{1/2}/(P \; d_{AB}^2 \; \Omega_{Dab})$$

where Ω_{Dab} is the collision integral which is a slowly varying dimensionless function of dimensionless temperature, of kT/ϵ_{AB} and of the intermolecular potential field for one molecule of gas A and one of gas B. M_i is the molecular weight of gas i. The collision integral is defined by the expression (Hirschfelder et al., 1954)

$$(2.19) \qquad \Omega_{Dab} = (2\pi \; K \; T/V_{AB})^{1/2} \int_0^\infty \int_0^\infty e^{-V_{AB}^2} V_{AB}^5 \; (1 - \cos \Delta) \; b \; db/dV_{AB}$$

where b is the impact parameter and Δ is the angle at which the molecules are deflected (Figure 2.2) and where V_{AB} is reduced initial relative speed between molecules A and B defined by

$$(2.20) \qquad V_{AB} = (\mu_{AB}/2\ KT)^{1/2}\ g_{AB}$$

The parameter g_{AB} is the initial relative velocity between the colliding molecules. The term μ_{AB} is the reduced mass defined by

$$(2.21) \qquad 1/\mu_{AB} = (1/m_A)(1/m_B)$$

Values of the collision integrals are given for values of dimensionless temperature, KT/e_{AB} in Table 2.4.

An alternate approach to determine the coefficient of diffusion based on kinetic theory and a correlation technique has been developed by Slattery and Bird (1958) and applied to available sets of diffusion flow data for self-diffusion and binary diffusion of dilute gases. The Slattery-Bird expression for the diffusion coefficient is written

$$(2.22) \qquad D_{AB} = [(P_A^C\ P_B^C)^{1/3}(T_A^C\ T_B^C)^{5/12}[(1/M_A)+(1/M_B)]]^{1/2}]/P \cdot a\ [T/(T_A^C\ T_B^C)^{1/2}]^b$$

where

P_C = critical pressure for designated gas,
T_C = critical temperature for designated gas,
a,b = constants.

The diffusion coefficient is inversely proportional to pressure, increases with increasing temperature, and somewhat insensitive to the composition of the gases at low temperatures. Values for the constants a and b are derived by a least squares method and computed for two classes of mixtures (Slattery and Bird, 1958). Experimental data on mixtures containing hydrogen, helium and water plotted on a trend separate from non-polar gases. Therefore, values for a and b used when determining the coefficient of diffusion of a pair of non-polar gases are different than values of a and b used for H_2 with a non-polar gas. The two pairs of constants are:

non-polar pairs: $a = 2.745 \times 10^{-4}$, $b = 1.823$

H_2O with a non-polar gas: $a = 3.640 \times 10^{-4}$, $b = 2.334$

Table 2.4 Functions for prediction of transport properties of gases at low densities, from Hirschfelder et al. (1954). Reprinted by permission of John Wiley & Sons, Inc. © (See page 15).

KT/ϵ_{AB}	$\Omega_\mu = \Omega_k^*$	$\Omega_{D,AB}^{**}$	KT/ϵ_{AB}	$\Omega_\mu = \Omega_k^*$	$\Omega_{D,AB}^{**}$
			2.50	1.093	0.9996
0.30	2.785	2.662	2.60	1.081	0.9878
0.35	2.628	2.476	2.70	1.069	0.9770
0.40	2.492	2.318	2.80	1.058	0.9672
0.45	2.368	2.184	2.90	1.048	0.9576
0.50	2.257	2.066	3.00	1.039	0.9490
0.55	2.156	1.966	3.10	1.030	0.9406
0.60	2.065	1.877	3.20	1.022	0.9328
0.65	1.982	1.798	3.30	1.014	0.9256
0.70	1.908	1.729	3.40	1.007	0.9186
0.75	1.841	1.667	3.50	0.9999	0.9120
0.80	1.780	1.612	3.60	0.9932	0.9058
0.85	1.725	1.562	3.70	0.9870	0.8998
0.90	1.675	1.517	3.80	0.9811	0.8942
0.95	1.629	1.476	3.90	0.9755	0.8888
1.00	1.587	1.439	4.00	0.9700	0.8836
1.05	1.549	1.406	4.10	0.9649	0.8788
1.10	1.514	1.375	4.20	0.9600	0.8740
1.15	1.482	1.346	4.30	0.9553	0.8694
1.20	1.452	1.320	4.40	0.9507	0.8652
1.25	1.424	1.296	4.50	0.9464	0.8610
1.30	1.399	1.273	4.60	0.9422	0.8568
1.35	1.375	1.253	4.70	0.9382	0.8530
1.40	1.353	1.233	4.80	0.9343	0.8492
1.45	1.333	1.215	4.90	0.9305	0.8456
1.50	1.314	1.198	5.0	0.9269	0.8422
1.55	1.296	1.182	6.0	0.8963	0.8124
1.60	1.279	1.167	7.0	0.8727	0.7896
1.65	1.264	1.153	8.0	0.8538	0.7712
1.70	1.248	1.140	9.0	0.8379	0.7556
1.75	1.234	1.128	10.0	0.8242	0.7424
1.80	1.221	1.116	20.0	0.7432	0.6640
1.85	1.209	1.105	30.0	0.7005	0.6232
1.90	1.197	1.094	40.0	0.6718	0.5960
1.95	1.186	1.084	50.0	0.6504	0.5756
2.00	1.175	1.075	60.0	0.6335	0.5596
2.10	1.156	1.057	70.0	0.6194	0.5464
2.20	1.138	1.041	80.0	0.6076	0.5352
2.30	1.122	1.026	90.0	0.5973	0.5256
2.40	1.107	1.012	100.0	0.5882	0.5170

* For viscosity and thermal conductivity.
**For mass diffusivity.

Diffusion coefficients for the range of temperature from 30° to 250°C have been calculated for H_2, Kr, CO_2, I_2 and CH_4 using the Slattery-Bird formula and the Chapman-Enskog formula (Figures 2.4 to 2.8). The gases are diffused into air in making the Chapman-Enskog calculations. Standard values for the critical temperature and critical pressure of air are not available. Because of this, diffusion coefficients were determined with the Slattery-Bird formula for gases diffused into N_2. The difference in diffusion coefficients calculated by each method is partially because the gases of interest are diffused into different gases.

The Chapman-Enskog expression for the diffusion coefficient for self and binary diffusion generally gives more accurate values than other methods except when the potential parameters are not experimentally determined and must be estimated from the critical proterties of the gas.

In general, the Chapman-Enskog calculation technique is employed when the Lennard-Jones potential for the gas is available. The Slattery-Bird technique is used when the Lennard-Jones potential is not available but the critical temperature and critical pressure of the substance are available. However, experimentally determined diffusion coefficients are used when possible (Bird et al., 1958).

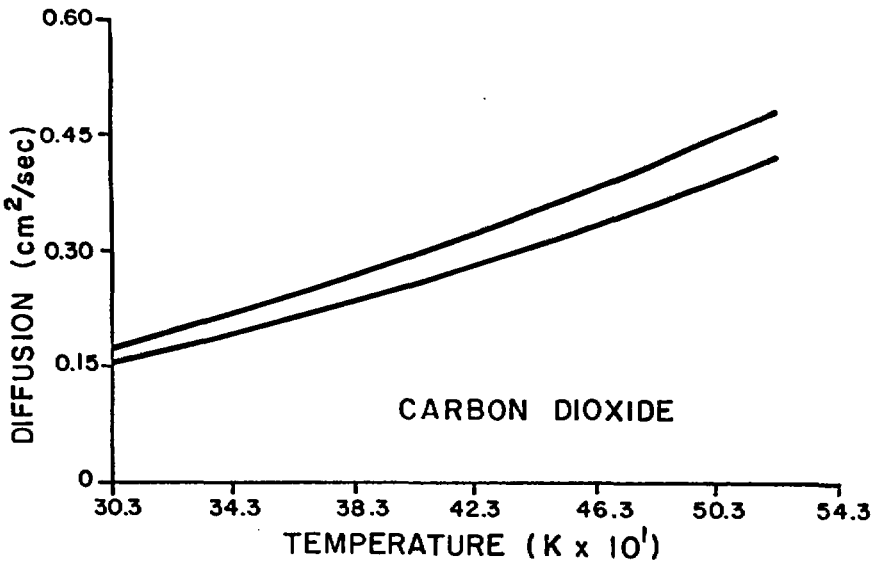

Figure 2.4. Diffusion coefficient (cm^2-sec^{-1}) for carbon dioxide versus temperature (°K). The top curve is determined by the Slattery-Bird method, the bottom curve is determined by the Chapman-Enskog method.

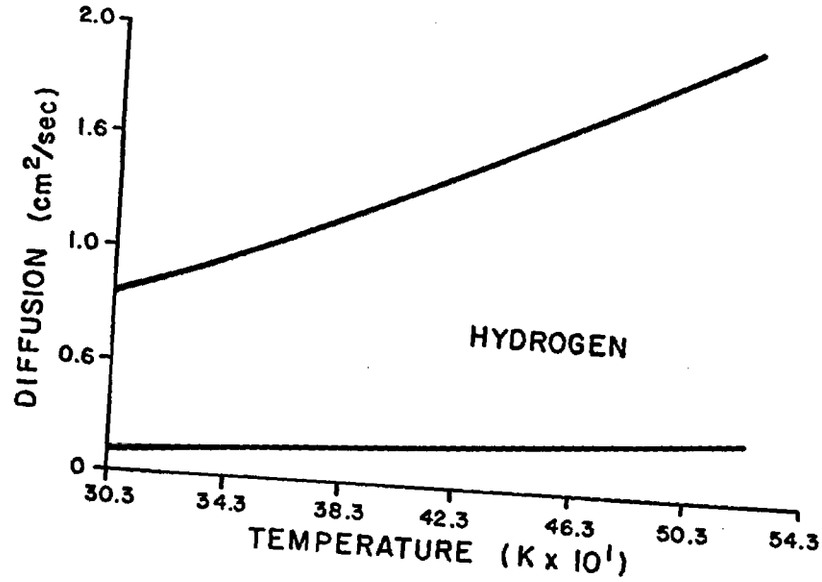

Figure 2.5. Diffusion coefficient (cm^2-sec^{-1}) for hydrogen versus temperature (°K). The top curve is determined by the Slattery-Bird method, the bottom curve is determined by the Chapman-Enskog method.

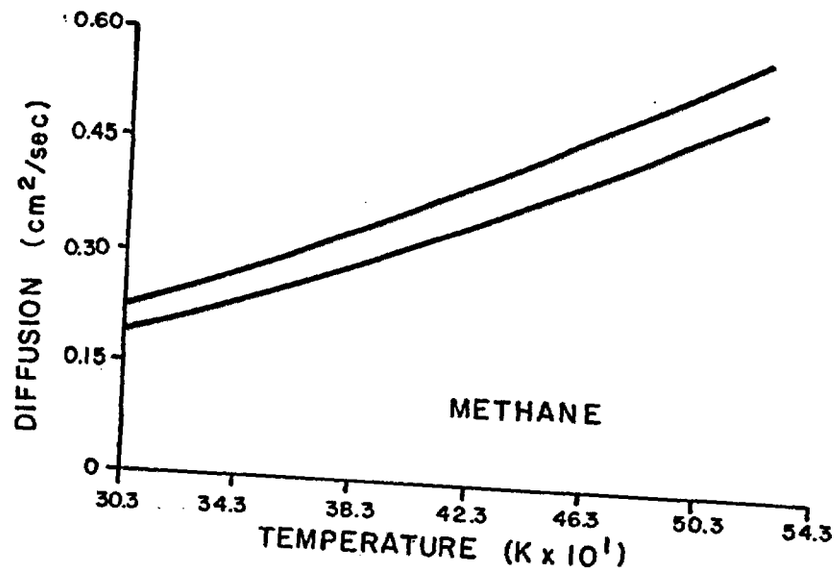

Figure 2.6. Diffusion coefficient (cm^2-sec^{-1}) for methane versus temperature (°K). The top curve is determined by the Slattery-Bird method, the bottom curve is determined by the Chapman-Enskog method.

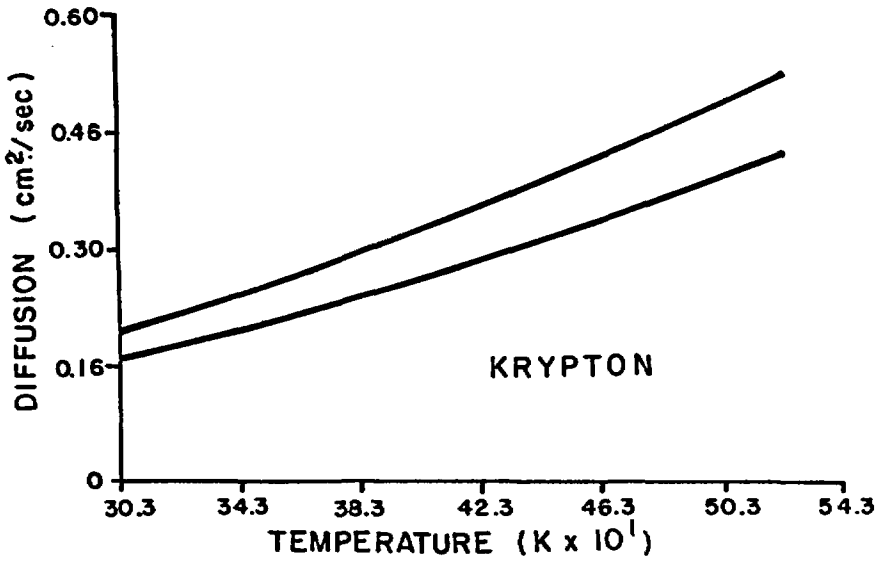

Figure 2.7. Diffusion coefficient (cm^2-sec^{-1}) for krypton versus temperature (°K). The top curve is determined by the Slattery-Bird method, the bottom curve is determined by the Chapman-Enskog method.

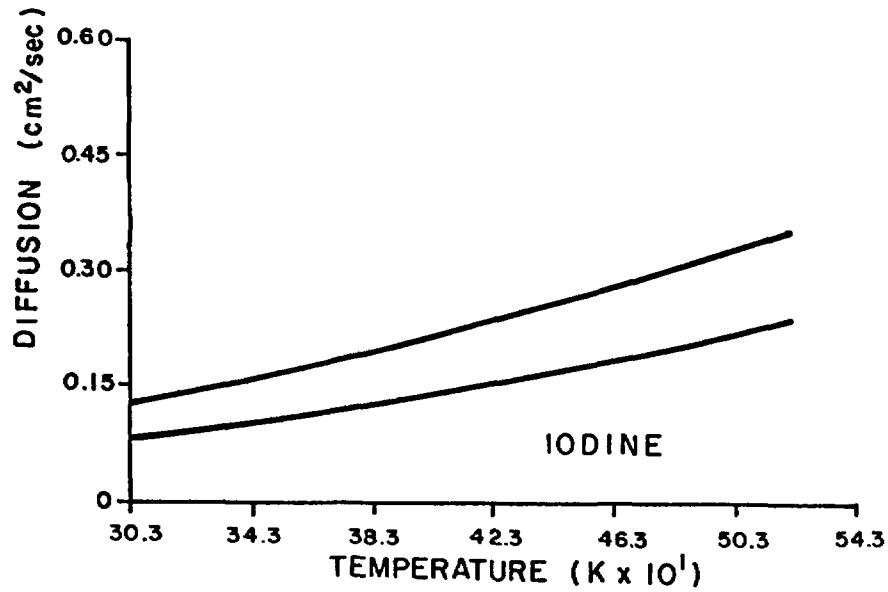

Figure 2.8. Diffusion coefficient (cm^2-sec^{-1}) for iodine versus temperature (°K). The top curve is determined by the Slattery-Bird method, the bottom curve is determined by the Chapman-Enskog method.

2.2.2 Knudsen Flow

Two fundamental assumptions are integral to the mathematical development of an expression which defines pure Knudsen diffusion. These assumptions are consistent with simplified gas theory. First, the number of impacts of gas molecules impinging upon a square centimeter of surface in the gas per second, n, is determined by the expression (Knudsen, 1950)

$$n = N \bar{v}/4 \tag{2.23}$$

where N is the gas molecule density (molecules/cm^3) and $\bar{v}$ is the arithmetic mean of the velocities of the gas molecules (Equation 2.11).

The remainder of the development of the Knudsen diffusion coefficient is, in general, adapted from the development by Loeb (1927). The second fundamental assumption is that Maxwell's distribution law is assumed valid when describing the velocity distribution of gas molecules. Thus, the number of gas molecules, dN, with velocity components between v and v + dv is given by Maxwell's distribution law in the expression

$$dN = (4N/\alpha^3(\pi)^{1/2})\ v^2\ \exp(-v^2/\alpha^2)\ dv \tag{2.24}$$

where α is the most probable gas molecule speed. The number of these molecules which strike a square centimeter of surface in the gas is 1/4 v dN.

A parallel plate model is used to represent an idealized fracture. The governing equation for Knudsen flow is initially developed for parallel plate geometry then for a capillary tube. A section of the parallel plates of interest has a length of dl and a circumference of L (Figure 2.9). The plates have an aperture of b and are of width h. The circumference (or hydraulic radius) is therefore 2h. The parallel plates are assumed to be of large enough lateral extent so that edge effects can be ignored. The cross sectional area normal to the direction of flow, A, is the aperture times the width or bh with units of cm^2.

The momentum given to the wall of the parallel plates by dN molecules is (1/4) v m v_t dN, where v_t is the component of velocity of translation parallel to the wall. The variable v_t can be written as kv where k is a constant of proportionality. The incremental momentum transfer, dB, is therefore

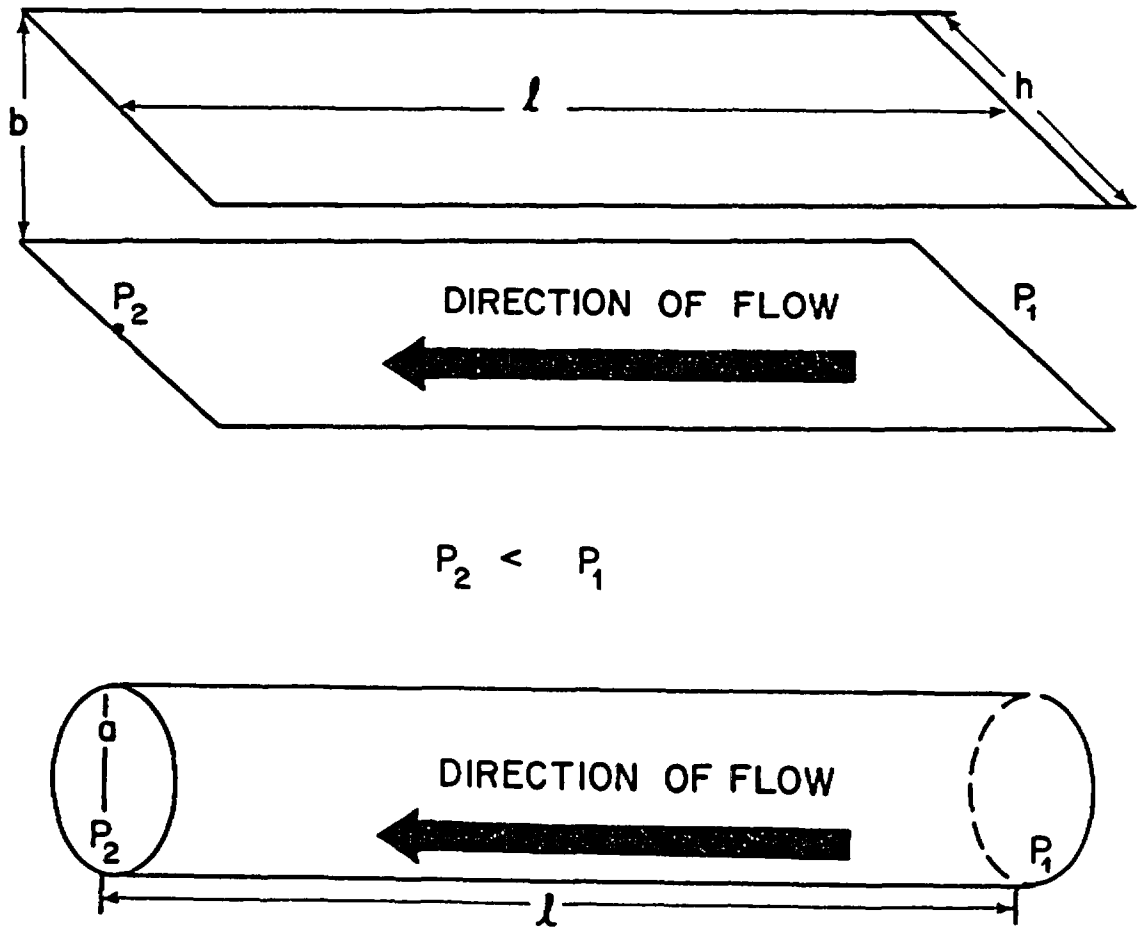

Figure 2.9. Parallel plate model (a) and capillary tube model (b) used to represent flow through an idealized fracture and an idealized porous medium, respectively.

(2.25) $dB = (1/4)\ k\ v^2\ m\ dN$

The momentum transfer, B, to the wall for all velocities is

(2.26) $B = (1/4)\ N\ k\ (4/\ \pi^{1/2})m \int_0^\infty v^4/\alpha^3\ \exp(-v^2/\alpha^2)\ dv$

which upon integration yields

(2.27) $B = (3/8)\ N\ k\ m\ \alpha^2$

$\bar{v}$ is equal to $\Sigma\ \bar{v}/N$ but can also be defined by the expression $2\ \alpha/\ \pi^{1/2}$. The term vk is equal to $\Sigma\ kv/N$ or $\Sigma\ v_t q/N$ which in turn is the definition of the drift velocity v_d. This velocity is therefore the geometric mean of the drift velocity of all molecules between the plates. After substituting for α and applying the definition of drift velocity Equation (2.27) becomes

(2.28) $B = (3\ \pi/32)\ N\ m\ \bar{v}\ v_d$

Equation (2.28) assumes that the velocity is constant across the aperture which is true only in Knudsen flow.

The pressure caused by a gas with density P can be expressed using the relation

(2.29) $P = (\pi/8)\ N\ m\ \bar{v}^2$

where the density of the gas, ρ, is equal to N m. If Equation (2.29) is solved for v and then substituted into Equation (2.28), the momentum can then be written

(2.30) $B = (3/8)\ \pi^{1/2}\ \rho(P/2)^{1/2}\ \rho\ v_d$

If it is further assumed that an area L dl along the parallel plates receives all the momentum resulting from the pressure drop along dl during time dt, then Equation (2.30) becomes

(2.31) $B = (3/8)\ \pi^{1/2}\ \rho\ \ (P/2\rho)^{1/2}\ v_d\ L\ dl\ dt$

The pressure drop along a section of the plate with length dl can be written -(dP/dl) dl. The momentum transfer, B^*, in time dt due to the pressure difference across area A is

(2.32) $B^* = -\ A\ (dP/dl)\ dl\ dt$

Conserving momentum within the two plates (equating Equations 2.31 and 2.32) yields the following expression

$$(2.33) \quad (3/8)\,(\pi/2)^{1/2}\,\rho\,(P/\rho)^{1/2}\,v_d\,L = -\,A\,dP/dl$$

The volume of gas, Q, which passes through A per second is

$$(2.34) \quad Q = A\,v_d$$

which when combined with Equation (2.33) (having been solved for drift velocity) yields

$$(2.35) \quad Q = -\,(8/3)\,(2/\pi)^{1/2}\,1/\rho\,(\rho/P)^{1/2}\,A^2/L\,dP/dl$$

Substituting the values for L and A into Equation (2.35) results in

$$(2.36) \quad Q = -(4/3)\,(2/\pi)^{1/2}\,b^2h\,1/\rho\,(\rho/P)^{1/2}\,dP/dl$$

Equation (2.36) is the general form of the equation defining Knudsen flow of a compressible gas.

Volumetric flow can be converted to mass flow by multipling by the density of the gas

$$(2.37) \quad G = Q\,\rho$$

where G has units of (g/sec). If G is divided by area and the molecular weight, then the mass flux per time per cross sectional area, J_k^p (gmoles/sec-cm^2), becomes

$$(2.38) \quad J_k^p = -\,(4/3)\,(2/\pi)^{1/2}\,b\,(1/RMT)^{1/2}\,dP/dx$$

where the term $(\rho/P)^{1/2}$ has been replaced by $(M/RT)^{1/2}$.

The derivation of the formulation for mass flux by Knudsen flow in a capillary tube is identical to parallel plate flow except that the cross-sectional area is πa^2 and the hydraulic radius is $2\pi a$ where a is the capillary radius (Figure 2.9).

The volumetric flux of gas, therefore, appears

$$(2.39) \quad Q = -\,(4/3)\,(2\pi)^{1/2}\,a^3\,1/\rho\,(\rho/P)^{1/2}\,dP/dl$$

and in terms of mass flux (gmoles/cm^2-sec) becomes

$$(2.40) \qquad J_k^c = - (4/3)\ (2/\pi)^{1/2}\ a\ (1/RTM)^{1/2}\ dP/dl$$

Equation (2.38) can be expressed in a more familiar form known as Fick's law

$$(2.41) \qquad J_k = - D_K\ dP/dl$$

where the Knudsen diffusion coefficient for parallel plate flow equals

$$(2.42) \qquad D_k^p = (4/3)\ (2/\pi)^{1/2}\ b\ (1/RMT)^{1/2}$$

and for capillary flow appears

$$(2.43) \qquad D_k^c = (4/3)\ (2/\pi)^{1/2}\ a\ (1/RMT)^{1/2}$$

As partial pressure is increased on a flow system with a relatively high Knudsen number (i.e., Kn > 1) self diffusion will begin to occur. The nature of molecular reflection at the fracture surface has a pronounced effect upon transitional flow. If wholly diffuse reflection occurs, each molecule leaves the solid surface according to the cosine law with no drift velocity component. Gas molecules obtain a component of drift velocity upon collision with other gas molecules between successive fracture surface collisions. A measure of the amount of drift obtained by a gas molecule can be gained by examining the ratio of the frequency of molecule-molecule collisions to molecule-wall collisions. For a section of unit length of parallel plates this becomes (Pollard and Present, 1948) $(b\ h\ n\ v/\lambda)/[2(b + h)\ n\ v/4]$ where h is the width of the fracture. For most cases, the width of a fracture will be much greater than the aperture ($h >> b$) and thus, the average number of molecule-molecule collisions per molecule-wall collisions can be approximated by $2\ b/\lambda$.

At smaller Knudsen numbers ($Kn << 1$), a component of diffusion flow, either self or binary diffusion, increases in importance relative to Knudsen flow. Expressions have been developed to describe the transitional flow between Knudsen flow and self-diffusion. Formulae evaluating flow in the transitional region are given by Pollard and Present (1948) for cylindrical geometry and by Hiby and Pahl (1952) for parallel plate geometry using the same approach. In both analyses, the number of molecules that pass through an elemental cross section of the flow path is evaluated. The molecules have encountered another gas molecule or the wall of the pore space upon passing through the

elemental cross section. The integrals which determine the two numbers are formulated and evaluated. Explicit evaluation is not always possible and in these cases the integral is evaluated numerically. In all cases the formulae are a function of the Knudsen number.

The diffusion coefficient at the transitional region between Knudsen flow and molecular diffusion for a cylinder of infinite length under isothermal conditions is (Pollard and Present, 1948)

$$(2.44) \qquad D_T = (1/3)\,\bar{v}\,\lambda[1 - (3/8)\,\lambda/a + 6/\lambda(\lambda/a)\,Q_c(a/\lambda)]$$

where $Q_c(a/\lambda)$ is defined

$$(2.45) \qquad Q_c(a/\lambda) = \pi/16 - \pi/6\,(a/\lambda) + \pi/3\,(a/\lambda)^2$$

$$- \pi/3(1.2264 - 3/4\,\ln(2\,Eu\,a/\lambda))(a/\lambda)^3 + \cdots$$

where Eu is Eulers constant (Eu = 0.5772....). For the case where $\lambda >> a$ Equation (2.44) reduces to

$$(2.46) \qquad D = (2/3)\,\bar{v}\,a\,[1 - (1.2264 + 3/4\,\ln(\lambda/2\ \ a))(a/\ \ ) + \cdots]$$

Similarly, when $\lambda << a$ one gets

$$(2.47) \qquad D = 1/3\,\bar{v}\,\lambda\,[1 - (3/8)(\lambda/a)]$$

At the limit where $Kn \to \infty$, Equations (2.46) and (2.47) are seen to be equal when the definition of mean gas velocity is substituted into Equation (2.42). Likewise, as $Kn \to 0$, Equation (2.47) reduces to the equation for self-diffusion (Equation (2.11)).

It is possible that unconsolidated rock matrix may not be adequately modeled using capillaries of infinite length. Capillaries of finite length may, in fact, better represent the flow channels through the rock matrix. The integrals from which Equations (2.44) to (2.47) are based are adapted to account for the finite length of the capillaries. It is then found that the diffusion coefficient at the transitional flow region between Knudsen flow and molecular diffusion for an isothermal system becomes (Pollard and Present, 1948)

$$(2.48) \qquad D = (1/3)\,\bar{v}\,\lambda[1 - (3/8)\,\lambda/a + (6/\pi)\,\lambda/a\,Q_c(a/\lambda\ )$$

$$- (3/2)(a/L)^2\,L/\lambda\,[e^{-L/\lambda} + L/\lambda\ \ Ei(-L/\lambda)]]$$

where L is the length of the capillary and $Ei(-L/\lambda)$ denotes the exponetial integral which is

$$(2.49) \qquad Ei(-L/\lambda) = \int_{\infty}^{-1/\lambda} - e^{-x}/x \; d(x)$$

The difference in the value of the diffusion coefficient for flow in a finite capillary and an infinite capillary becomes negligible when the half-length of the tube is greater than a few times the mean free path length.

The diffusion coefficient for Knudsen flow through a finite length capillary can be determined using Equation (2.48) when $\lambda >> L >> a$. This expression is written

$$(2.50) \qquad D = (2/3)\ \bar{v}\ a\ [1 - (3/4)a/L - (0.4764 + 3/4\ \ln(L/2a))(a/\lambda)]$$

Upon comparing Equations (2.46) and (2.50), Knudsen flow is less through capillaries of infinite length than through capillaries of finite length. This result is corroborated by a graph by Massignon (1979) which illustrates a greater permeability for Knudsen flow through a short capillary than a long capillary (Figure 2.10).

A similar treatment of flow for the transition between low and high Knudsen numbers has been evaluated for parallel plate geometry by Hiby and Pahl (1952). Evaluating the integrals which define the number of gas molecules which pass through an elemental cross section normal to flow between two plates of infinite extent results in the following expression for the diffusion coefficient for isothermal conditions

$$(2.51) \qquad D = \bar{v}\ b\ [\lambda/3b - \lambda^2/8b^2 + (\lambda^2/2b^2)\ Q_p(b/\lambda)]$$

where $Q_p(b/\lambda)$ for parallel plate geometry is defined

$$(2.52) \qquad Q_p(b/\lambda) = e^{-b/\lambda}/4\ [1 - (5/3)b/\lambda\ -b^2/6\ \lambda^2 + b^3/6\lambda^3]$$

$$+ [(b/\lambda)^4 - 12(b/\lambda)^2]/24\ Ei(-b/\lambda)$$

The diffusion coefficient is defined for a section of parallel plates of unit width. For Knudsen flow ($\lambda >> b$) Equation (2.51) reduces to

$$(2.53) \qquad D = \bar{v}\ b/4\ (3/4 - \ln(b/\lambda))$$

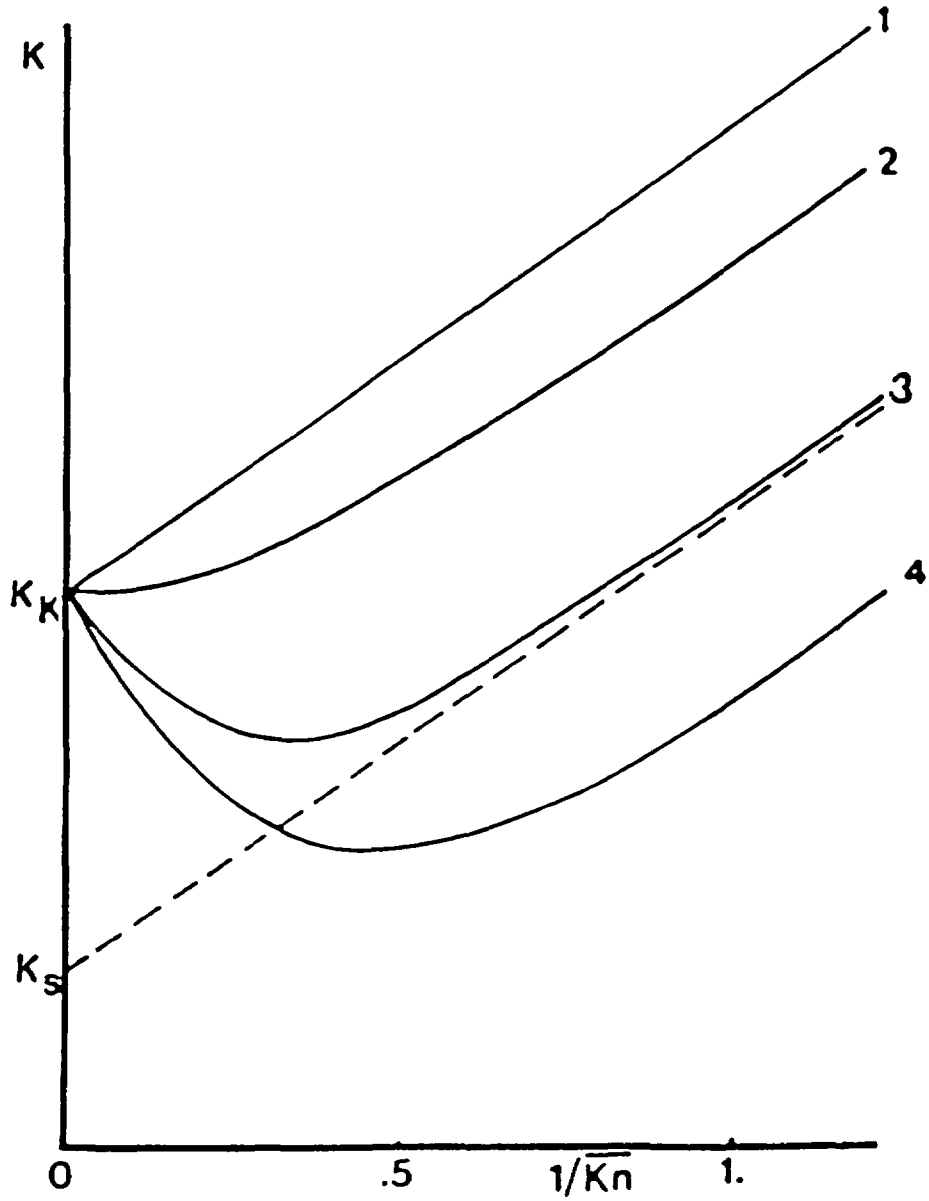

Figure 2.10. Experimental permeability k for different pore geometries: 1) bed of spheres; 2) short capillary (l = 5a); 3) long capillary and 4) parallel plates. k_K and k_S are Knudsen and slope permeabilities (from Massignon, D., "Gaseous Diffusion," in Uranium Enrichment, ed. by S. Villani, Springer-Verlag, New York, 1979. Reprinted with permission.)©

When molecular diffusion predominates ($\lambda << b$) Equation (2.51) becomes

$$(2.54) \qquad D = \bar{v}\, h\, [\lambda/3b - \lambda^2/8b^2]$$

Although the apparent applicability is not in evidence in a fractured rock system, the diffusion coefficient for parallel plate geometry of finite extent is now calculated. The lack of applicability arises in the fact that the aperture of a fracture is generally several orders of magnitude less than either the length or width of a fracture in rock and edge effects can be assumed to be negligible. Nevertheless, if edge effects do exist, the following expressions are approximations of diffusion coefficients for Knudsen flow through a fracture. For the case where the length of the fracture is greater than the width which, in turn, is greater than the aperture, the diffusion coefficient is expressed (Hiby and Pahl, 1952)

$$(2.55) \qquad D = \bar{v}\, b/4\, (1/2 + \ln(2\, h/b)) \qquad L >> h >> b$$

and for the situation where the width is greater than the length and both are greater than the aperture, the diffusion coefficient appears

$$(2.56) \qquad D = \bar{v}\, b/4\, (1/2 + \ln(L/b)) \qquad h >> L >> b$$

2.2.3 Surface Diffusion

The occurrence of surface flow (or diffusion) can greatly augment the flow of a gas through a microscopic system. A microscopic system is one in which the passageways through a medium (either fractures or capillary-like tubes) have an aperture of a magnitude of 10^2 Å. Surface diffusion is parallel flow of an adsorbable gas in the presence of a concentration gradient along a surface covered with a few monolayers of an adsorbant.

Surface diffusion only occurs when the diffusing gas sorbs onto the surface of the medium through which its travels. Adsorption of gases and surface diffusion are important to gas movement when a partial layer of gas is adsorbed onto the surface of the medium or when only a few layers at most are present on the surface. If the solid surface has more than several layers of gas molecules, gas molecules adsorbed onto the surface behave as a fluid and are governed by laws of diffusion and hydrodynamics. Ultimately, concentration can increase until the entire cross-section of a capillary is blocked by the adsorbed gas molecules. This condition is referred to as capillary condensation. Although the flux of gas transported by surface diffusion may exceed other diffusion

fluxes, surface diffusion is generally less than fluid flow and therefore deemed insignificant relative to fluid flow because surface diffusion affects relatively few molecules compared to the multitude of molecules affected by fluid flow.

Adsorption can be categorized as either localized or non-localized. In the first case, adsorbed molecules take up fixed positions and are at equilibrium with the surface only when occupying adsorption sites. They may, however, move from one position to another when locally adsorbed.

Non-localized adsorption occurs when the surface has no favored positions with respect to potential energy and molecules can move about freely under stable conditions. A molecule under this condition would have the same energy at any point on a surface. Consequently, if a molecule obtained momentum in a direction parallel to the surface, it could move about freely in the absence of a lateral energy barrier. Likewise, if lateral energy barriers in the localized adsorption case have a value of E_a which is less than the kinetic energy of the molecule, RT, then molecules under localized adsorption conditions could move about laterally in a manner similar to non-localized adsorption.

Gases that exist under the abovementioned conditions are said to possess a two-dimensional property called spreading pressure. Spreading pressure represents the force per unit width necessary to compress the adsorbed layer of gas molecules (Gregg, 1961).

Surface diffusion at low concentrations is a two-dimensional process analogous to three-dimensional Knudsen flow because molecular collisions between pairs of adsorbed molecules are very rare. Conditions which favor the existence of Knudsen diffusion (i,e., $Kn >> 1$) are also the conditions necessary for surface diffusion to occur when an adsorbable gas is present.

The relationship between the quantity of gas molecules sorbed on a surface and the pressure at which adsorption occurs is defined by an adsorption isotherm. There are five general classes of of isotherms (Brunauer, 1945) which are Type I (Langmuirs isotherm for monolayer adsorption), two isotherms for multilayer adsorption (Types II and III) predicated on the Brunauer, Emmet and Teller (BET) isotherm equation and finally Type IV and Type V isotherms which are bounded at high values of condensation by capillary condensation. Types I, II and III have no upper bound (Figure 2.11). At very low values of surface coverage, the isotherms are nearly linear and are thus analogous to Henrys law.

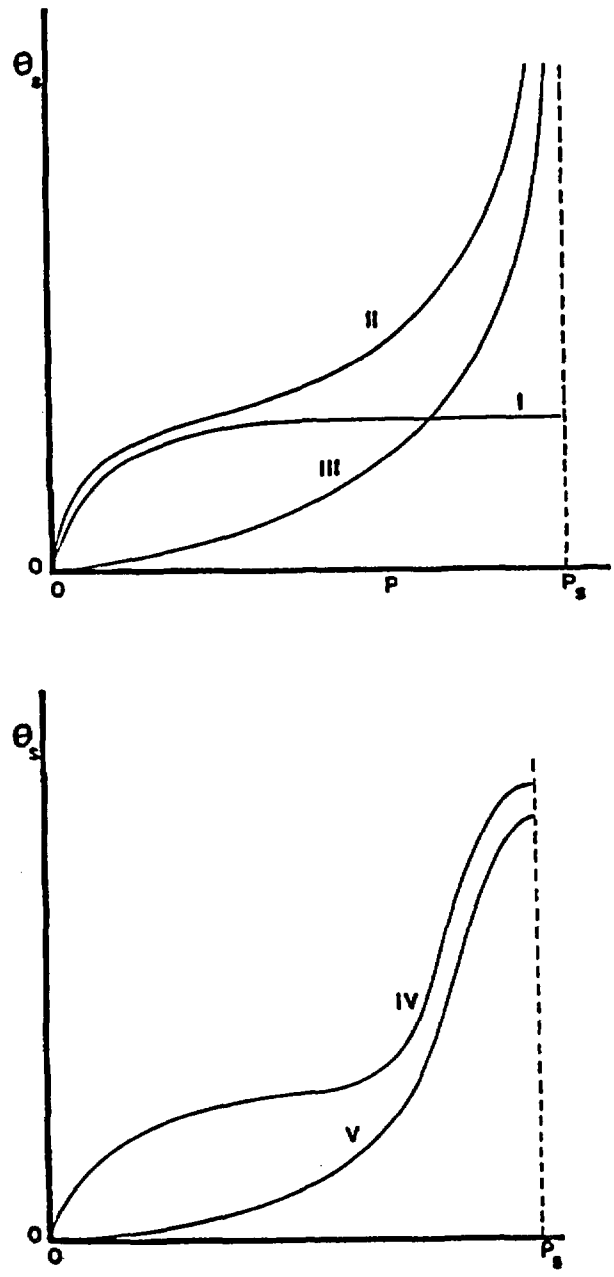

Figure 2.11. Types of adsorption isotherms: 1) monolayer adsorption; 2) and 3) multilayer adsorption; 4) and 5) bounded at high condensation values by capillary condensation. P_S is saturation vapor pressure and θ_S is saturation surface coverage (from Massignon, D., "Gaseous Diffusion," in Uranium Enrichment, ed. by S. Villani, Springer-Verlag, New York, 1979. Reprinted with permission.)©

Henrys law can be succinctly stated as $X = k\ P$ where X is the solubility, k is some constant of proportionality and P is the partial pressure of the solute. The region of low pressure where surface coverage is proportional to pressure is referred to as Henrys law region (Gregg, 1961).

The relationship between surface coverage and pressure during two-dimension surface diffusion is not adequately represented by a general isotherm. Instead, a two-dimensional form of van der Waals equation appears to offer the best approximation for surface coverage as a function of pressure. Van der Waals two-dimensional isotherm is written (Gregg, 1961)

$$(2.57) \qquad P = K_h(\theta_s)\ \theta_s/(1 - \theta)\ \exp(\theta_s/(1 - \theta_s) - 2\ a_c\ \theta_s/(A\ K\ T))$$

θ_s is the fraction of surface coverage, $K_h(\theta_s)$ is a function of the heat of adsorption which will vary with θ_s, A is area and a_c is a two-dimensional attraction constant analogous to the constant a in a three-dimensional form of van der Waals equation.

Isotherms predicted by van der Waal's equation are in close agreement with experimental data for specified instances (Dacey, 1965), thus supporting the premise that two-dimensional gas behavior does exist at low coverage on uniform surfaces. Using simplified kinetic theory, Dacey determined the coefficient of surface diffusion to be the expression

$$(2.58) \qquad D_s = 1/2\ \bar{v}\ \lambda_s$$

where the mean free path, λ_s, along the surface is defined as

$$(2.59) \qquad \lambda_s = 1/2\ d_m\ c_s$$

and where d_m is the molecular diameter and c_s is the surface concentration. The flux resulting from surface diffusion is therefore

$$(2.60) \qquad J_s = -\ D_s\ dc_s/dx$$

Frequently, the energy barriers present at localized adsorption are greater than the kinetic energy of the gas and the gas does not diffuse in two dimensions. The movement of gas molecules in this case is referred to as activated surface diffusion and the molecules move or slip from one site to another in random walk fashion. The diffusion coefficient is related to the length of each slip by the formula (Hill, 1956)

(2.61) $D_s = \lambda_s'^2/2\ T_t$

where λ_s' is the distance between adsorption sites and where T_t is the travel time between sites calculated by the expression

(2.62) $T_t = T_o\ e^{E_a/RT}$

T_o is a property of the solid surface and E_a is the potential of the barrier on the surface which must be exceeded for a molecule to change sites.

Hagashi et al. (1963) noted that D_s is dependent on surface coverage and suggested that the surface diffusion coefficient be expressed

(2.63) $D_s = D_{so}\ 1/(1 - \theta_s)\ \exp(-E/\ kT)$

where D_{so} is a gas dependent constant. Equation (2.63) differs from Hill's formulation because the surface diffusion coefficient increases with the degree of surface coverage instead of decreasing as Hill's equation predicts.

Although flow rates for two-dimensional surface diffusion are considerably greater than activated surface diffusion (up to 10^5 times greater (de Boer, 1953)), surface obstructions diminish the importance of two-dimensional surface diffusion to such an extent that activated surface diffusion is the dominate mechanism of transport at low concentrations.

2.2.4 Total Contribution by Ordinary Diffusion

The mathematical expressions defining the contributions to concentration diffusion flux are now formulated. The total flux resulting from a concentration gradient is represented by the expression

(2.64) $J_o = J_k + J_{self} + J_b + J_s$

where the particular equation to be substituted for each contributor flux is selected based upon the nature of the gas (or gases) and the type of medium. Table 2.5 lists all the variations of the diffusion coefficient as they appear in the text. By stating the transport mechanisms in this manner, an isothermal system is assumed when temperature is not contained in the driving force. A non-isothermal system requires that variations in temperature are accounted for when

solving the appropriate equations. The non-isothermal nature of a HLW repository dictates that the driving forces resulting from temperature gradients are fully acknowledged.

Mean velocity and mean free path length are both temperature dependent variables as illustrated in Equations (2.10) and (2.11). Therefore, these two variables must be incorporated into the driving force for the non-isothermal case. Occasionally the diffusion term cannot be separated from the driving force by simple mathematical manipulation. In these cases, temperature dependent terms remain couched in the coefficient of diffusion and the equation of gas flow can not be easily factored.

Additional information is required when the driving force contains more than one variable. For example, data based upon either laboratory measurements, field measurements or computer simulations are available which provide the relationship between the spacial variation of both pressure and temperature for different scenarios of site locations and engineering designs at different times after emplacement (Wang et al., 1983; Pruess and Wang, 1985). A numerically determined curve representing the values of pressure versus temperature can be inserted into the flow equation with a complex driving force. The equations describing concentration diffusion can either be integrated analytically or numerically and solved for a particular scenario.

Expressions are presented which define the flow of gas by diffusion through fractured media for a vast range of expected flow scenarios. The selection of a flow equation (or equations) depends on the scope of the problem, the driving force present and the nature of the medium. Laboratory and field tests of gas movement can indicate which expressions best represent the medium. For example, gas-phase permeability experiments by Reda (1985) reveal an order of magnitude increase in permeability of nitrogen through densely welded tuffaceous materials as total gas pressure is decreased from 13.1 to 0.1 MPa. The mean free path between molecular collisions increased as pressure decreased. The higher than expected flow predicted by pressure flow verified the occurance either of Knudsen flow, slip flow or surface diffusion through micropores and the order of magnitude increase in flow rate over that predicted by pure pressure flow attests to the importance in recognizing the phenomenon.

Table 2.5 Coefficient of diffusion for the isothermal case (with comments), driving force is ∇C unless otherwise noted.

(eq. no.)	Coefficient of diffusion
(2.16)	$D_{AA} = 2/3\ (K^3/\pi^3 M_a)^{1/2}\ t^{2/3}/pd_a^2$ (self diffusion, simplified kinetic theory)
(2.17)	$D_{AB} = 2/3(K^3/\pi^3)^{1/2}(1/2M_a + 1/2M_b)^{1/2} \cdot t^{3/2}/p[(d_a + d_b)/2]^2$ (binary diffusion, simplified kinetic theory)
(2.18)	$D_{AB} = 0.0018583\ [t^3(1/M_a + 1/M_b)]^{1/2}/(pd^2_{ab}\ \Omega_{Dab})$ (binary diffusion based on rigorous kinetic theory)
(2.22)	$D_{AB} = [(p^c_A\ p^c_B)^{1/3}(T^c_A\ T^c_B)^{5/12}[(1/M_a)+(1/M_b)]^{1/2}]/P \cdot a\ [T/(T^c_A\ T^c_B)^{1/2}]^b$ (binary diffusion, kinetic theory and correlation of available data, Slattery - Bird)
(2.42)	$D^k_p = (4/3)\ (2/\pi)^{1/2}\ b(1/RMT)^{1/2}$ (Knudsen diffusion, parallel plates, driving force is ∇P)
(2.43)	$D^k_c = (4/3)\ (2/\pi)^{1/2}\ a(1/RMT)^{1/2}$ (Knudsen diffusion, cylindrical flow, driving force is ∇P)
(2.44)	$D_T = (1/3)\ \bar{v}\ \lambda[1 - (3/8)\ \lambda/a + 6/\pi(\lambda/a)\ Q_c(a/\lambda)]$ (Knudsen/self-diffusion transition flow, infinite cylinder)
(2.46)	$D_T = (2/3)\ \bar{v}\ a[1 - (1.2264 + 3/4\ \ln(\lambda/2ga)(a/\lambda) + \cdots)]$ (Knudsen/self-diffusion transition flow, infinite cylinder $\lambda >> a$)
(2.47)	$D = 1/3\ \bar{v}\ \lambda\ [1 - (3/8)(\lambda/a)]$ (Knudsen/self-diffusion transition flow, infinite cylinder $\lambda << a$)
(2.48)	$D = (1/3)\ \bar{v}\ \lambda[1 - (3/8)\ \lambda/a + (6/\pi)\ \lambda/a\ Q_c(a/\lambda) - (3/2)(a/L)^2\ L/\lambda\ [e^{-L/\lambda} + L/\lambda\ Ei(-L/\lambda)]]$ (Knudsen/self-diffusion transition flow, finite cylinder)

Table 2.5 (Continued)

(2.50) $D = (2/3)\,\bar{v}\,a\,[1 - (3/4)a/L\,] - (0.4764 + 3/4\,\ln(L/2a))(a/\lambda)$
(Knudsen/self-diffusion transition flow,
finite cylinder $\lambda \gg L \gg a$)

(2.51) $D = \bar{v}\,b\,[\lambda/3b - \lambda^2/8b^2 + (\lambda^2/2b^2)\,Q_p(b/\lambda)]$
(Knudsen/self-diffusion transition flow,
infinite parallel plate)

(2.53) $D = \bar{v}\,b/4\,(3/4 - \ln(\,b/\lambda))$
(Knudsen/self-diffusion transition flow,
infinite parallel plate $\lambda \gg b$)

(2.54) $D = \bar{v}\,h\,[\lambda/3b - \lambda^2/8b^2]$
(Knudsen/self-diffusion transition flow,
infinite parallel plate $\lambda \ll b$)

(2.55) $D = \bar{v}\,b/4\,(1/2 + \ln(2\,h/b))$
(Knudsen/self-diffusion transition flow $L \gg h \gg b$)

(2.56) $D = \bar{v}\,b/4\,(1/2 + \ln(L/b))$
(Knudsen/self-diffusion transition flow,
finite parallel plate $h \gg L \gg b$)

(2.58) $D_S = 1/2\,\bar{v}\,\lambda_S$
(surface diffusion, two-dimensional, driving force is ∇C_S)

(2.61) $D_S = \lambda_S'^2/\,2\,T_t$
(surface diffusion, activated diffusion, driving force is ∇C_S)

- -

2.3 Viscous Flow

Laminar or turbulent flow of gas resulting from a total pressure gradient is referred to as viscous flow. Viscous flow of gas, J_v is defined to include pressure flow, J_p, and a slip flow term, J_{sf}, (Figure 2.12) or

$$(2.65) \qquad J_v = J_p + J_{sf}$$

In this development, the governing equations which define slip flow also account for pressure flow, thus, either J_p or J_{sf} represent a flow system but not both, thus J_v is more exactly defined by the expression $J_p \cup J_{sf}$.

Although turbulent flow may occur near a HLW canister at early times, total pressure will be close to one bar after about 100 years based on results by Pruess and Wang (1984), thus, total pressure gradients are assumed to be small enough so that flow is laminar and not turbulent at later times.

2.3.1 Pressure Flow

The governing equation for viscous flow is derived from Stokes equation. Stokes equation defines slow, laminar flow which is characteristic of Poiseuille (or Couette) flow of an incompressible fluid and is written (Neuman, 1981)

$$(2.66) \qquad \rho \, \partial v / \partial t = -\nabla p + \rho g + \mu \nabla^2 v$$

where t is time, g is the acceleration of gravity and μ is absolute viscosity. Small total pressure gradients in the system permit the assumption of an incompressible fluid.

Stokes equation is solved assuming steady, one-dimensional, horizontal flow between two parallel plates with no slip boundaries. The velocity in the direction of flow is

$$(2.67) \qquad v_x = (4 z^2 - b^2)/8\mu \, \partial P / \partial x$$

Figure (2.12) illustrates the coordinate system for Poiseuille flow between two parallel plates with no slip boundaries.

Velocity in the x-direction when averaged over the entire fracture becomes

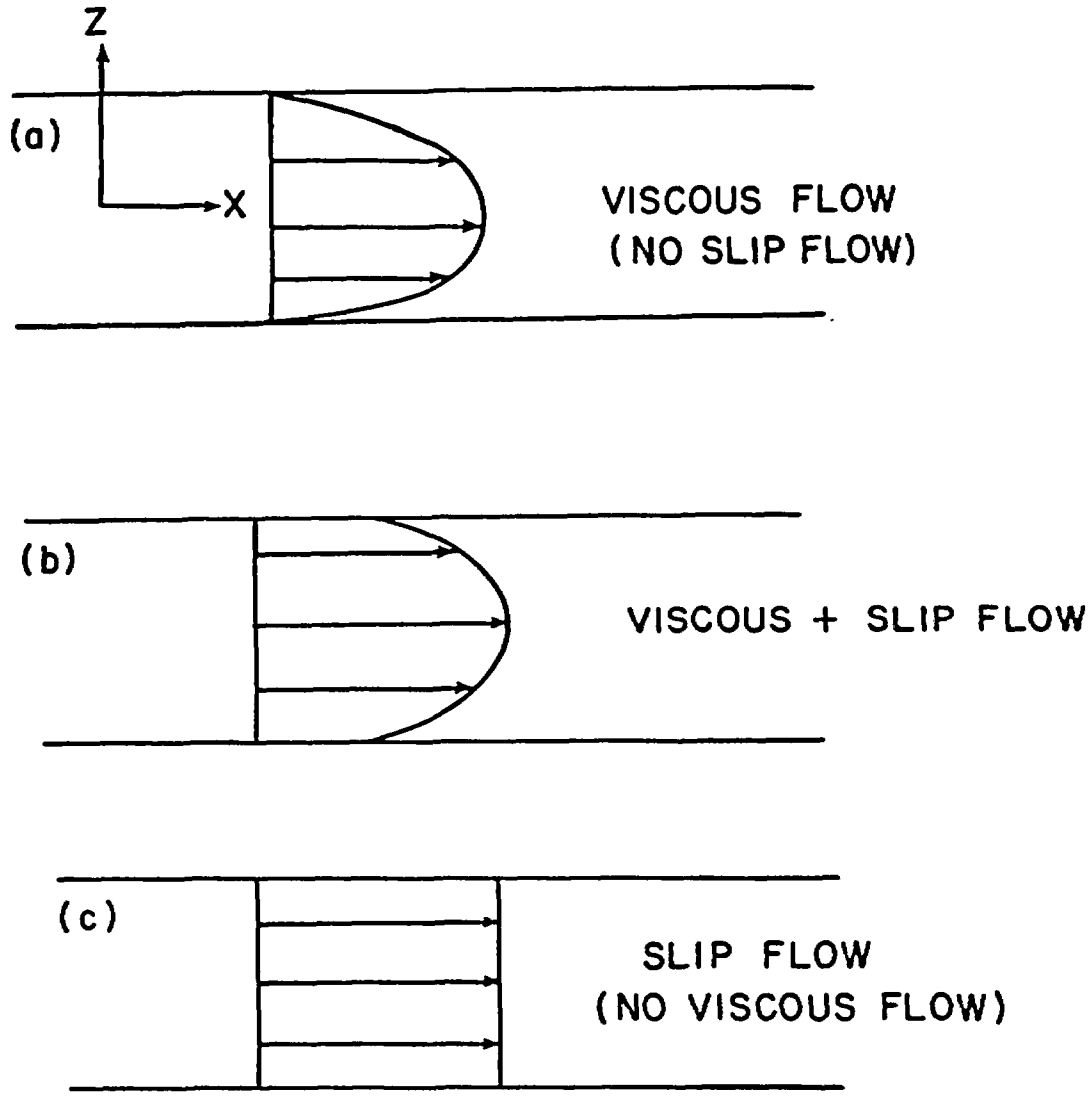

Figure 2.12. Velocity profiles of idealized gas flow through either parallel plates or capillary tube: a) total viscous flow-no slip flow; b) viscous and slip flow and c) total slip flow-no viscous flow.

$$(2.68) \qquad v^p = -b^2/12\mu \, \partial P/\partial x$$

The mass flux of a species can be calculated once the velocity has been determined by multipying velocity with the density of the species of interest. If the resulting quantity is divided by the molecular weight, the mass flux caused by laminar flow can be expressed in gmoles/cm^2-sec by the expression

$$(2.69) \qquad J_i^p = -b^2 \, \rho/(12 \, \mu \, M) \, \partial P/\partial x$$

Laminar flow gas velocity through a capillary is determined by a similar development to that used to define parallel plate flow. Stokes equation is expressed in cylindrical coordinates with the same boundary conditions as parallel plate flow. The velocity is thus calculated to be

$$(2.70) \qquad v^c = -a^2/8\mu \, \partial P/\partial z$$

and likewise, the mass flux of gas by laminar flow through a capillary of radius a is found to be

$$(2.71) \qquad J_i^c = -a^2 \, \rho/(8 \, \mu \, M) \, \partial P/\partial z$$

Equation (2.71) can be adapted to evaluate the velocity of gas mixtures by replacing the viscosity for a single gas with the viscosity for gas mixtures, μ_{mix}. Wilke (1950) used simplified kinetic theory to calculate μ_{mix} based upon the viscosities and molecular weights of the individual gases of the gas mixture in the expression

$$(2.72) \qquad \mu_{mix} = \sum_{i}^{n} \mu_i / \left[1 + 1/x_i \sum_{j \neq i}^{n} x_j \, \phi_{ij}\right]$$

where x_i is the mole fraction of component i of the gas mixture and where ϕ_{ij} is given by the equation

$$(2.73) \qquad \phi_{ij} = [1 + (\mu_i/\mu_i)^{1/2}(M_j/M_i)^{1/4}]^{1/2}/(4/(2)^{1/2})[1 + (M_i/M_j)]^{1/2}$$

2.3.2 Slip Flow

It is possible that slip flow occurs at the fracture surface-gas interface during viscous flow. Slip flow may occur when the mean free path is similar in length to the aperture of a fracture. Greater gas

flow velocities will be experienced with slip flow at the boundaries than with a no-slip boundary.

The boundary layer of gas flowing next to the fracture surface is referred to as the Knudsen layer. The thickness of the Knudsen layer is of the same order of magnitude as the mean free path. The boundary condition at the fracture surface becomes

$$(2.74) \quad v(\pm b/2) = u_o$$

where u_o is the velocity of the gas at the fracture surface-gas interface. The equation for viscous flow between parallel plates becomes

$$(2.75) \quad v_x = (4\ z^2 - b^2)/8\mu \ \partial P/\partial x - u_o$$

where the additional velocity term is attributed to slip.

Gas flow velocity, u_o, at the surface of a fracture can be determined by examining momentum at the fracture surface-gas interface. Viscous shearing stress, S_s, in flowing gas varies with distance from the fracture surface according to an empirically based formula based on Newton's law of viscosity (Freeze and Cherry, 1979)

$$(2.76) \quad S_s = \mu\ dv_x/dz$$

where the z-direction is normal to the fracture surface.

The following development by Present (1958) examines momentum transfer to determine u_o. The shearing stress is equal to the momentum transferred to the fracture surface per unit time per unit area during steady flow. The momentum carried to the fracture wall is determined by the location of the site of the gas molecules last collision. The average distance from the collision site to the wall is $2\ \lambda/3$ and accordingly, the momentum, B, carried by this molecule is

$$(2.77) \quad B = m\ (u_o + 2\ \lambda/3\ \ dv_x/dz)$$

Since the number of collisions per unit time per unit area is $n\ v/4$, the total momentum transfer to a unit area of the wall per unit time is

$$(2.78) \quad B = (n\ \bar{v}/4)\ m\ (u_o\ + 2\ \lambda/3\ dv_x/dz)$$

Equating the shearing stress in the gas (Equation 2.76) to momentum transfer at the wall (Equation 2.78) and substituting in the value of $m\ n\ v\ \lambda/3$ for viscosity yields

$$(2.79) \qquad m\ n\ \bar{v}\ \lambda/3\ \ dv_x/dz = m\ \bar{v}\ n\ u_o/4 + n\ \bar{v}\ m\ \lambda/6\ dv_x/dz$$

Solving for slip flow velocity yields the expression

$$(2.80) \qquad u_o = 2\ \lambda/3\ \ dv_x/dz$$

The derivative of v_x with respect to the z-direction can be determined from Stokes equation for parallel plate flow to be

$$(2.81) \qquad dv_x/dz = 1/\mu\ b/2\ \partial P/\ \partial x$$

where the derivative has been evaluated at the fracture surface-gas interface. Substituting this expression for dv_x/dz into (2.80) yields

$$(2.82) \qquad u_o = (2\ \lambda/3)\ b/2\mu\ \partial P/\ \partial x$$

again replacing μ gives the expression

$$(2.83) \qquad u_o = b/(m\ n\ \bar{v})\ \partial P/\ \partial x$$

By employing the same arguments, a similar expression for slip flow through a capillary tube is

$$(2.84) \qquad u_o = (2\ \lambda/3)\ a/2\mu\ \partial P/\ \partial x$$

or

$$(2.85) \qquad u_o = a/(m\ n\ \bar{v})\ \ \partial P/\ \partial x$$

Equation (2.83) is modified by the inclusion of a dimensionless term c

$$(2.86) \qquad u_o = c\ b/(m\ n\ \bar{v})\ \partial P/\ \partial x$$

to account for discrepancies in the slip flow velocity term. The b term here denotes either capillary radius or parallel plate aperture. Various analytical and empirical values for c range from 1 to 4/3. Massignon (1979) presents a discussion of these values.

The total average viscous flow expression containing a pressure flow term plus slip flow between parallel plates is

(2.87) $$v_x^p = -[b^2/12\rho + c\ b/(m\ n\ \bar{v})]\ \partial P/\partial x$$

The flux term corresponding to v_x^p is

(2.88) $$J_p = -(\rho/M)[b^2/12\mu + c\ b/(m\ n\ v)]\ \partial P/\partial x$$

Similarly for capillary flow, the velocity of total viscous flow appears

(2.89) $$v_x^c = -[a^2/8\mu + c\ a/(m\ n\ v)]\ \partial P/\partial x$$

The corresponding equation for flux is

(2.90) $$J_{sf}^c = -(\rho/M)[a^2/8\mu + c\ a/(m\ n\ v)]\ \partial P/\partial x$$

Expressions for slip flow also contain the pressure flow component, thus, either J_p of J_{sf} represent viscous gas flow but not both. Concluding this section is Table 2.6 which lists the various forms of the equaton for viscous flow including both pressure and slip flow.

2.4 Diffusion-Viscous Flow Transition

As the magnitude of the driving force varies, the nature of the transport mechanism may change. For example, if partial pressure is increased on a system where Knudsen flow is present, self-diffusion may be experienced. However, if total pressure is increased in a system where Knudsen flow is present, then slip flow may occur.

When pressure is increased in a system at low pressure where Knudsen flow is occurring, the total gas flow rate does not experience a monotonic increase. Instead, the gas flow rate will decrease to a minimum, then increase momotonically according to the physics that governs pressure flow as pressure is increased. This minimum in the total gas flow rate is referred to as the Knudsen minimum. The Knudsen minimum can be explained using an hypothesis fostered by Weber (1963) whereby pressure flow, slip flow, and free molecular flow are assumed to be additive. This additivity is illustrated in Figure 2.13 (from Massignon, 1979). The fact that Knudsen flow decreases at a greater rate than the increase in viscous flow (Poiseuille flow plus slip flow) causes the Knudsen minimum. Basic to Weber's hypothesis is the observation that Knudsen flow does not tend to zero as pressure is decreased.

Table 2.6 Equations of viscous flow.

eq. no.	equation	comments
(2.67)	$V_x^p = -b^2/12\mu I_x$	parallel plates, Poiseuille, infinite
(2.68)	$J_p = -b^2\ \rho/(12\ \mu\ M)I_x$	parallel plates, Poiseuille, infinite
	$J_p = (\bar{v}b/4L)\ (\lambda e Pc/b)[\ 1.173(P_1 - P_2)$	finite parallel plate Poiseuille flow
	$-\ (P_1 \ln P_1 - P_2 \ln P_2)$	transitional to slip/Knudsen
	$-\ 2.15(P_1^2 - P_2^2)$	(total pressure gradient)
	$+\ 0.49(P_1^2(\ln^2 P_1 - \ln P_1)$	
	$-\ P_2^2(\ln^2 P_2 - \ln P_2 2))]$	
(2.86)	$V_p = -\ [b^2/12\rho + c\ b/(m\ n\ \bar{v})]I_x$	infinite parallel plate Poiseuille and slip flow
(2.87)	$J_p = -\ \rho/M[b^2/12\mu + c\ b/(m\ n\ v)]I_x$	infinite parallel plate Poiseuille and slip flow
(2.88)	$V_x^c = -\ [a^2/8\mu + c\ a/(m\ n\ \bar{v})]I_x$	capillary flow, infinite capillary, slip flow
(2.89)	$J_c = -\ \rho/M[a^2/8\mu + c\ a/(m\ n\ v)]I_x$	capillary flow, infinite capillary, slip flow
(2.69)	$V_x^c = -\ a^2/8\mu I_x$	capillary flow, infinite lenght
(2.70)	$J_c = -\ a^2\ \rho/(8\ \mu\ M)I_x$	capillary flow, infinite lenght

where $I_x = \partial h/\partial x$

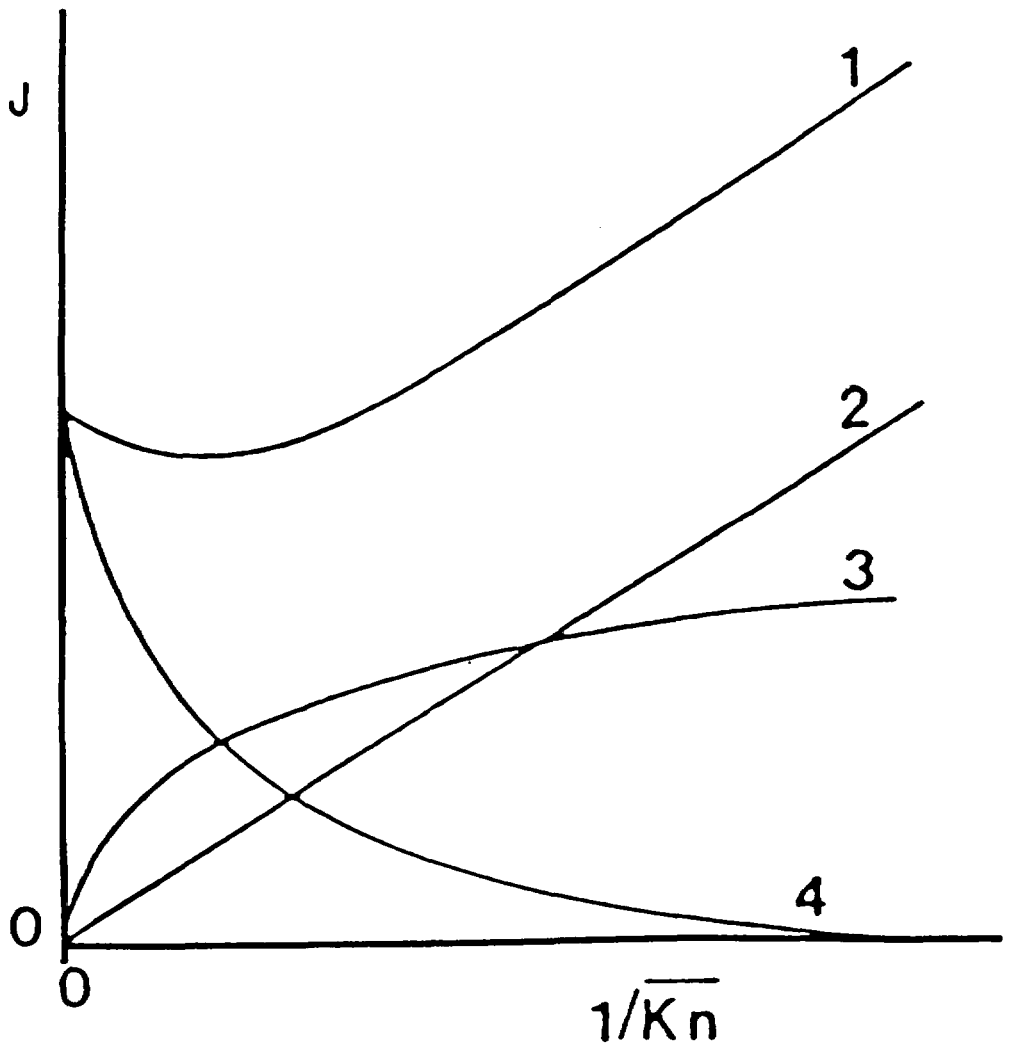

Figure 2.13. Transition from Knudsen to viscous flow through a long capillary tube as Knudsen number decreases: 1) total flow rate; 2) viscous flow; 3) slip flow and 4) Knudsen flow (from Massignon, D., " Gaseous Diffusion," in Uranium Enrichment , ed. by S. Villani, Springer-Verlag, New York, 1979. Reprinted with permission.©

Analogous behavior by gas flow through parallel plates is assumed to occur. Illustrating this hypothesis is a graph of the relative magnitude of flow versus an inverse in the Knudsen number for several representative geometries. As is illustrated in Figure 2.10, the Knudsen minimum for flow through parallel plates (curve 4) is actually more pronounced than the minimum for flow through either a bed of spheres (curve 1), a short capillary (curve 2), and a long capillary (curve 3). The more pronounced Knudsen minimum in gas flow through parallel plates is attributed to the unique opportunity of gas molecules to travel unimpeded in two directions rather than none as in the case of the bed of spheres and only one as in the case of capillary flow before interaction with pore walls.

2.5 Ordinary Diffusion--Example at Large Distances

The significance of ordinary diffusion at a large distance is largely dependent upon the characteristics of the rock medium through which the gas moves. Nevertheless, examination of heuristic idealized case studies can lend valuable information concerning the importance of radionuclide transport by ordinary diffusion from a HLW canister to the accessible environment at some distance.

The equation of continuity of a gas states

$$(2.91) \qquad -\nabla \cdot J = \partial c / \partial t$$

where t denotes time. Combining Equations (2.14) and (2.90) results in the expression

$$(2.92) \qquad D \nabla^2 c = \partial c / \partial t$$

where a constant density and isothermal medium have been assumed.

An indication of the importance of mass flux by diffusion can be gained by examining the time required for diffusive flux to approximate steady state.

For this example, an open mineshaft and borehole absent of backfill are assumed. The diffusive path is equated to a 300 m long cylindrical conduit with no retardation and an absense of convective forces. Concentration at the far end of the conduit located at the accessible environment is zero and contaminants that reach the far end are immediately released. The boundary and initial conditions imposed on Equation (2.92) are therefore

(2.93a) $c(0,t) = 1 \quad t > 0$

(2.93b) $c(300,t) = 0 \quad t > 0$

(2.93c) $c(z,0) = 0 \quad 0 < z < 300$

The one-dimensional analytical solution to Equation (2.92) in the z-direction is (Carslaw and Jaeger, 1959)

$$(2.94) \quad c(z,t) = \frac{2D\pi}{L^2} \sum_{i=1}^{\infty} i \exp\left(\frac{-Di^2\pi^2 t}{L^2}\right) \sin\left(\frac{i\pi z}{L}\right) \int_0^t \exp\left(\frac{Di^2 2\lambda^2}{L^2}\right) c(0,t)d\lambda$$

where L is the length of the conduit. Solving the integral in Equation (2.93) and rearranging terms yields the infinite series

$$(2.95) \quad \frac{c(z,t)}{c(0,t)} = \frac{2}{\pi} \sum_{i=1}^{\infty} \sin\left(\frac{i\pi z}{L}\right) \frac{1}{i} \left[1 - \exp\left(\frac{-Di^2\pi^2 t}{L^2}\right)\right]$$

A diffusion coefficient of 0.15 cm^2/sec is assumed. This value is believed to be reasonable since it equals the approximate value for either I_2, Kr, CH_4, H_2, or CO_2 diffusing through air at 300°K and atmospheric pressure. Figure (2.14) illustrates normalized concentration, c(z,t)/c(0,t), versus distance at times 1 to 75 years. Constant diffusive flux has been approached by about 75 years.

The rates of contaminant emission from a HLW canister have yet to be calculated because the exact nature of waste containment is not specified. However, calculating the source term based on a specified release rate of waste to the accessible environment is possible when several assumptions are made. The proposed release rate to the accessible environment is 1000 curies (Ci) per 1000 metric tons of heavy metal (MTHM) over a 10,000 yr period for any gamma- or beta-emitting radionuclide (40CFR191). This is an average of 0.0001 Ci/yr per MTHM at a constant release rate.

In the first case analyzed, the source term is calculated for gas diffusion through a 300 m long cylindrical conduit that is 35 cm in diameter and abutts a canister containing approximately 0.5 MTHM. This amount of high-level waste translates to an allowable constant release rate of 1.6×10^{-12} Ci/sec per canister. At steady state, the diffusive flux from a beta- or gamma-emitting radionuclide in the canister will be 1.6×10^{-15} Ci/cm^2-sec at the accessible environment. It is assumed that no retardation has occurred, the coefficient of diffusion is constant, and that 100% of the flux from the canister is released to the

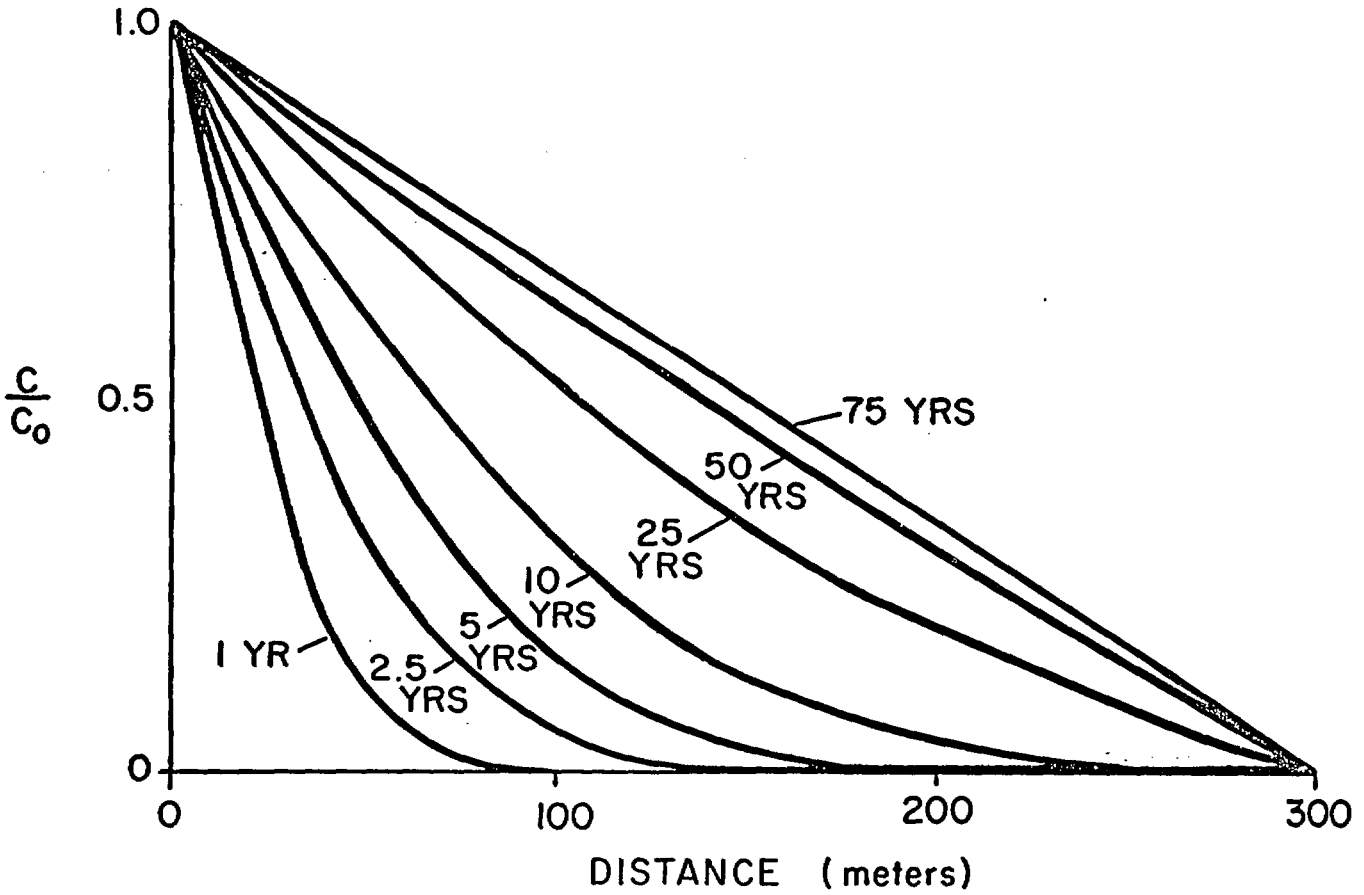

Figure 2.14. Diffuse flux versus normalized concentration for a 300 m long cylindrical conduit at time 1 to 75 years.

accessible environment through a 35 cm diameter borehole. An additonal assumption made in this calculation is that once a canister is breached, the entire canister cladding is deemed inoperative and contaminants are introduced into the geologic medium over 100% of the surface area of the canister. The diffusive flux (per unit area) from the surface of a canister is calculated to be 3.9×10^{-18} Ci/cm^2-sec. Once the diffusive flux at the canister surface is known, the concentration of gas at the surface of the canister is determined using Fick's law (Equation 2.14) as 7.8×10^{-13} Ci/cm^3.

One curie is emitted by approximately 5770 g of ^{129}I, thus, a concentration of 7.8×10^{-13} Ci/cm^3 corresponds to 4.5×10^{-9} g/cm^3 of ^{129}I. Therefore, an average concentration of greater than 4.5×10^{-9} g/cm^3 of ^{129}I over the entire surface area of the canister will exceed the proposed release rate of 1.6×10^{-18} Ci/sec at the accessible environment for the conditions given.

A second case study analyzes ordinary diffusion from a repository overlain with a 300 m thick layer of homogeneous unsaturated fractured rock. The rock matrix is considered an equivalent porous medium with a constant effective gas porosity. The repository is assumed to cover a 1 x 2 km area and contain about 50,000 MTHM (100,000 canisters). The time to approach steady state in this case would be slightly greater than the 75 years required in the first case study.

Equation (2.14), when accounting for porosity and tortuosity, becomes (Weeks et al., 1982)

$$J = -\beta_t \, \theta_d \, D \, \nabla c \qquad (2.96)$$

Tortuosity, β_t, can be related to the drained porosity, θ_d, by the empirically derived expression (Millington, 1959)

$$\beta_t = (\theta_d)^{1/3} \qquad (2.97)$$

An equivalent porous medium with a drained porosity of 10% will have a calculated tortuosity of 0.46. Therefore, the rate of diffusive flux through the rock would be 4.6% of the diffusive flux through an open borehole of similar cross-sectional area for the same concentration gradient.

Each canister will influence an average area of 2.0×10^5 cm^2 if 100,000 canisters are uniformly spaced over a 2 km^2 area. It is assumed that no retardation has occurred, the coefficient of diffusion is constant and

equals 0.15 cm^2/sec, and that 100% of the flux of beta- or gamma-emitting radionuclides at the canister is released through a 2.0×10^5 cm^2 area at the accessible environment.

Since the proposed allowable release rate of a beta- or gamma-emitting radionuclide from each canister is an average of 1.6×10^{-12} Ci/sec, the flux will be 7.9×10^{-18} Ci/cm^2-sec to the accessible environment at steady state. The flux at the surface of a canister will be 3.9×10^{-18} Ci/cm^2-sec. An average concentration of less than 1.7×10^{-11} Ci/cm^3 is necessary over the entire surface of a canister (4.1×10^5 cm^2) to meet the proposed standards. If the radionuclide is ^{129}I, a concentration of 1.7×10^{-11} Ci/cm^3 corresponds to a concentration of 9.7×10^{-8} g/cm^3 of ^{129}I.

There is a lack of definitive design and analysis of the characteristics of high-level waste, the canister, and associated engineering barriers. The rate and chemical nature of high-level waste exposed to the geologic medium after canister failure has not been specified. However, this analysis indicates that steady-state diffusive flux at the accessible environment is attained in a relatively short period of time for two extreme cases. The analysis also suggests source term limits at the canister that should not be exceeded if gaseous ^{129}I is released.

3. FORCED DIFFUSION

Mass flux of a gas by forced diffusion is, under most conditions, considered insignificant when compared to ordinary diffusion. However, gamma radiation emitted during decay of high-level waste can induce an electric field caused by Compton scattered electrons which in turn can create conditions conducive to forced diffusion. The magnitude of the resulting electric field and the related forced diffusion of an ionized gas through the air space of a partially saturated fracture will depend upon the physical characteristics of the high-level waste, specific engineering design and site characteristics.

The mass flux (ions/cm^2-sec) of gas resulting from forced diffusion caused by an electric field can be expressed as (McDaniel and Mason, 1973)

(3.1) $$J = n_i \; M \; E_e$$

where

n_i = number density of ions (ions/cm^3)
E_e = electric field (V/cm)
M = mobility (cm^2/V·sec)

The mobility term, M, is a measure of the ease at which an ion can move through a gas. The mobility term is related to the diffusion coefficient by the expression

(3.2) $$M = e\, D/\,(KT)$$

where e = ionic charge (coulombs)
D = diffusion coefficient (cm^2/sec)
K = 1.38 x 10^{-23} (joules/°K), Boltzmann constant
T = temperature (°K)

Equation (3.2) is known as the Einstein relation.

McDaniel and Mason (1973) use an electric field parameter to investigate the importance of electric fields on ion transport in the vapor phase. This parameter indicates if a system is classified as having low or high field energy. Expressions which govern the flow of ions in an electric field are different for low energy and high energy fields. The field parameter can be expressed as either E_e/N or E_e/P where N is the gas number density and P is the total pressure. Using the ideal gas law, the two forms of the field parameter are related by the expression

(3.3) $E_e/N = (1.0354 \times 10^{-2}\ T)\ E_e/P$

Field energy is low when the following inequality is valid

(3.4) $(m_g/m_i + m_i/m_g)\ e\ E_e\ \lambda \ll KT$

where m_g and m_i are the molecular mass of the gas molecules and ions, respectively. If a singly charged ion is transported through a gas of similarly sized molecules and the collision cross-section is assumed to be 5×10^{-15} cm^2, the inequality reduces to approximately

(3.5) $E_e/P \ll 2$ V/cm·Torr

Thus, at atmospheric pressure, the energy field is considered low when the external electric field is less than about 1500 V/cm.

Mobility of a gas or a gas mixture can be considered a constant at low field levels. The mobility of a gas mixture at low field level can be determined using Blanc's law. Blanc's law is based on simplified kinetic theory and is written

(3.6) $M_{mix}(0) = [\sum_j x_j/M_j(0)]^{-1}$

where $M_j(0)$ is the mobility of the j^{th} gas in the absence of an electric field and x_j is the mole fraction of the j^{th} species.

Also at low energy, the drift velocities of ions along the field lines are directly proportional to the electric field as described by the relation

(3.7) $v_d = M\ E_e$

When field energy is high (that is, greater than 1500 V/cm), the relationship described by Equation (3.7) is not linear. Two physical mechanisms are observed in the electric field when this occurs. First, the drift velocity contains the velocity component directed along field lines and, secondly, an additional random element is introduced by collisions of ions with gas molecules. The mobility term is not constant at high field energy, rather it is dependent upon the magnitude of the field energy. The diffusion coefficient in Equation (3.2) is a scalar in low field energy but a second order tensor in high field energy. Equation (3.2), therefore, does not apply for the latter case.

Although data are sparse, deviations between observed mobility and predicted mobility range from 0.05% to 20% when a constant mobility term is used and field energy is high (McDaniel and Mason, 1973). Since accurate determination of mobility in high field energy is complex and difficult, mobility is considered a constant for these calculations and is determined by Equation (3.2) for all cases.

However, as will be demonstrated, the predicted electric field intensity is usually low enough to assume low energy status. Even when field energy approaches the threshold between low and high energy level, the energy level is not excessive enough to warrant employing the approximations necessary to determine mobility at high field energy.

Compton current creates a displacement of electrons away from the canister. This sets up an electric field which causes a return flow of conduction electrons. The electric field grows in strength until the return flow exactly balances the Compton current. The electric field is related to the return flow (or current density), j (amps/cm^2), and the resistivity of the medium, ρ (ohms·cm), by Ohm's law which can be expressed as

$$E_e = \rho j \tag{3.8}$$

Although the Compton current is not governed by Ohm's law, the return current is, and Equation (3.8) can be used to calculate the electric field. Current density is by definition related to the electric current, I (amps), by the expression

$$j = I/A \tag{3.9}$$

where A is area (cm^2). The electric field surrounding a HLW repository can therefore be determined if current density and resistivity are known.

3.1 Photon Transport Model--COMPMC

The attenuation of photons in a medium and the electric field created during interaction between photons and the medium are not successfully determined using first guess approximation techniques (Goldstein, 1959). I have developed a photon transport computer program to chart the movement of photons as they collide with the particles in a medium in order to determine the outward flux of electrons. From this, the electric current density, electric field and ion drift velocity can be predicted.

Gamma radiation (or photons of electromagnetic radiation) loses a relatively large amount of energy when it interacts with matter. Interaction of gamma radiation with matter can occur during several different processes. Three of the more important processes are 1) the photoelectric effect, 2) the Compton effect, and 3) pair production (Spinks and Wood, 1976). Only the Compton effect has a significant effect on induced electric fields around a HLW canister.

The Compton effect results from an interaction of a photon with either a bound or free electron in the absorbing material. During the collision, energy is transferred to the electron. If the transferred energy is in excess of the binding energy of the electron bound to the atom, the electron moves off in a new direction. Another photon of lower energy, E', is deflected in a different direction (Figure 3.1). Energy and momentum are conserved during the collision. The resulting preferential movement of electrons results in the Compton current in the absorbing medium.

A photon emitted during a collision from whence a Compton scattered electron is produced, can theoretically cause a series of subsequent collisions provided each collision-produced photon has sufficient energy to cause Compton scattering. A Monte Carlo algorithm has been written as part of the photon transport code to record the movement of photons emitted from a HLW canister. Each photon is followed from collision to collision keeping track of its energy losses and the Compton electrons emitted. A history is terminated when the photon's energy becomes too small to cause further Compton scattering. The simulation program, COMPMC (Appendix A), follows a sufficient number of histories to account for the random nature of photon interactions.

As an example, a graph of the total attenuation coefficient per atom or molecule A_c (cm^2/molecule) of water resulting from three different attenuating processes is shown in Figure 3.2 (from Spinks and Wood, 1976). The variable A_c is also referred to as the microscopic cross section. Gamma ray attenuation in other material and air is similar to the atternuation in water.

The Compton effect of a photon interacting with either a bound or free electron is important for photon energies between 0.5 and 5.0 MeV in high atomic number materials and between 0.1 and 20 MeV in low atomic number materials such as water (Meyers, 1970). In general, the Compton effect is the dominant process affecting photon attenuating over the photon energy range of about 0.1 to 10 MeV. Below about 0.03 MeV,

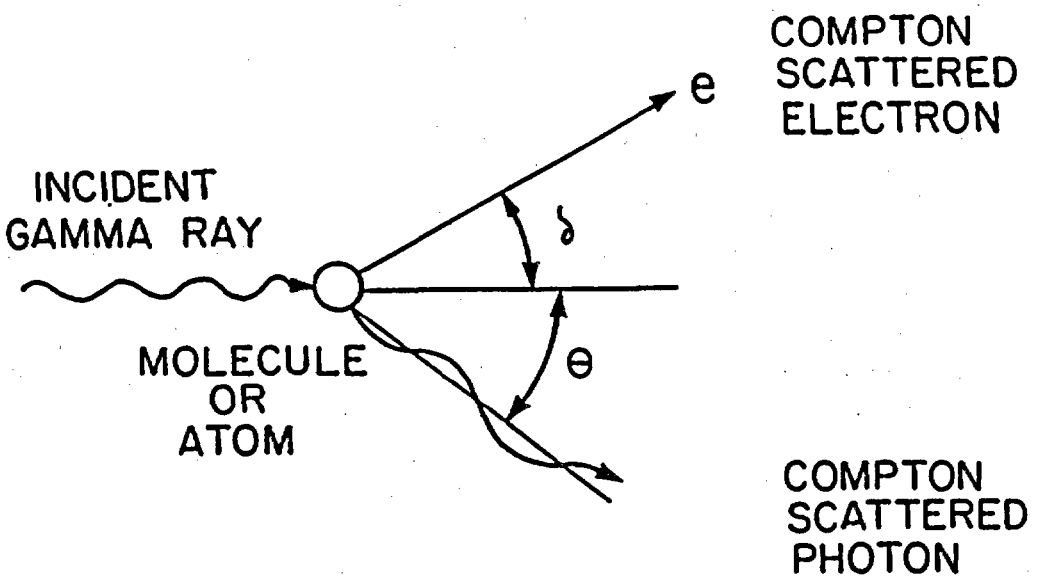

Figure 3.1. Collision of incident photon on molecule or atom causing scattering of Compton electron and collision photon.

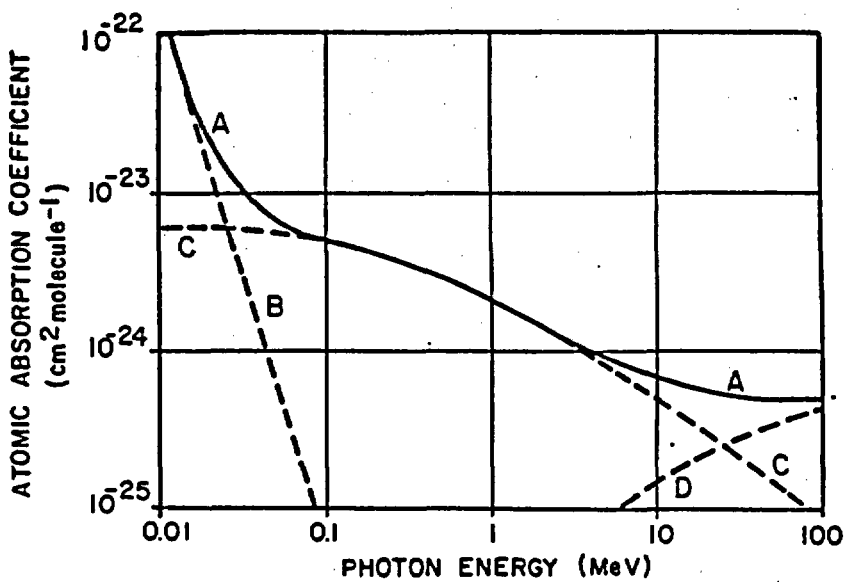

Figure 3.2. Attenuation coefficients for water. Curve A: total attenuation coefficient; B: photoelectric attenuation coefficient; C: Compton attenuation coefficient; D: pair-production coefficient (from Spinks, J.W.T. and R.J. Woods, An Introduction to Radiation Chemistry, Wiley-Interscience, New York, 1976.) Reprinted by permission of John Wiley & Sons, Inc. ©

photoelectric attenuation becomes the dominant absorption process of gamma radiation in water. During the photoelectric process only an electron is emitted during a collision. Therefore, the chain reaction of collision induced photons traveling through the medium is terminated. The Compton effect will be the most important process involved in reducing the intensity of gamma radiation, and more importantly, the principal cause of an electric current in the absorbing matter.

The waste package is characterized as an infinite line source. Thus end or edge effects are ignored. A typical waste package is approximately 240 cm long and 35 cm in diameter. Additionally, forced diffusion caused by an electric field will most probably be a phenomenon in the zone near the repository and, therefore, will only be important in the immediate region surrounding the waste package (less than 1-2m). Because of these two facts, the assumption of treating the 240 cm long cylinder as an infinite line source is believed justified.

A further assumption made in this simulation is that the HLW canister is located in an homogeneous, isotropic medium. This assumption simplifies the procedure employed in tracking individual photons. Two cases are investigated 1) Compton scattering in rock mass and 2) Compton scattering in air. However, once the Compton current is calculated for the rock mass case, partially drained fractures which intersect the canister are introduced into the system. Forced diffusion or ion drift velocity in partially drained fracture can then be calculated. The effect of the canister per se upon photon transport, however, has not been considered. For the conservative case, it is assumed that the canister has failed and no canister cladding is present.

The Compton current density, $\hat{j}(r)$, is formally given by the expression

$$(3.10) \qquad \hat{j}(r) = \iiiint A(\hat{\Omega}',E',\hat{\Omega},E)\ \hat{\Omega}\ R_{eff}\ \phi_e(\hat{r},\hat{\Omega}',E')\ e\ dE\ d\Omega\ dE'\ d\Omega'$$

where

R_{eff} = effective range of electron with energy E

$A(\hat{\Omega},E,\hat{\Omega}',E')$ = microscopic cross section for producing a Compton electron of direction Ω and energy E from a photon of direction Ω' and energy E'.

$\phi_e(\hat{r},\hat{\Omega}',E')$ = gamma flux (photons per unit solid angle, per unit area, per unit energy.

$\hat{\Omega}$	=	direction of electron
$\hat{\Omega}'$	=	direction of photon
E	=	electron energy
E '	=	photon energy

A separate routine, SR, calculates the effective range of the electrons and COMPMC calculates the rest of the integral. The procedure which determines current density is described in detail in this section.

The procedure used to record the path of a photon (more exactly, a series of photons) from collision to collision, makes use of a combination of cartesian and spherical coordinate systems. In general, a collision is assumed to occur after traveling a weighted randomly selected distance. The trajectory of the collision or emitted photon is chosen and expressed in terms of a local coordinate system which is defined relative to the trajectory of the incident photon. The trajectory of the collision photon is chosen using spherical coordinates, but the unit vector of the new trajectory is recorded in terms of its cartesian coordinates.

The trajectory of the collision photon is dependent upon the energy of the incident photon. As energy increases, the microscopic cross section, A(E), becomes more narrowly peaked in the forward direction. Conversely, at lower energy levels, the microscopic cross section tends to be less peaked and there is a higher probability that the collision photons are isotropically emitted. Figure 3.3 illustrates the dependence of the collision cross section on the energy of the incident photon. Figure 3.3 and the following discussion on cross-sections are adapted from Goldstein (1959).

The microscopic cross section can be thought of as a measure of the probability per atom or molecule that a collision will result from a specific photon. The Klein-Nishini equation defines the probability of attenuation of energy by scattering of a photon. It can be calculated from the energy of the incident photon using the following equation (expressed in Thomson units)

$$(3.11) \quad A(E) = 3/4 \langle (1 + E)/E^3 [2E(1 + E)/(1+2E) - \ln(1 + 2E)] + 1/2E - \ln(1 + 2E) - (1 + 3E)/(1 + 2E)^2 \rangle$$

A Thomson unit equals 0.655 barns, or 0.655×10^{-24} cm^2.

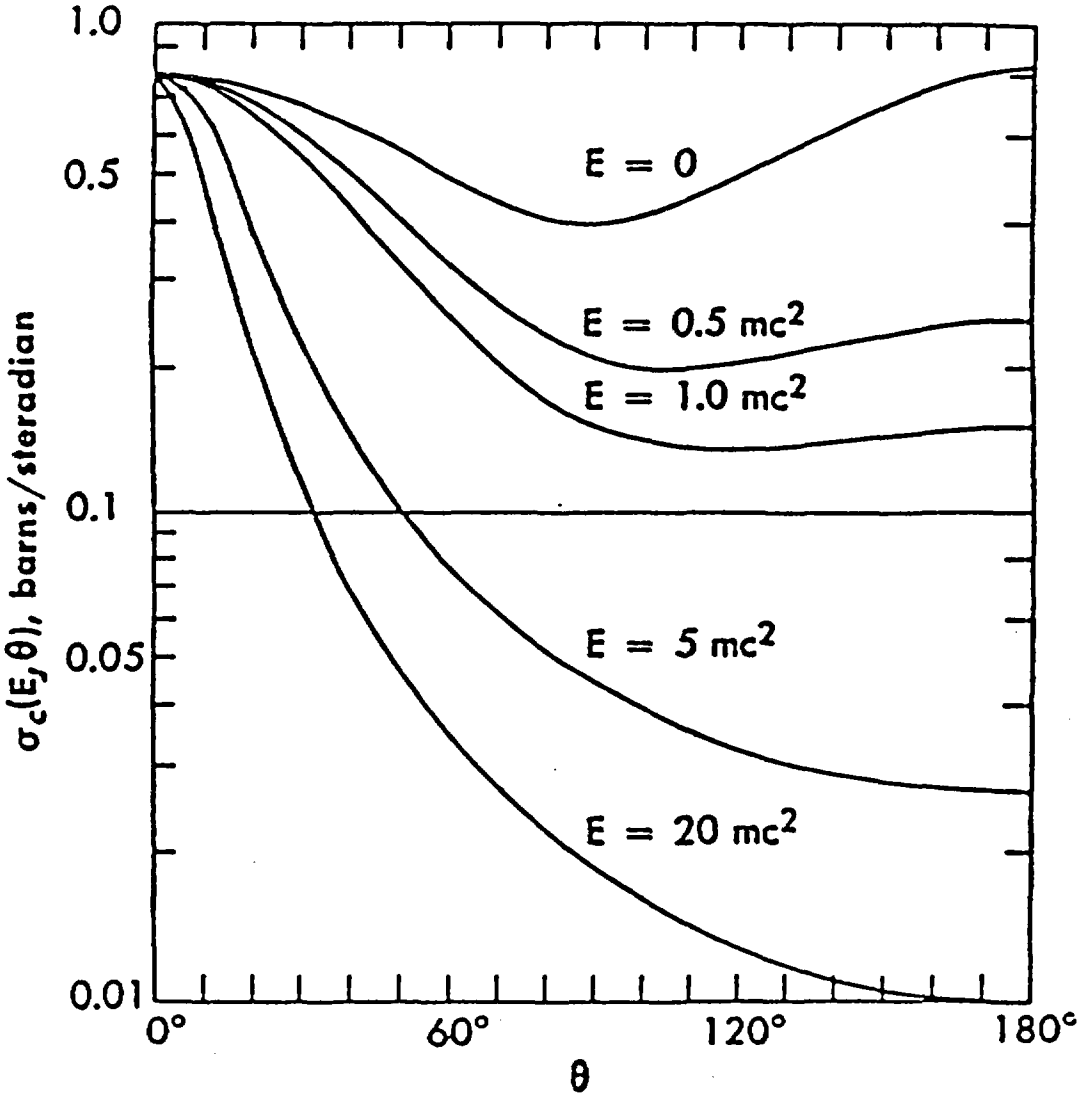

Figure 3.3. Differential cross section for the Compton effect (from Goldstein, 1959).

The differential cross section it the incremenatal cross section available for scattering at a given differential angle and can be defined

$$(3.12) \qquad A(e_0)d\Omega_s = 3/16\pi\ (E'^2/E^2)(E/E' + E'/E - \sin^2 e_0)d\Omega_s$$

where e_0 is the angle of deflection between the trajectory of the incident photon and the collision photon, $A(e_0)$ is the microscopic cross section due to the Compton effect, E' is the energy of the collision photon and $d\Omega_s$ is the differential solid angle. Equation (3.12) describes how the cross section varies with the differential scattering solid angle. The o-subscript denotes the newly determined angles which define the trajectory of the collision photon in the locally defined coordinate system.

The conversion from microscopic cross section to macroscopic cross section, μ (cm^2/g) is accomplished by the relationship

$$(3.13) \qquad \mu = A(E)\ N_s$$

where N_s the number of scatterers per unit volume. The term macroscopic cross section is used interchangably with either the absorption coefficient or the attenuation coefficient. The term attenuation coefficient is generally associated with photon transport and will be used here.

The energy of the incident photon and the collision photon are related by the expression

$$(3.14) \qquad E' = E/(1 + E(1 - \cos e_0))$$

The azmuthal angle, ϕ_0, of the trajectory of the emitted photon is randomly chosen between 0°and 360° in the plane perpendicular to the trajectory of the incident photon (Figure 3.4). The cartesian components of the unit vector aligned with the new photon trajectory are e'_x, e'_y, and e'_z when expressed in the local coordinate system. The local coordinate system is denoted by the prime notation. The unit vectors e'_x and e'_z lie in the same plane in which the azmuthal angle is defined. The y'-axis is colinear to the trajectory of the collision photon. The deflection angle relative to the y'-axis, however, abides by the cosine law and is therefore chosen such that the solid angle through which the photon proceeds is a weighted random selection.

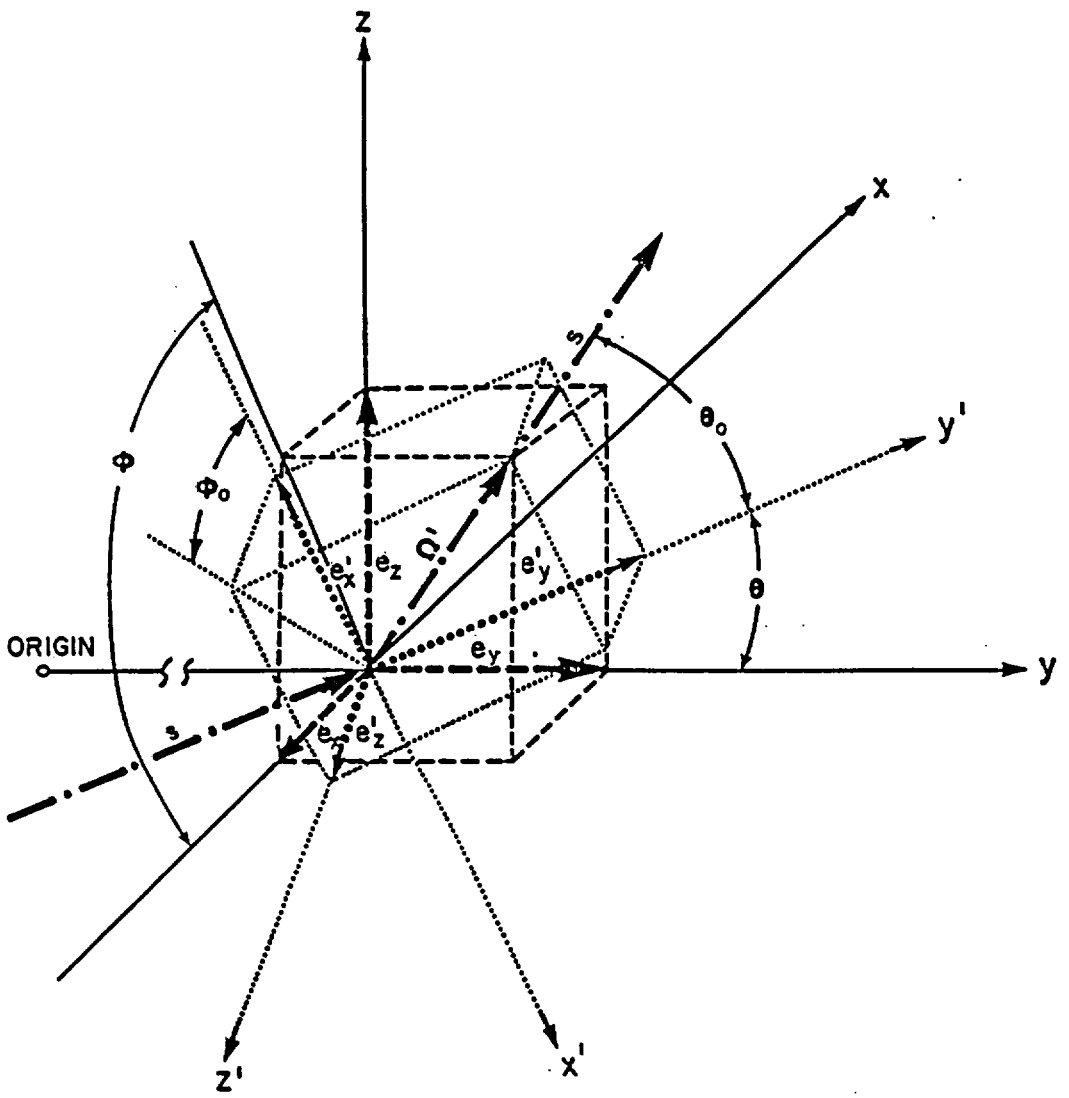

Figure 3.4. Illustration of rotation from local cartesian coordinate system (x', y', z') to global cartesian corrdinate system (x, y, z). Deflection angle is θ and azmuthal angle is ϕ.

A rejection technique is used to randomly select the deflection angle subtended by the y'-axis of the local coordinate system and the trajectory of the emitted photon. The first step in the rejection procedure is to randomly select the deflection angle between 0 and 180°.

The second step is to randomly select a microscopic cross section for that angle. The possibilities range from 0 to $3/16\pi$ when expressed in Thomson units. The microscopic cross section for the selected angle is computed using the Klein-Nishini equation. Values for the microscopic cross section as defined by the Klein-Nishini equation are determined relative to the deflection angle for values of 0 to 180° at different energy levels. This relationship is plotted for selected energy levels in Figure 3.3. The computed microscopic cross section is compared to the randomly selected microscopic cross section. If the latter is greater, the randomly selected microscopic cross section and angle are rejected and step one is repeated. The process is continued until an angle and microscopic cross section are selected which fulfill the rejection criterion. By using the Klein-Nishini equation as the acceptance or rejection criterium, the ultimate selection is influenced or weighted according to the cross section of the incident photon.

Consequently, there is a lower probability of rejection at lower photon energy levels where the microscopic cross section is more constant and less peaked than at higher energy levels (Figure 3.2). This fact is supported by COMPMC. As many as 250 random angles and cross sections are rejected before an acceptable angle and cross section are chosen for a 10 MeV photon. However, fewer than 5 angle and cross section selections are needed before the selection criterion is fulfilled and rarely as many as 15 selection attempts necessary for a 1.0 MeV photon.

The basic premise of this Monte Carlo simulation is the recording of the travel history of many individual particles. It is imperative to use an efficient program to record each history because a large number of histories are required to ensure a statistically sound result. For this reason, the deflection angle is determined using the cosine law where $\cos^{-1}e_0$ is randomly selected in lieu of randomly selecting the angle e_0. By selecting $\cos^{-1}e_0$ rather than e_0, the solid angle subtended by e_0 is equally likely instead of e_0. A 10% reduction in the C.P.U. requirement is realized by employing this technique in COMPMC.

The effect of matter on gamma radiation is a reduction in the intensity of incident gamma radiation by the above mentioned collision processes. The intensity of gamma radiation, I_g (ergs/cm^2-sec), is defined as the radiation energy (the number of photons multiplied by their average

energy) passing through a sphere of unit (maximum) cross-sectional area in unit time at the point of interest. A basic property of photons is the exponential decrease in intensity as they travel a finite distance, Δs, through matter as defined by the expression (Kaplan, 1955)

$$I_g = - \mu_o I_g \Delta s \tag{3.15}$$

where μ_o is the total linear attenuation coefficient (cm^{-1}). The value of the total linear attenuation coefficient is a composite of all interactions which reduces the intensity of gamma radiation in matter and depends upon the nature of both the incident gamma radiation and the absorbing matter (Spinks and Woods, 1976).

The distance of travel of a photon can be calculated using physical laws (Fillipone, 1985). Integration of Equation (3.15) yields

$$I_g/I_g^o = e^{-\mu s} \tag{3.16}$$

where μ is the attenuation coefficient attributed to Compton scattering. Equation (3.16) is referred to as Lambert's law of absorption and gives the intensity of gamma radiation after a beam of initial intensity I_g^o has traveled a distance of s.

The quantity I_g/I_g^o can also be thought of as the probability of reaching a distance s without a collision and μds is the probability of a subsequent reaction in ds. The probability of having a reaction in ds about s can be stated

$$P(s)ds = e^{-\mu s} \mu ds \tag{3.17}$$

where P(s) is the probability of an event occurring in s.

Let ρ be uniformly probable over the range [0,1]. Additionally, let each ρ with range [0,1] correspond to an s with range $[0,\infty)$ which can be written

$$P(\rho)d\rho = P(s)ds \tag{3.18}$$

However, the probability of ρ is unity and Equations (3.17) and (3.18) can be combined to yield

$$d\rho = e^{-\mu s} \mu ds \tag{3.19}$$

Integration of Equation (3.19) results in

(3.20) $\rho = -e^{-\mu s} + c$

where the boundary conditions are

(3.21a) $\rho(\infty) = 1$

and

(3.21b) $\rho(0) = 0$

The constant of integration is therefore 1 and Equation (3.16) can be written

(3.22) $e^{-\mu s} = 1 - \rho$

However, $1 - \rho$ is as equally likely to occur as ρ, thus Equation (3.22) can be restated

(3.23) $s = -(\ln \langle \rho \rangle)/\mu$

Therefore, if the attenuation coefficient is known, randomly selecting ρ between 0 and 1 determines the distance a photon will travel before a collision occurs. The selection of trajectory and distance of travel of a photon between collisions is complete.

The procedure used to track the pathway of a photon from one collision to the next collision requires that the randomly selected collision photon vector, $\hat{\Omega}'$, which is initially defined in a local coordinate system, be redefined in terms of a global coordinate system (Figure 3.5). The redefined vector can then be projected outward to the point of the subsequent collision given the distance between collisions. The redefined vector, $\hat{\Omega}$, is, therefore, the incident photon vector for the subsequent collision defined in the global coordinate system. As will be shown, there is a single vector transformation, $\bar{T}$, that will perform the redefinition from local to global coordinate systems or

(3.24) $\hat{\Omega}' = \bar{T}\hat{\Omega}$

Initially, the new trajectory is described in terms of the principal cartesian coordinates aligned orthogonally with the trajectory of the incident photon. The y'-axis is aligned colinearly with the incident photon trajectory. Next, the three principal components of the cartesian coordinate system which define the local coordinate system are

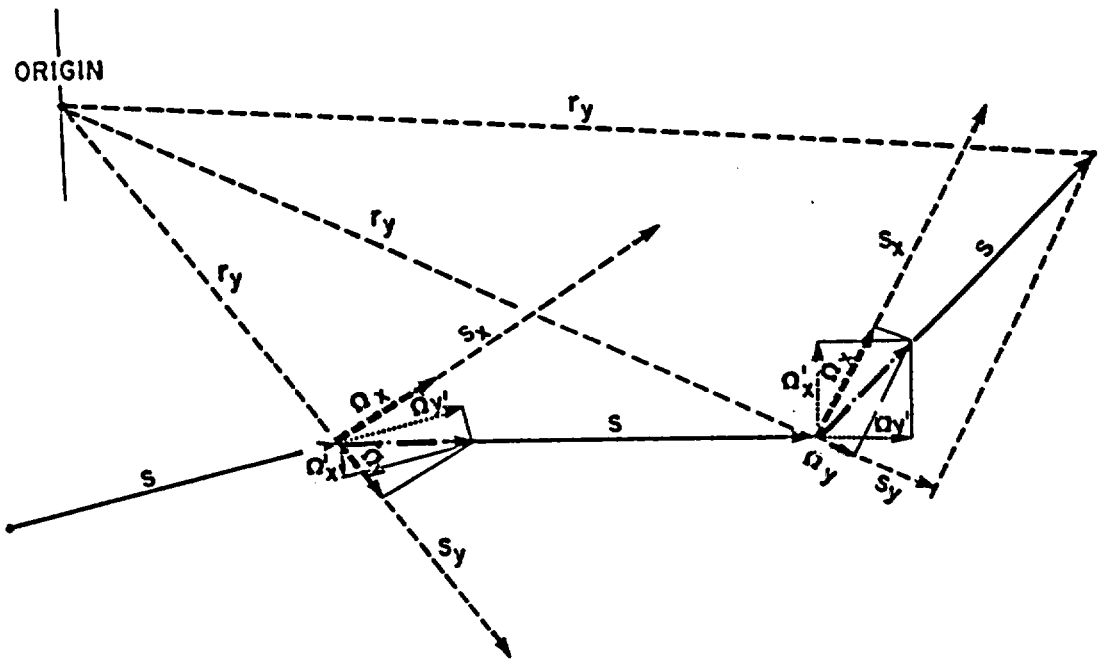

Figure 3.5. Trajectory of photons from collision to collision along S in two-dimensions. r_y is radial distance from initial photon origin; $\hat{\Omega}_x$, $\hat{\Omega}_y$ components to unit vector in global coordinate system; $\hat{\Omega}$ unit vector in global coordinate system; $\hat{\Omega}_x'$, $\hat{\Omega}_y'$ components to local coordinate system; S_x, S_y magnitude of photon travel in global coordinate system.

redefined in terms of the global system. The global system is oriented orthogonally with respect to a position vector from the source of the original gamma ray located along the line source to the point of collision.

An important aspect of the tracking procedure is that although the global coordinate system is redefined at each collision site in terms of cartesian components, it remains the same system in terms of spherical coordinates. There are two major reasons supporting the use of this methodology. First, only the radial distance from the origin of the initial photon to the point of collision and the trajectory of the collision photon at the point of collision are important in terms of accounting for Compton scattered electrons. The azmuthal angle of the radial component of the position vector, $\hat{r}_y$, is neglected because of the radial symmetry of the system. As such, accountability of collisions reduces to a one-dimensional array averaged over 2π times the radial distance to adjust for radial spreading. Secondly, it is easier to record trajectories in a cartesian coordinate system than in a spherical system since the trajectories are linear vectors not necessarily oriented in the radial direction.

The first step involved in the redefinition of the collision photon vector, Ω, from a local to global coordinate system is to arbitrarily define the local x'-direction component, $\hat{e}'_x$, of the unit vector in the local coordinate system such that it is perpendicular to the plane defined by the global unit vector, $\hat{\Omega}$, which is aligned colinearly with the incident photon trajectory and by the y-direction component to the unit vector of the global coordinate system, $\hat{e}_y$ (Figure 3.4). The y-direction component to the global coordinate system is defined as the vector that originates at the initial origin of the gamma ray and goes through the point of collision. The local x'-direction component to the locally defined unit vector, $\hat{\Omega}'$, can therefore be defined using the cross product by the expression

$$\hat{e}'_x = \hat{\Omega} \times \hat{e}_y / |\hat{\Omega} \times \hat{e}_y| \qquad (3.25)$$

where the magnitude of the cross product is defined

$$|\hat{\Omega} \times \hat{e}_y| = |\hat{\Omega}|\ |\hat{e}_y| \sin \theta \qquad (3.26)$$

and where θ is the globally defined angle subtended by $\hat{\Omega}$ and $\hat{e}_y$. Equation (3.25) is rewritten as

$$\hat{e}'_x = -\sin \phi\ \hat{e}_x + \cos \phi\ \hat{e}_z \qquad (3.27)$$

where ϕ is the azmuthal angle in the x-z plane of the global coordinate system. The azmuthal angle is always defined as the angle subtended by the x-axis and the projection of the Ω vector onto the x-z plane for both the local and global coordinate systems.

The local z'-direction component to the unit vector, $\hat{e}'_z$, is similarly defined relative to the trajectory of the incident photon and the previously defined local x'-direction unit vector component. This expression appears

$$\hat{e}'_z = \hat{\Omega} \times \hat{e}'_x / |\hat{\Omega} \times \hat{e}'_x| \tag{3.28}$$

or

$$\hat{e}'_z = \hat{\Omega} \times \hat{e}'_x \tag{3.29}$$

because the two vectors in the cross product are of unit length and orthogonal. Expansion of the cross product yields

$$\hat{e}'_z = \cos\theta \cos\phi \, \hat{e}_x - \sin\theta \, \hat{e}_y + \cos\theta \sin\phi \, \hat{e}_z \tag{3.30}$$

Lastly, the local y'-direction or radial component to the local unit vector along the trajectory of the incident photon is defined

$$\hat{e}'_y = \hat{\Omega} \tag{3.31}$$

which can be expanded to appear

$$\hat{e}'_y = \hat{\Omega}_x \hat{e}_x + \hat{\Omega}_y \hat{e}_y + \hat{\Omega}_z \hat{e}_z \tag{3.32}$$

Examination of Figure (3.6) yields the basic relations between a spherical and cartesian coordinate system

$$\Omega_x = \sin\theta \cos\phi \tag{3.33a}$$

$$\Omega_y = \cos\theta \tag{3.33b}$$

and

$$\Omega_z = \sin\theta \sin\phi \tag{3.33c}$$

Equation (3.31) can be rewritten using these relations to give the following expression

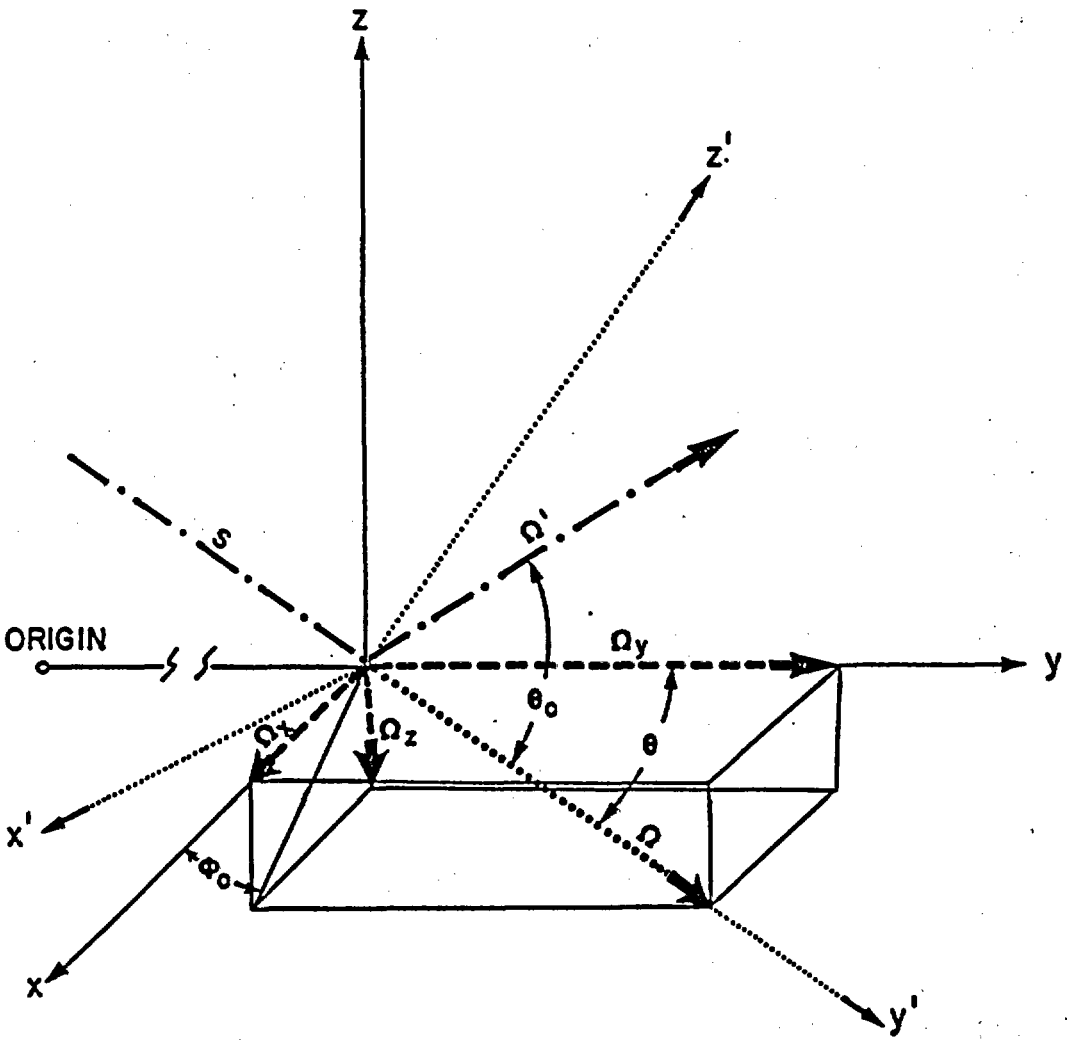

Figure 3.6 Illustration of conversion from local spherical to local cartesian coordinate system, where ϕ is the local azmuthal angle; θ_0 local angle of deflection; (x, y, z) global cartesian system; (x', y', z') local coordinate system; $\hat{\Omega}'$ unit vector in direction of collision photon

(3.34) $\hat{e}'_y = \sin\theta\cos\phi\,\hat{e}_x + \cos\theta\,\hat{e}_y + \sin\theta\sin\phi\,\hat{e}_z$

Equations (3.27), (3.30), and (3.34) therefore express the unit vector components in the local coordinate system in terms of the global coordinate system.

The local collision photon unit vector, $\hat{\Omega}'$, is defined

(3.35) $\hat{\Omega}' = \hat{\Omega}'_x\hat{e}'_x + \hat{\Omega}'_y\hat{e}'_y + \hat{\Omega}'_z\hat{e}'_z$

Again using the basic relations stated in Equations (3.33a-c), the unit vector of the collision photon (Equation 3.35) is expressed in the local coordinate system by the relation

(3.36) $\hat{\Omega}' = \sin\theta_0\cos\phi_0\hat{e}'_x + \cos\theta_0\hat{e}'_y + \sin\theta_0\sin\phi_0\hat{e}'_z$

Substitution of Equations (3.27), (3.30), and (3.34) into Equation (3.36) defines the unit vector of the trajectory of the collision photon in the global coordinate system. Rearranging yields the complete expression

$$\begin{aligned}(3.37)\quad \hat{\Omega}' = {} & (-\sin\theta_0\cos\phi_0\sin\phi + \cos\theta_0\sin\theta\cos\phi \\ & + \sin\theta_0\sin\phi_0\cos\theta\cos\phi)\,\hat{e}_x \\ & + (\cos\theta_0\cos\theta - \sin\theta_0\sin\phi_0\sin\theta)\,\hat{e}_y \\ & + (\sin\theta_0\cos\phi_0\cos\phi + \cos\theta_0\sin\theta\sin\phi \\ & + \sin\theta_0\sin\phi_0\cos\theta\sin\phi)\,\hat{e}_z\end{aligned}$$

Equation (3.37) is an expansion of the transformation $\bar{T}$ defined in Equation (3.24).

After the distance of travel of the collision photon has been calculated, the global x- and y-direction components to S are determined using the global components to the unit vector. These magnitude of these two vector components appear as S_x and S_y in Figure 3.5 and are calculated using the equations

$$\begin{aligned}(3.38a)\quad S_x = {} & (-\sin\theta_0\cos\phi_0\sin\phi + \cos\theta_0\sin\theta\cos\phi \\ & + \sin\theta_0\sin\phi_0\cos\theta\cos\phi)\,\hat{e}_x \cdot \hat{S}\end{aligned}$$

(3.38b) $S_y = (\cos \theta_0 \cos \theta - \sin \theta_0 \sin \phi_0 \sin \theta)\, \hat{e}_y \cdot \hat{S}$

The radial vector from the initial origin of the photon to the end point of the distance vector of the collision photon is updated with each collision. The x-direction component of the global position vector r equals the x-direction component to the $\hat{S}$ vector. The magnitude of the y-component to the position vector, r_y, is calculated using the Pythagorean Theorem as is illustrated in Figure 3.5 and is expressed

(3.39) $$r_y^{new} = [(r_y^{old} + S_y)^2 + (r_y^{old})^2]^{1/2}$$

A basic premise in this investigation of forced diffusion is the assumption that the source of gamma rays is an infinite line source. Consequently, the z-component of the position vector does not enter into the calculations of the distance and position vectors. The z-component is, however, necessary in calculations concerning the position unit vector.

The tracking of a photon from its inception at a collision to the subsequent collision is now complete. The procedure is repeated until the energy of the collision photon is deemed insignificant (about 0.03 MeV). At 0.03 MeV, Compton scattering becomes insignificant relative to photoelectric attenuation.

3.2 Electron Transport

Each Compton collision involving a photon and a molecule or atom results in the emission of a photon and an electron. The trajectory of the collision (or Compton) electron (Figures 3.1 and 3.7) is dependent upon the trajectory of the collision photon and the energy level of the incident photon. Energy and momentum are conserved during the collision. Consequently, the azmuthal angle, ϕ^e_0, of the electron is 180° different from the azmuthal angle of the photon in the x-z plane of the local coordinate system. This is expressed

(3.40) $$\phi^e_0 = \phi_0 + 180$$

The deflection angle relative to the y'-axis of the trajectory of the Compton electron, θ^e_0 is contingent upon the energy of the incident photon and the deflection angle of the collision photon and is stated (Meyers, 1970)

(3.41) $$\theta^e_0 = \tan^{-1} (1/(1 + E/h\beta)) \cdot \cot^{-1} (\theta_0/2)$$

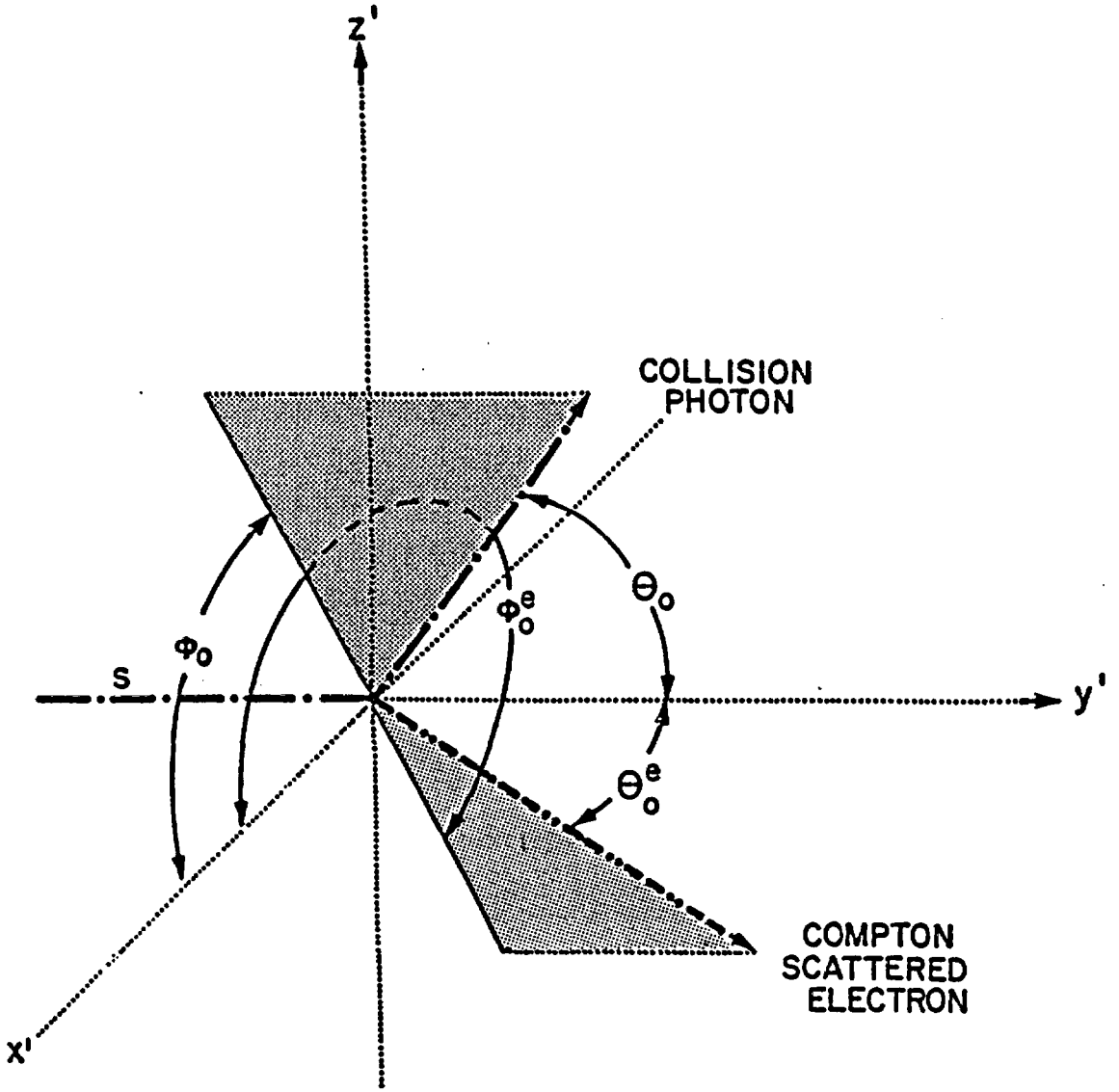

Figure 3.7. Collision trajectories of the collision photon and the Compton scattered electron relative to the incident photon. ϕ_0 and θ_0 are azmuthal and deflection angles of collision photons in local corrdinate system ϕ_0^e and θ_0^e are the same for the Compton scattered electron.

where h is Plancks constant and β is the frequency of the photon. The quantity $h\beta$ is the energy of a photon. It is assumed that the energy of the incident photon is equal to the sum of the energies of the collision photon and the Compton electron which is stated

$$E = E' + E^* \tag{3.42}$$

The distance of travel of the collision or Compton scattered electron through a medium is a difficult parameter to determine because each Compton electron is, in turn, capable of causing the movement of many other electrons through a series of subsequent collisions. The effective range (net displacement) of the electron is determined by a separate computer routine, SR, which uses the streaming ray method (Filippone et al., 1980; and Woolf et al., 1986) to solve the electron transport equation. The effective range depends on the electron energy and the medium through which it is traveling.

3.3 Photon Transport Code (COMPMC) Validation

There is no analytic solution available to validate the full extent of COMPMC (which is based upon transport theory), that is, to calculate the radial density of collisions between anisotropically scattered photons and particles in the medium. However, an analytic solution based upon diffusion theory approximation is available to calculate diffusion of isotropically scattered photons emitted from an infinite line source. In general, photons emitted from a line source will not propagate in a manner resembling diffusion because of the preferential outward movement of the photons. However, with isotropic scattering, diffusion theory agrees well with transport theory except near sources and sinks. Therefore, by making the collisions isotropic and maintaining the photon energy at 1 MeV, it should be possible to make the results of the COMPMC code agree well with those predicted by one speed diffusion theory in regions away from the line source. The one speed diffusion theory equation to this problem is referred to as the scalar Helmholtz equation and can be expressed analytically (Lamarsh, 1966)

$$\nabla^2 \phi_e - (1/L_D^2)\, \phi_e = - S_p/D_p \tag{3.43}$$

where ϕ_e is the flux (per unit energy) emitted from a line source, L_D is the diffusion length, D_p is a diffusion coefficient and S_p is the strength of the source expressed in terms of photons per sec per unit length of line source. The diffusion coefficient, D_p, is defined here by the expression

(3.44) $$D_p = 1/[3\mu_{tr}(1 - \bar{\mu})]$$

where $\bar{\mu}$ is the average cosine of the scattering angle. The term μ_{tr} is referred to as the transport attenuation coefficient and is defined

(3.45) $$\mu_{tr} = \mu - \mu_s \bar{\mu}$$

where μ_s is the scattering attenuation coefficient and μ is the total attenuation coefficient. Since isotropic scattering is assumed, $\bar{\mu}$ is zero, the transport attenuation coefficient equals the total attenuation coefficient, and the diffusion coefficient becomes

(3.46) $$D_p = 1/3\mu$$

The term L is a constant referred to as the diffusion length and is defined by the expression

(3.47) $$L^2 = D_p/\mu_a$$

where μ_a is the absorbing attenuation coefficient. By definition, the total attenuation coefficient equals the sum of the absorbing attenuation coefficient and the scattering attenuation coefficient. Substitution of the definition of the diffusion coefficient into Equation (3.47) yields

(3.48) $$L^2 = 1/3\mu_a$$

An initial photon energy of 1 MeV and an assumed scatterer density of about 10^{24} electrons/cm^3 yields a value of 0.205 cm^{-1} for the total attenuation coefficient. If 10% of the incident photons are absorbed upon collision, the diffusion coefficient has a value of 1.62 cm and the diffusion length has a value of 8.90 in dimensionless units.

The analytical solution for the line source case of Equation (3.43) is given by (Lamarsh, 1966)

(3.49) $$\phi_e = (S_p/2\pi D_p)\, K_0(r/L)$$

where K_0 is the zeroeth order modified Bessel function of the second kind.

The total number of collisions per unit length, N_c, observed in a cylindrical annulus encompassing the line source is defined

(3.50) $$N_c = \phi_e\, \mu V/S_p$$

where V is the volume of the annulus per unit length and is defined

(3.51) $V = 2\pi r \Delta r$

Substitution of (3.49) and (3.51) into (3.50) yields

(3.52) $N_c = \mu \Delta r K_0(r/L)/(2\pi D_p)$

which is the analytical solution based on diffusion theory calculated at radial increments (Δr = 1 cm).

The condition which assumes that 10% of all incident photons are absorbed during the collision is applied to both the analytic solution and to COMPMC. This means that there is a 90% chance that a photon is emitted during the initial collision between a photon emitted from the line source and a particle in the medium. The collision produced photon is available to travel on to a second collision. Similarly, there is a 81% chance of a photon being emitted after two collisions have occurred. Since collision or emitted photons are terminated by COMPMC after 100 collisions, irrespective as to whether they are absorbed, there is a $(0.9)^{100}$ or 0.0027% chance that a photon is terminated prematurely. Since the validation simulation records the history of 200,000 photons emitted from the line source, only about 5 particles are prematurely absorbed.

The normalized radial collision density determined from the transport theory based results of COMPMC is compared with the analytical solution to the diffusion equation approximation. As is illustrated in Figure 3.8, there is a discrepancy between the results near the line source where diffusion theory does not adequately represent the initial preferential outward movement apparent in the results from COMPMC. However, after the region where the initial collisions occur and beyond where outward preferential movement is observed, the results from COMPMC and the diffusion equation are very close. The slight discrepancy between the two solutions below approximately 10^{-4} collisions may the result of several different effects. Although the histories of 200,000 particles are recorded, this number may not be sufficiently large to adequately simulate isotropic scattering at relativley large distances. Alternatively, there is the possibiltiy that the analytic solution to the diffusion equation is not an exact solution to isotropic scattering at relativeily large distances. It is assumed, however, that both solutions are sufficiently similar to each other and that they both represent the same process within an acceptable margin of error.

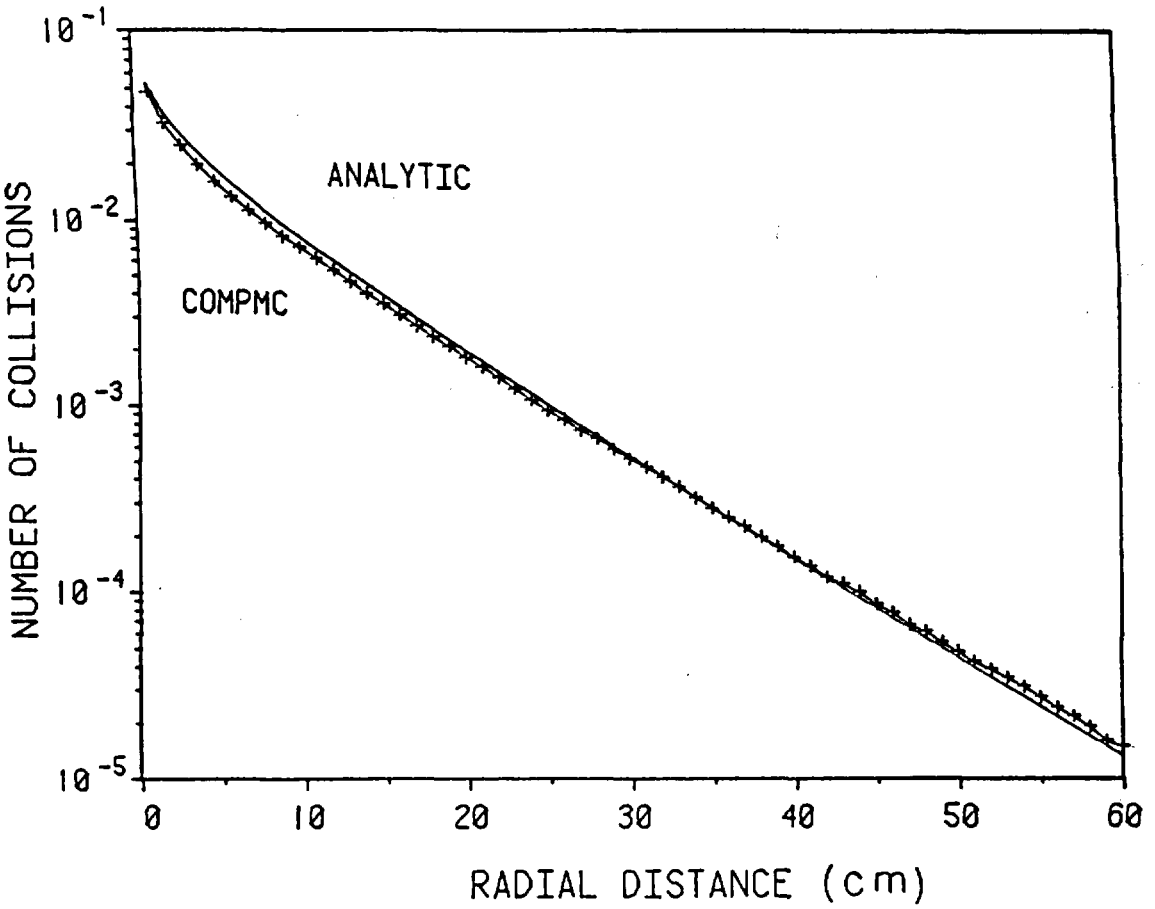

Figure 3.8. Comparison of computer program COMPMC with diffusion theory approximation solution. COMPMC is based on transport theory. Both assume 10% absorption and isotropic scattering.

3.4 Error Analysis of COMPMC

An additional routine was incorporated into COMPMC to indicate the degree of accuracy of the values for the current density for different numbers of histories. Ideally, several large computer simulations should be undertaken to determine at what level (number of histories) does increasing the number of histories not contribute appreciably to the accuracy of the simulation. As the number of histories is increased, the mean value of the calculated current density should approach the true value. However, a major constraint in determining the level of a Monte Carlo simulation is the associated computer cost. Therefore, the standard deviation of the values of the current density for each compartment is determined to indicate the accuracy of the resulting normalized values.

The Central Limit Theorem determines the probability that the difference between the Monte Carlo approximation for current density, j, and the true value of the current density, $\langle j \rangle$, is less than a given e. This theorem is stated as

$$(3.53) \qquad P(|j - \langle j \rangle| < e) \underset{n \to \infty}{\to} (2/\pi)^{1/2} \int_0^{(en)/\Sigma_d} \exp(-t^2/2)\, dt$$

where n is the number of histories and Σ_d is the standard deviation which is estimated by the expression

$$(3.54) \qquad \Sigma_d^2 = \overline{j^2} - \overline{j}^2$$

The right hand side of Equation (3.53) is referred to as the confidence level. In this work it is assigned the conservative value of 0.9. Thus, 90% of the values for the current density determined by COMPMC are assumed to be accurate to ±e of their true value.

The value of Σ_d is calculated for current density at each compartment to give an indication of the scatter of the results at various number of history levels. One possible assessment of the accuracy is to determine at what radial distance is e as large as the value of the current density. Monte Carlo simulation of 200 histories of a 1 MeV photon indicates that e is as large as j at a radial distance of 3 cm. Likewise, it is observed that an approximate parity between e and j occurred at 12 cm for 2,000 histories, 20 cm for 10,000 histories, 27 cm

for 20,000 histories and finally at 39 cm when 100,000 histories are recorded.

3.5 Analysis of Forced Diffusion Using COMPMC

The Compton current density is calculated using Equation (3.10). Once the Compton current density is determined at a particular radial distance, the individual current density contribution is added to the appropriate discrete radial compartment. Each radial compartment represents an annulus one cm wide. The final values of current density are presented as a one-dimensional array that is normalized for radial spreading by dividing each compartamental value by 2π times the radial distance. Electric field intensity is determined at each radial compartment when electrical resistivity is known. The gamma ray source employed in COMPMC is normalized so that any HLW inventory can be represented and examined in terms of the resulting forced diffusion caused by emitted photons.

The significance of the electric fields, ion drift velocities and forced diffusion is examined for two limiting cases: 1) Compton scattering in an infinite homogeneous space of rock and 2) Compton scattering in an infinite homogeneous space of air. In both cases, the photon source is a typical HLW canister represented by an infinite line source.

3.5.1 Radionuclide Source

The particular gamma ray source used in this analysis is based on the radionuclide inventory of a single fuel assembly of defense high-level waste (DHLW) from a light water reactor (LWR) predicted using the SANDIA-ORIGEN code (Sutherland and Bennett, 1979). The particular reactor type is a pressurized water reactor (PWR). Spent fuel from the pressurized water reactor is assumed to be canistered without being reprocessed. It is assumed that the fuel assembly has been immobilized in a matrix and placed in a canister. The dimensions of the canister are 240 cm in length and an outer diameter of 34 to 60 cm containing about 0.63 m^3 of DHLW. Fuel assemblies which are placed in the canisters are a product of a 3-yr, 3-cycle exposure of 3.3 weight percent ^{235}U enriched fresh fuel. The uncertainty of the integrated or total quantites used in this study is assumed to be in the range of 10 to 20%.

COMPMC determines the Compton electric current density per photon per second at a designated initial photon energy. The number of and energy level of photons are determined from results from a summary of the gamma

spectrum (photons/sec) per fuel assembly (as described above) at 10^2, 3 x 10^2, 10^3, 10^4, and 10^5 yrs after emplacement. All photons originating in the structural material, actinides, and fission products of the fuel assembly are included in the summary. Values of the gamma-spectrum at discrete energy levels are listed in Table 3.1. The electric current density caused by Compton scattered electrons in a dry tuff are calculated using the gamma ray source defined in this table.

Table 3.1. Summary of gamma spectrum (photons/sec) per fuel assembly (structural materials + actinides + fission products)(from Sutherland and Bennett, 1979).

	Time (years)				
MeV	100	300	1,000	10,000	100,000
0.30	2.4E13	1.8E13	7.8E12	1.1E12	5.6E10
0.63	1.6E14	1.8E12	2.5E11	1.1E11	1.4E10
1.10	1.4E11	7.6E10	7.2E10	3.7E10	9.8E09
1.55	5.6E06	3.2E06	1.8E07	7.6E08	6.1E09
2.75	1.3E09	1.3E09	1.3E09	1.2E09	6.9E08

3.5.2 Compton Current in a Rock Matrix

Current density, ion drift velocity and forced diffusion are investigated for a limiting case of Compton current generated in an infinite homogeneous rock medium to assess the importance of Compton scattering in the immediate neighborhood of a HLW canister. The effect of fractures on the electric field generated in rock matrix is neglected. Fractures are superimposed onto the rock matrix, however, when investigating ion drift velocities (Figure 3.9).

3.5.2.1 Effective Electron Range in Rock.

For the rock mass case, the effective range of electrons is calculated using SR for a total of 27 different electron energies. A graph of the effective range of a electron in the hypothesised material (with properties resembling the properties of an unsaturated tuff, i.e.: atomic weight of 33 and atomic mass of 68, Table 3.2) is plotted versus electron energy in Figure 3.10. Three second order polynomials are used

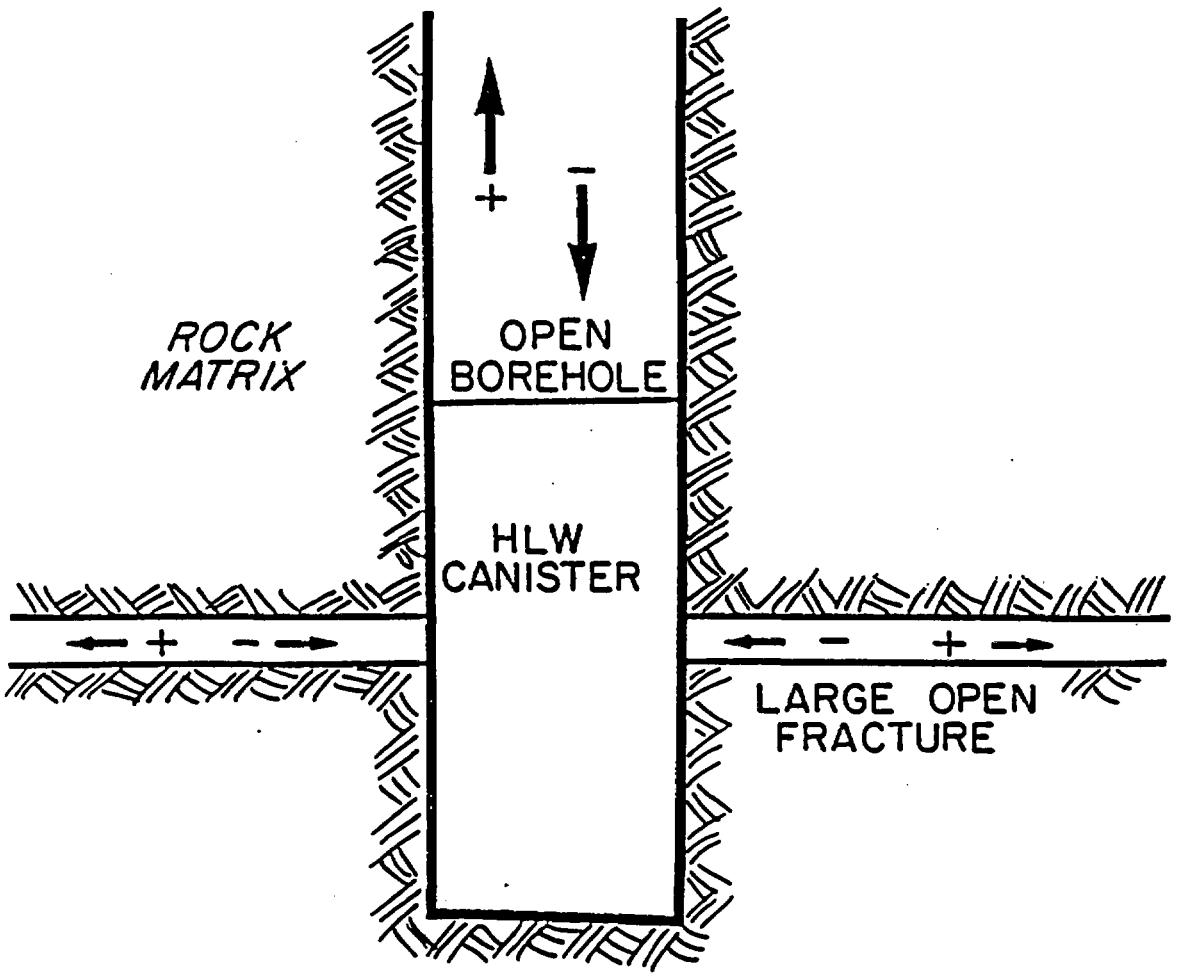

Figure 3.9. Fractures and open borehole intersecting a high-level waste cansiter.

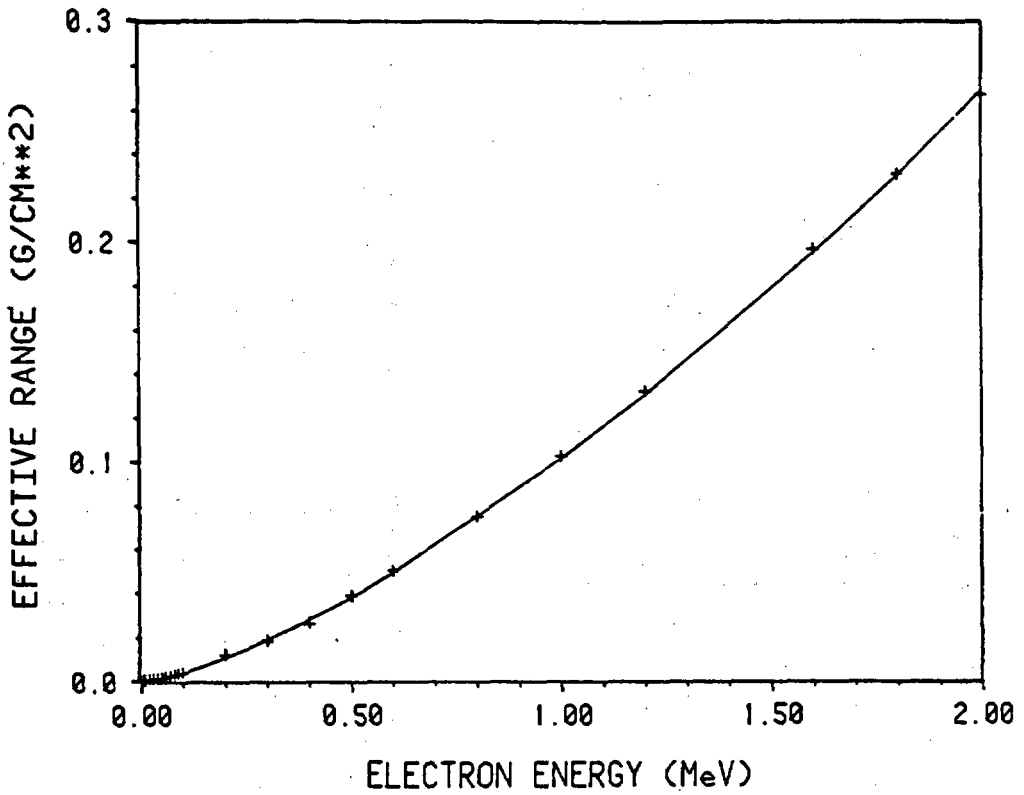

Figure 3.10. Effective range of electrons in tuff versus electron energy level.

Table 3.2 Simplified tuff sample, average composition of rhyolite.

composition	(wt. %)	no. electrons	wt. ave. electrons	atomic mass	wt. ave.
SiO_2	73.7	30	22.11	60.086	44.28
Al_2O_3	13.5	50	6.75	101.970	13.77
Fe_2O_3	1.3	76	0.99	159.694	2.39
MgO	0.3	20	0.06	71.847	0.21
CaO	1.1	28	0.31	40.312	0.44
Na_2O	3.0	30	0.90	61.980	1.86
K_2O	5.3	46	2.43	94.204	4.99
			33.56		67.94

One 'monomer' has a molecular weight (M) of 67.94 and 33.56 electrons (E_0). Rhyolitic tuff (highly welded) has a bulk density (d) of 2.4 g/cc. Avogadrous number (N_0) = $6.02 * 10^{23}$.

Electron density (N) = E_0N_0d/M.
N = $7.137 * 10^{23}$ electrons/cc.

to approximate a smooth line through the data in a spline-like fashion and are indicated with a solid line. The polynomials are determined using a discrete least-squares approximation. Six points are used to calculate the first polynomial over the range of 0.005 to 0.07 MeV. The second polynomial is determined using nine points over the range Of 0.07 to 0.7 MeV while 12 points are used to calculate the coefficients for the polynomial for energies greater than 0.7 MeV. The three second order polynomials are, respectively,

(3.55a) $4.937E\text{-}7 + 6.607E\text{-}3\ x + 2.744E\text{-}1\ x^2 = y$

(3.55b) $-2.246E\text{-}3 + 5.019E\text{-}2\ x + 5.638E\text{-}2\ x^2 = y$

and

(3.55c) $-7.351E\text{-}3 + 7.769E\text{-}2\ x + 2.978E\text{-}2\ x^2 = y$

where x denotes energy (MeV) and y effective range. A straight line interpolation is used to approximate the value of the effective range for values with energy in the range of 0.0 to 0.005 MeV. Following convention, effective range is expressed in g/cm^2 units. Units of range in centimeters are calculated by dividing by the density of the medium through which the electrons are transmitted.

The effective range-electron energy relationship is incorporated into COMPMC using the three polynomials and the straight line interpolation. Results from COMPMC suggest that about 50% of the collision electrons resulting from an initial gamma ray with an energy of 1.0 MeV have an effective range in the radial direction corresponding to an energy of less than 0.005 MeV. Likewise, about 15% of the collision electrons have an effective range in the radial direction corresponding to electron energies of greater than 0.07 MeV with the remainder in the 0.005 to 0.07 MeV range. Therefore, after each collision, the radial distance travelled by each electron can be calculated.

3.5.2.2 Current Density in Rock.

The values of current density and e determined for a 90% confidence interval are plotted versus radial distance in Figures 3.11 to 3.15 for energy levels 0.30, 0.63, 1.10, 1.55, and 2.75 MeV, respectively. A total of 100,000 histories are recorded at each energy level. As is illustrated, the accuracy of the values determined by Monte Carlo simulation appears to be slightly better at lower photon energies than at higher energies.

Values for current density are very high near the canister. This trend is not entirely understood. It may be partially attributed to edge effects at the surface of the canister. The assumption of an infinite line source in COMPMC does not adequately represent the behavior of photons near a HLW canister which has a diameter of 35 cm. thus, these values may be misleading. If the trend is not erroneous, however, relatively large electric fields may be experienced at the surface of the waste canister and certain precautionary procedures will be required so that the effect of the electrical field does not adversely affect the performance of the waste package.

The erratic behavior in the results of COMPMC beyond about 40 cm is attributed to the fact that only a finite number of realizations are computed during the simulations. Nevertheless, the basic trend of the values of current density versus radial distance is apparent at distances beyond 40 cm.

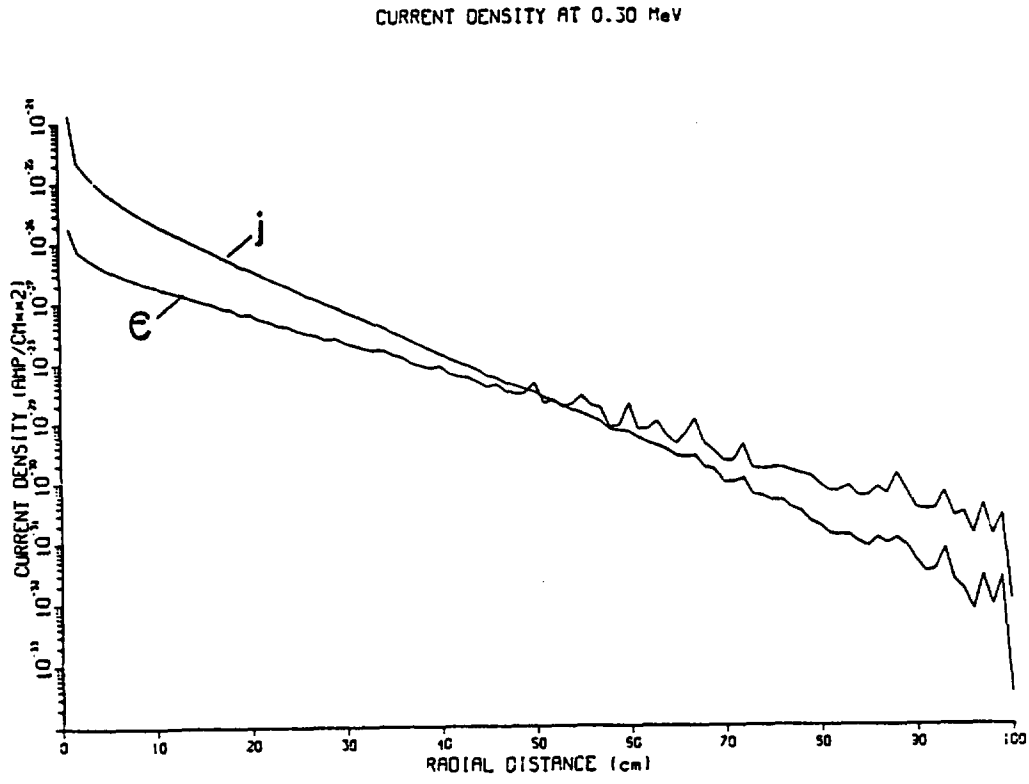

Figure 3.11. Electric current density in tuff from a 0.30 MeV photon emitted from an infinite line source. Values for e indicate accuracy relative to magnitude of current density.

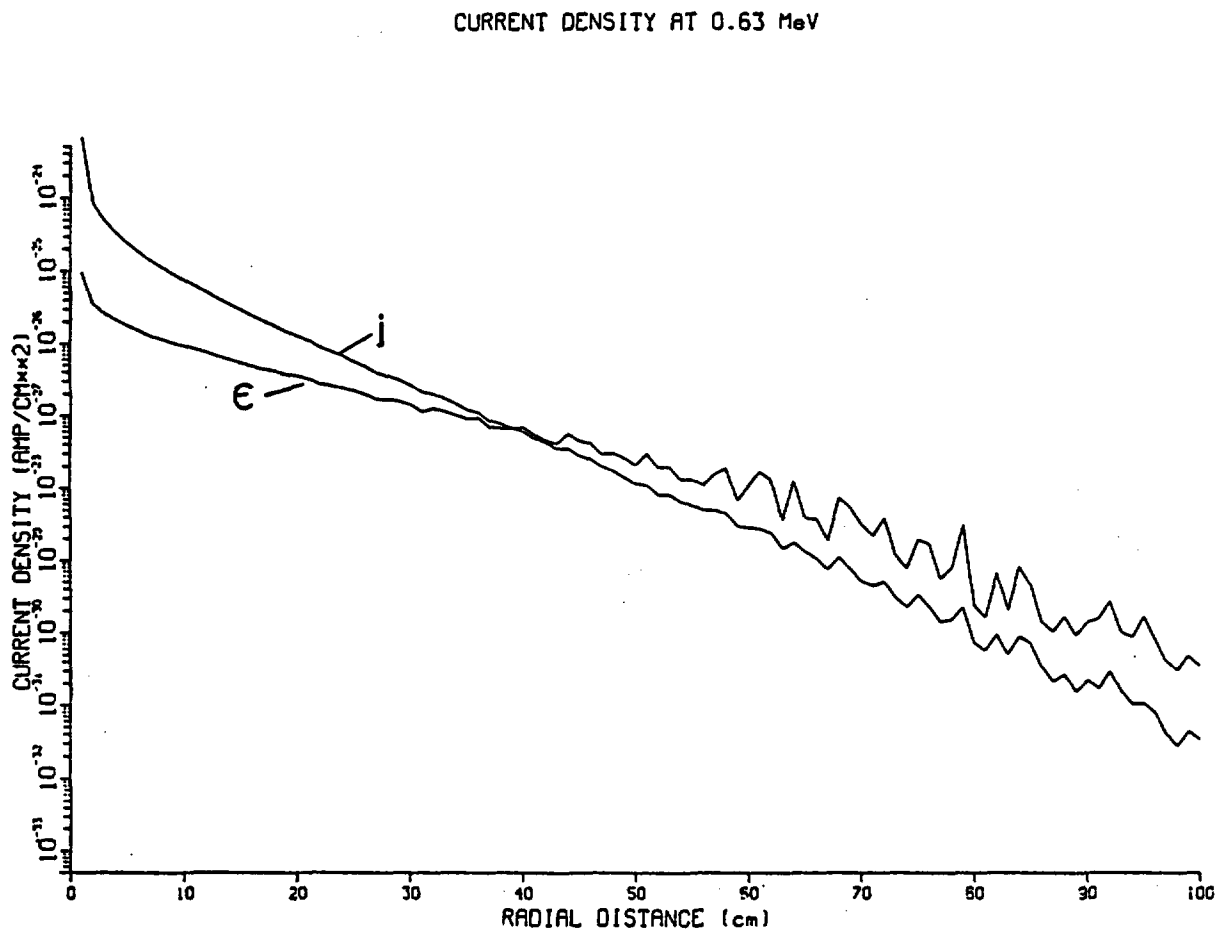

Figure 3.12. Electric current density in tuff from a 0.63 MeV photon emitted from an infinite line source. Values for ϵ indicate accuracy relative to magnitude of current density.

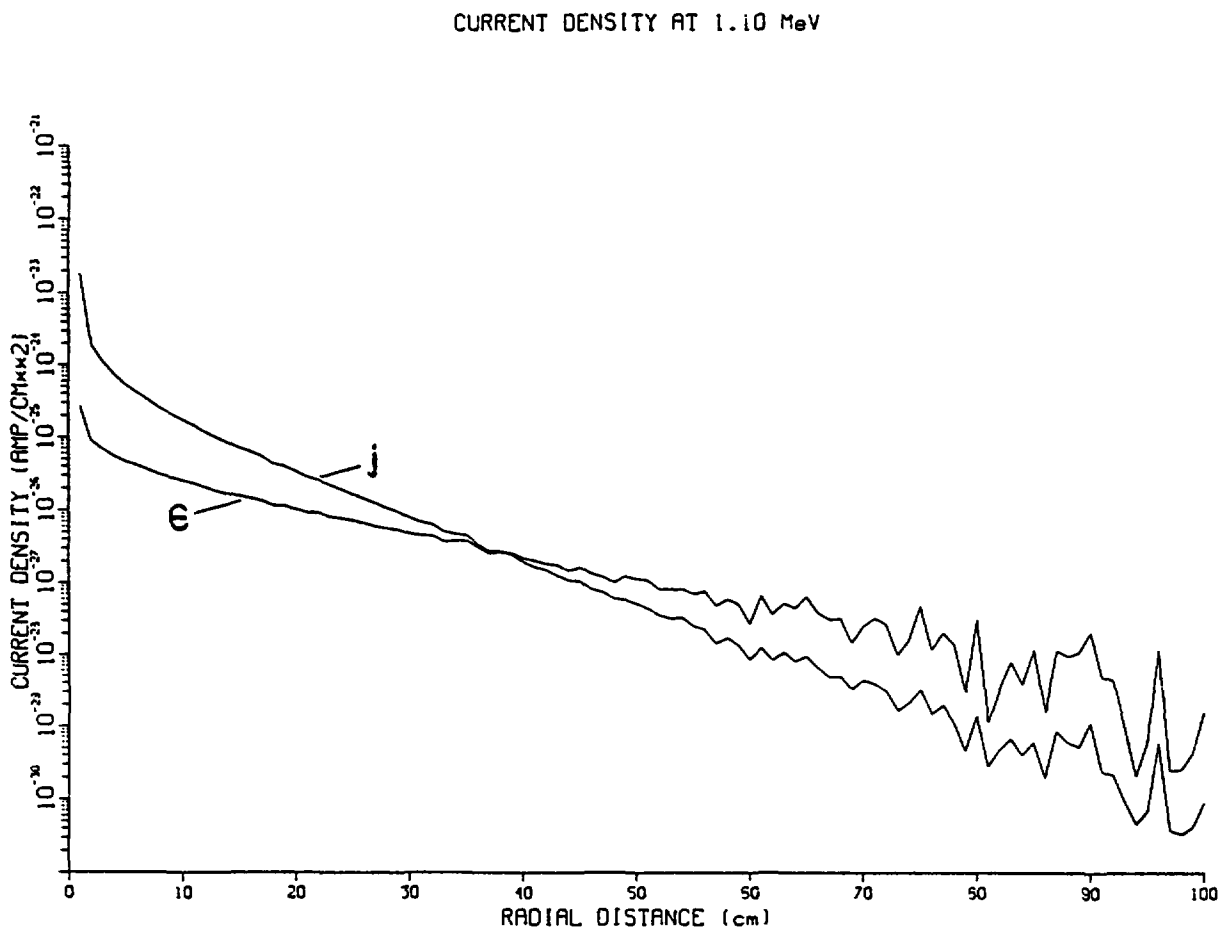

Figure 3.13. Electric current density in tuff from a 1.10 MeV photon emitted from an infinite line source. Values for e indicate accuracy relative to magnitude of current density.

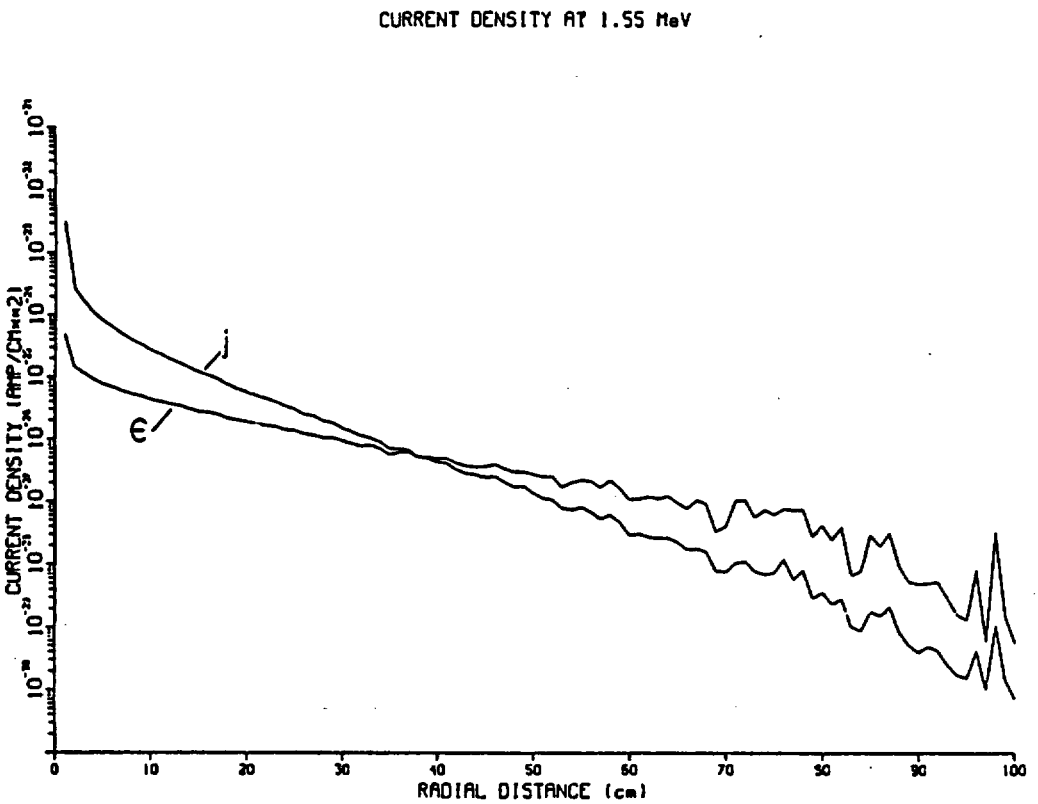

Figure 3.14. Electric current density in tuff from a 1.55 MeV photon emitted from an infinite line source. Values for e indicate accuracy relative to magnitude of current density.

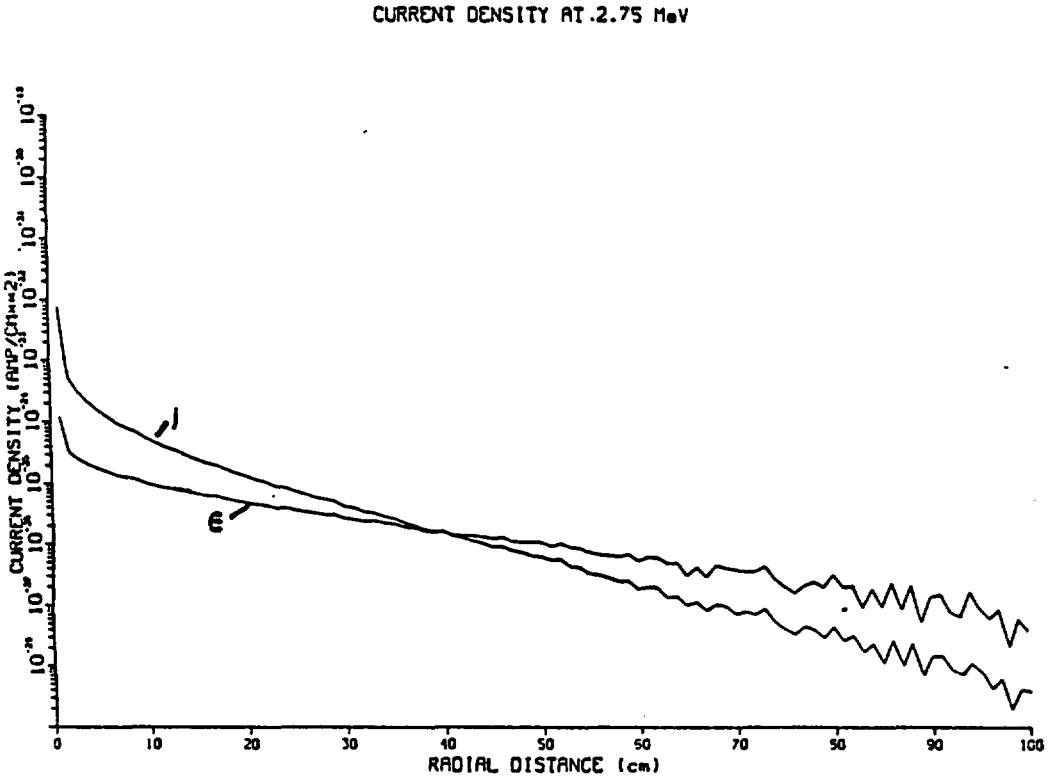

Figure 3.15. Electric current density in tuff from a 2.75 MeV photon emitted from an infinite line source. Values for e indicate accuracy relative to magnitude of current density.

3.5.2.3 Electric Field Intensity in Rock.

The electric current density is determined at each radial compartment using Ohm's law (Equation 3.8) at discrete gamma ray energies for each of five time periods. The total electric field encompassing the HLW canister is the summation of the electric field values determined at the five discrete energy levels. The resulting quantities are plotted versus radial distance at 10^2, 3×10^2, 10^3, 10^4, and 10^5 yrs in Figure 3.16. A value of 10^6 ohm-cm is assigned to the resistivity of unsaturated tuff in this calculation (Telford et al., 1976). This relatively high resistivity value is believed justified because the high temperatures expected at the canister will vaporize most liquid water proximal to the canister, thus, increasing the resistivity of the rock.

3.5.2.4 Ion Drift Velocities for Rock Case.

If it is assumed that a partially saturated fracture can be superimposed onto the rock mass without affecting the Compton current nor the resulting electric field, then ion drift velocities in the air space of the fracture can be calculated using Equation (3.7). Ion drift velocities are determined directly from electric field predictions using Equation (3.7) when mobility is known. A typical value for the mobility of ions in air is 2 $cm^2/V\text{-sec}$ (McDaniel and Mason, 1973). Ion drift velocities illustrated in Figure 3.16 are calculated at the above determined electric field intensities for this value of mobility. Ion drift velocities do not exceed about 10^{-6} cm/sec even at early times at regions proximal to the HLW canister.

3.5.3 Compton Current in Air

A second scenario is investigated to determine the potential of forced diffusion in air near a HLW canister. The importance of forced diffusion in a significantly large air space immediately proximal to a canister will exceed that for the case where the canister is completely encapsulated in rock mass. Significant air spaces around a canister can occur in large fractures in the disturbed zone around the canister borehole. These fractures or air spaces can be induced by a thermal load caused by the canister, by mechanical loading and unloading of stress in the rock or by dissolution of the material along a fracture surface and even the rock matrix itself. Large spaces can also occur where a borehole intersects a region of highly fractured rock. Leaving the borehole absent of backfill has been suggested (Fernandez and Freshley, 1983) as a means of reducing liquid flow under conditions of

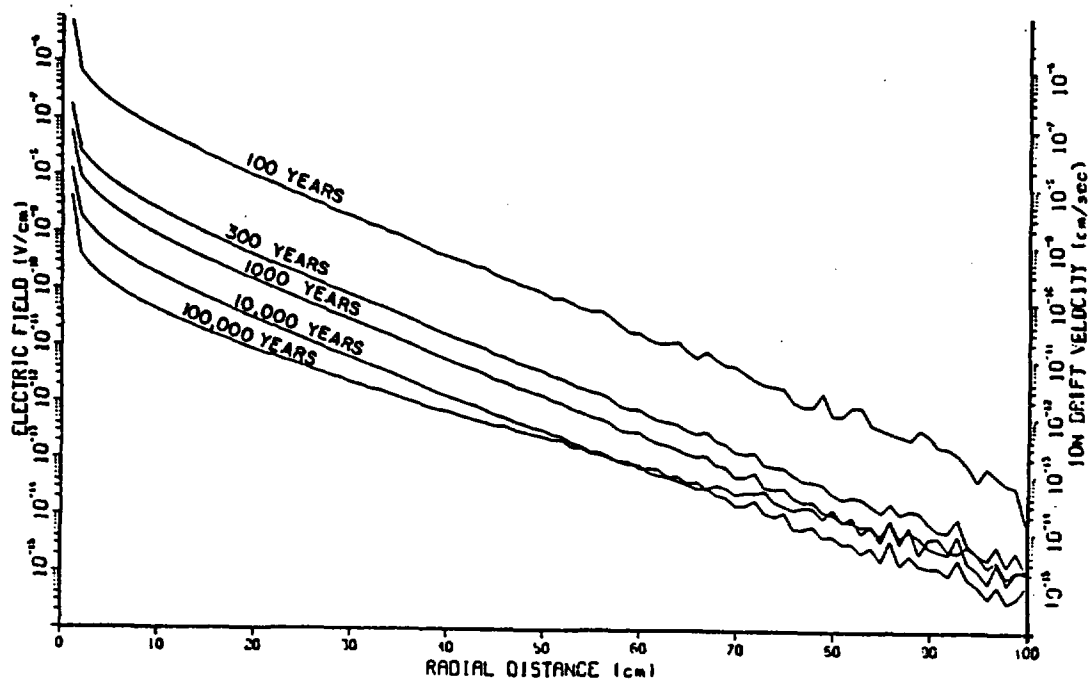

Figure 3.16 Electric field intensity (left axis) and ion drift velocity (right axis) in tuff at 10^2, 3 x 10^2, 10^3, 10^4 and 10^5 years versus radial distance from an infinite line source. Resistivity of the tuff is 10^6 ohm-cm and mobility is 2 $cm^2/V\text{-}cm$.

negative water pressure (Figure 3.9). Additionally, significant air spaces may result at locations where canister cladding fails.

COMPMC and SR are used to predict current density in air by the same methodology that was used for the rock mass model. SR is used to calculate the effective range/electron energy relationship for electrons travelling through air. The atomic mass of air has an assigned value of 28.9 and the atomic number has the value of 14.2 in these calculations. Air is assumed to be composed of 78% N_2 and 21% O_2.

3.5.3.1 Effective Electron Range in Air.

Similar to the case of the rock mass model, the coefficients for three second order polynomials are calculated from 23 data points to approximate the effective electron range/electron energy relationship. A straight line approximation is used for energy values of 0 to 0.01 MeV. The three polynomials appear as follows.

(3.56a) $-6.235E\text{-}2 + 2.318E\text{-}1\ x + 1.429E\text{-}2\ x^2 = y$

(3.56b) $-7.295E\text{-}3 + 1.102E\text{-}1\ x + 8.739E\text{-}2\ x^2 = y$

and

(3.56c) $-5.394E\text{-}5 + 1.128E\text{-}2\ x + 4.576E\text{-}1\ x^2 = y$

Figure 3.17 illustrates the computed values of effective electron range versus the electron energy and the associated approximating polynomials.

3.5.3.2 Current Density in Air.

COMPMC determines current density in air for the same five energy levels of the gamma ray source summarized in Table 3.1. The variable e is calculated at a 90% confidence interval for each energy level. The values of current density and e are plotted versus radial distance and are illustrated in Figures 3.18 to 3.22.

In order to obtain values of current density in air with a level of accuracy similar to the level of accuracy obtained by COMPMC for the rock mass simulation, it is necessary to record double the realizations for the air scenario (or 200,000 histories per photon energy level) compared to the number of realizations that were recorded for the rock mass. The necessity of doubling the number of simulations is attributed

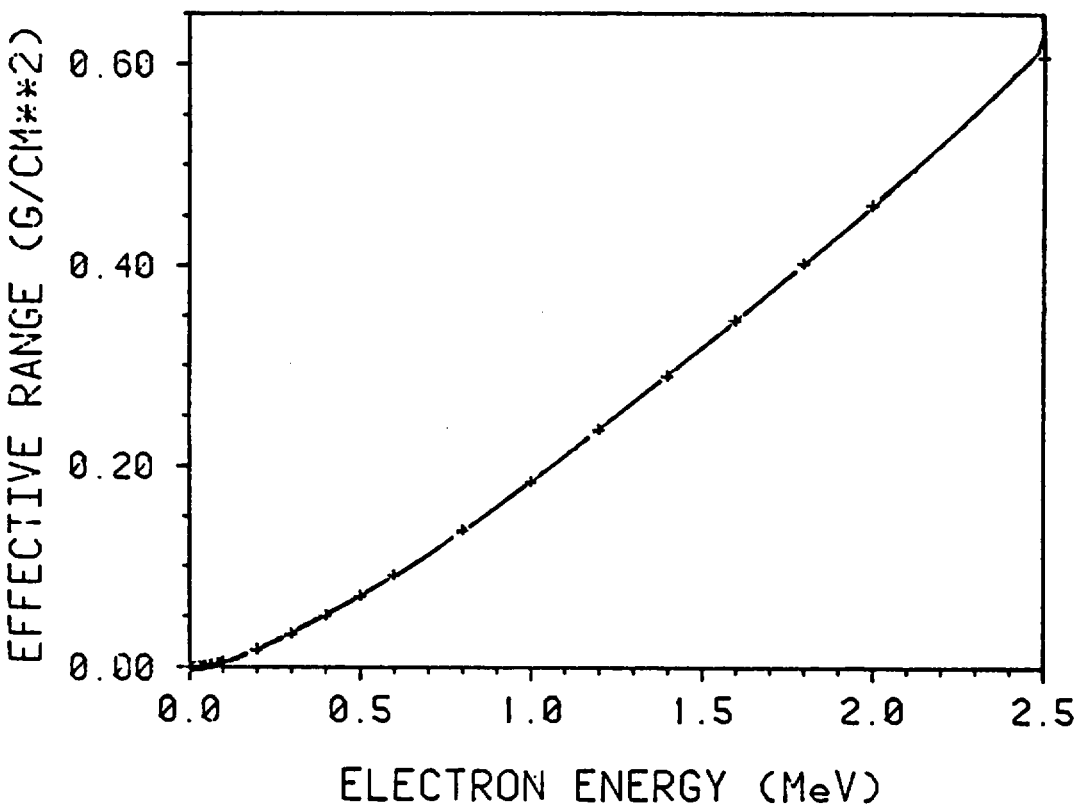

Figure 3.17. Effective range of electrons in air versus electron energy level.

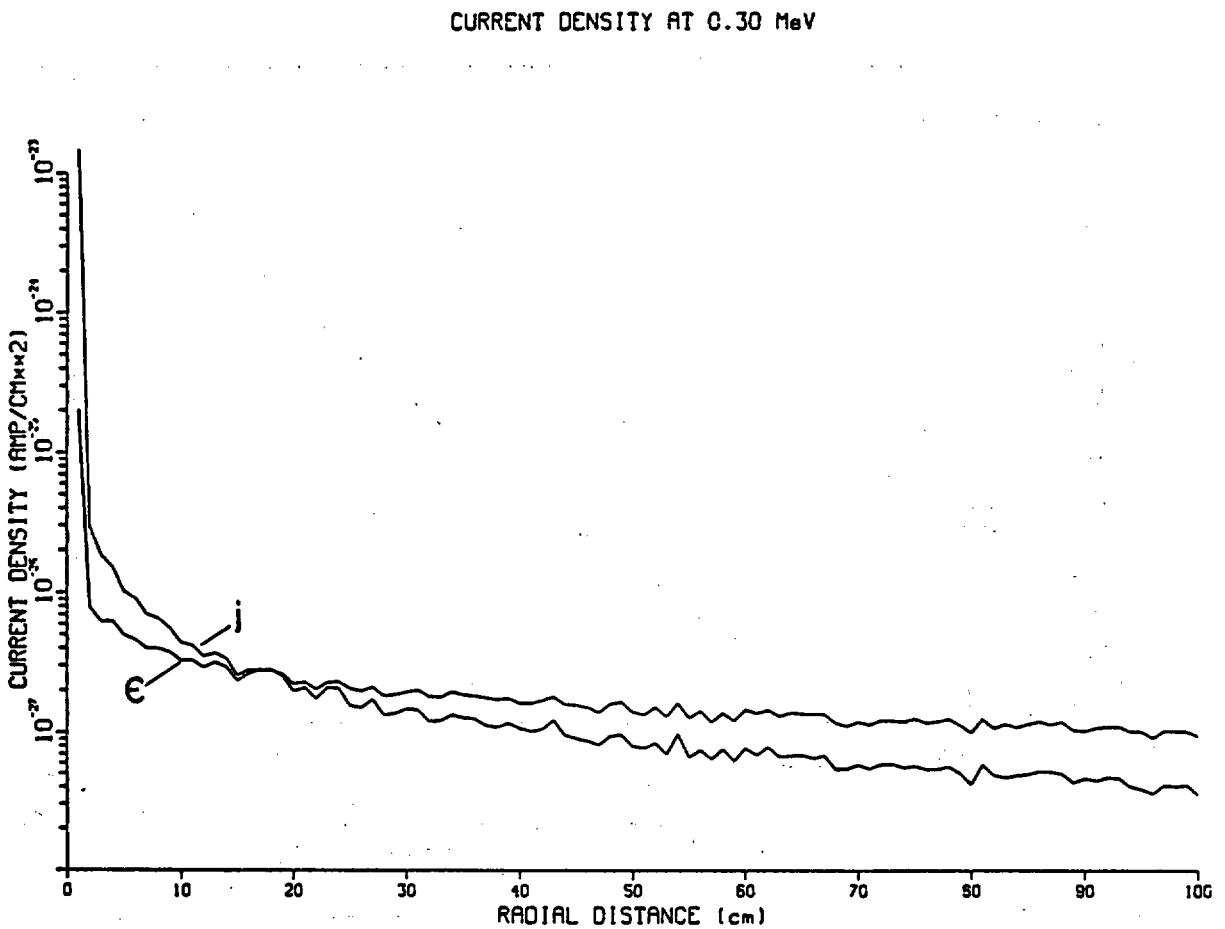

Figure 3.18. Electric current density in air from a 0.30 MeV photon emitted from an infinite line source. Values for e indicate accuracy relative to magnitude of current density.

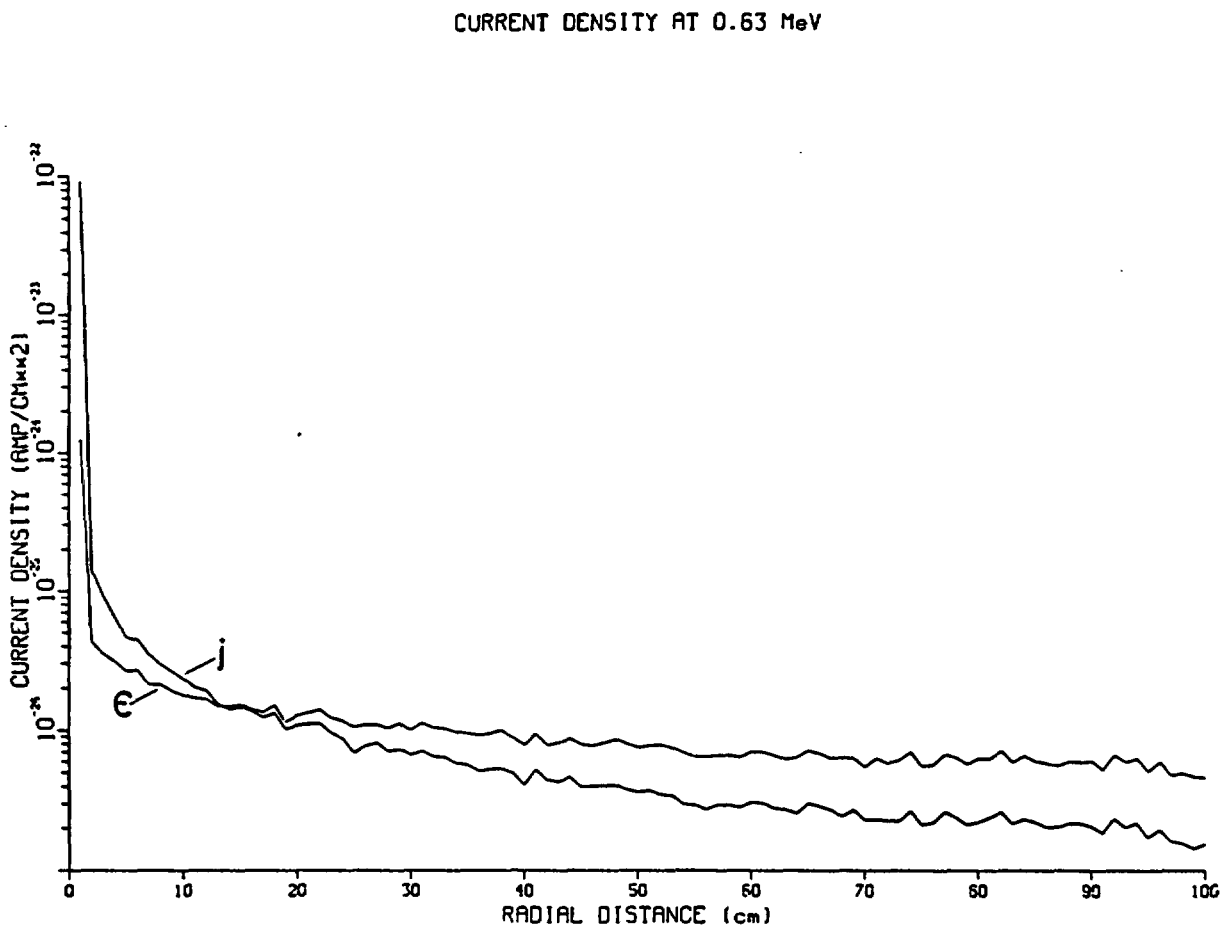

Figure 3.19. Electric current density in air from a 0.63 MeV photon emitted from an infinite line source. Values for e indicate accuracy relative to magnitude of current density.

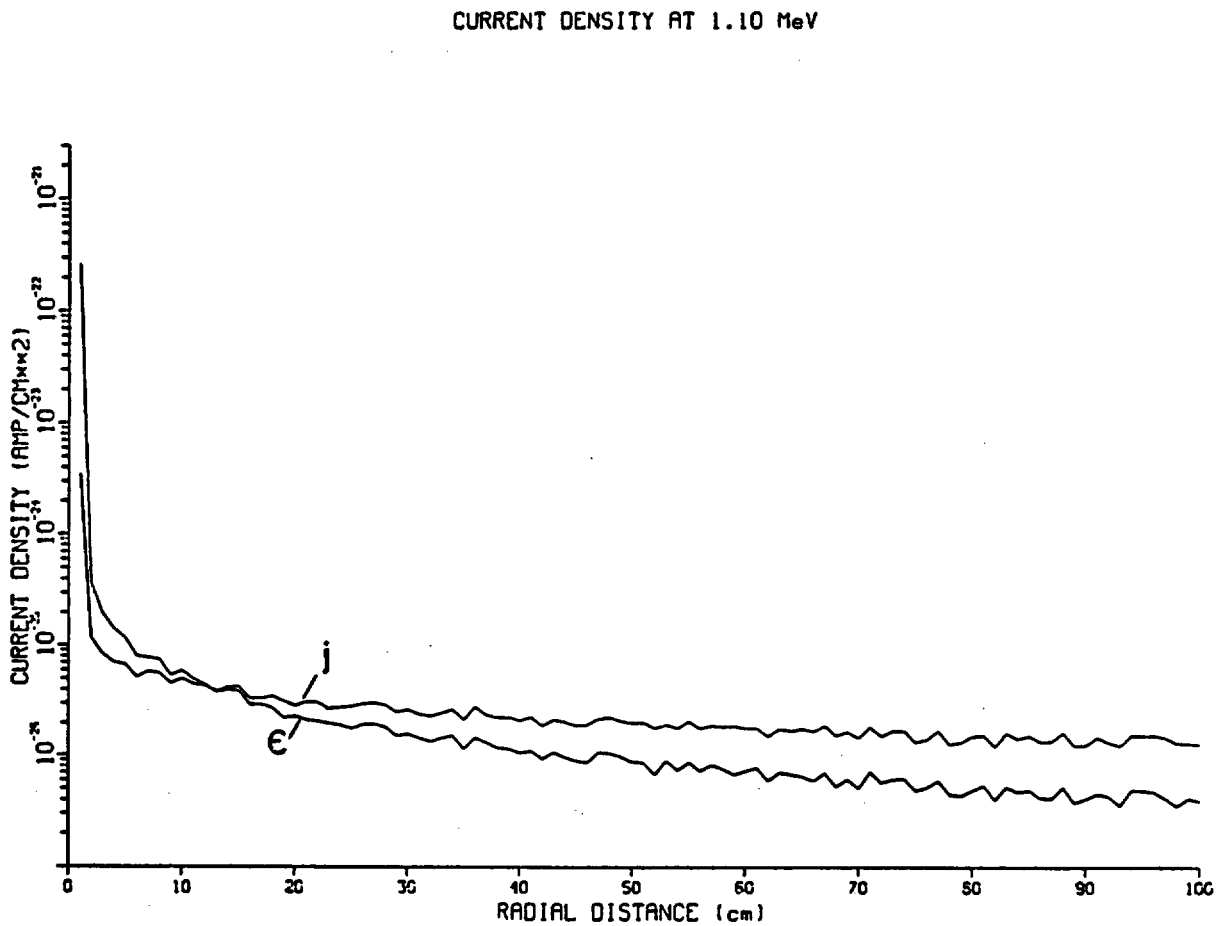

Figure 3.20. Electric current density in air from a 1.10 MeV photon emitted from an infinite line source. Values for e indicate accuracy relative to magnitude of current density.

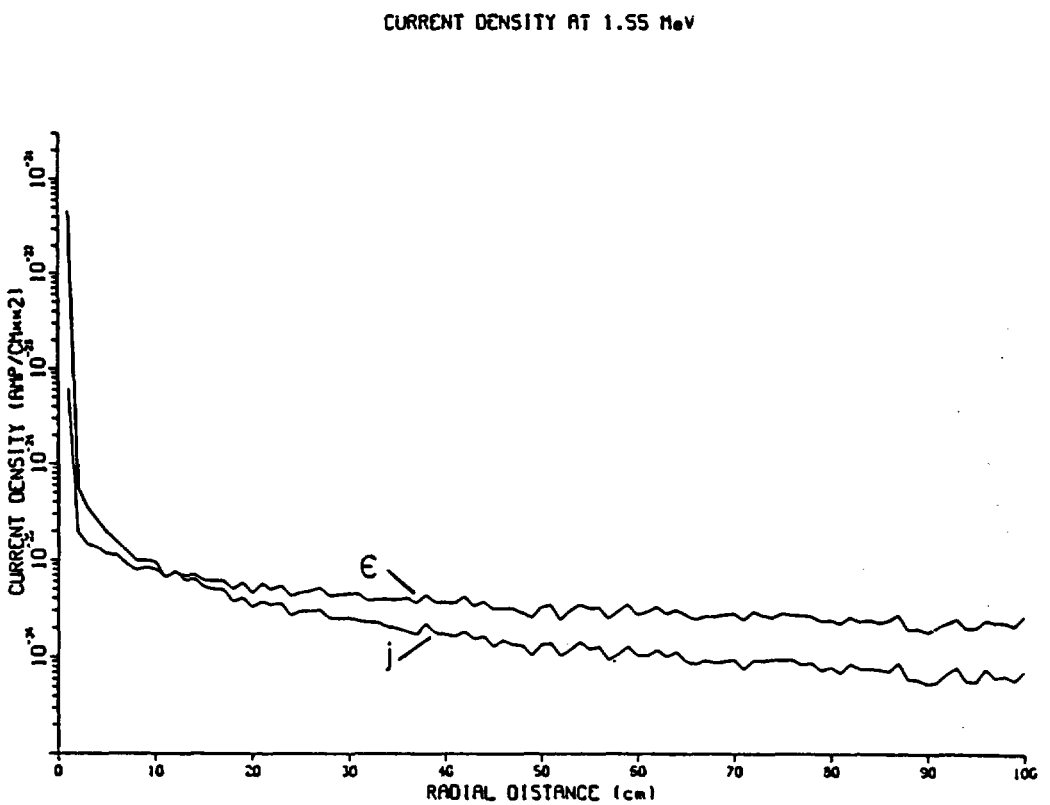

Figure 3.21. Electric current density in air from a 1.55 MeV photon emitted from an infinite line source. Values for e indicate accuracy relative to magnitude of current density.

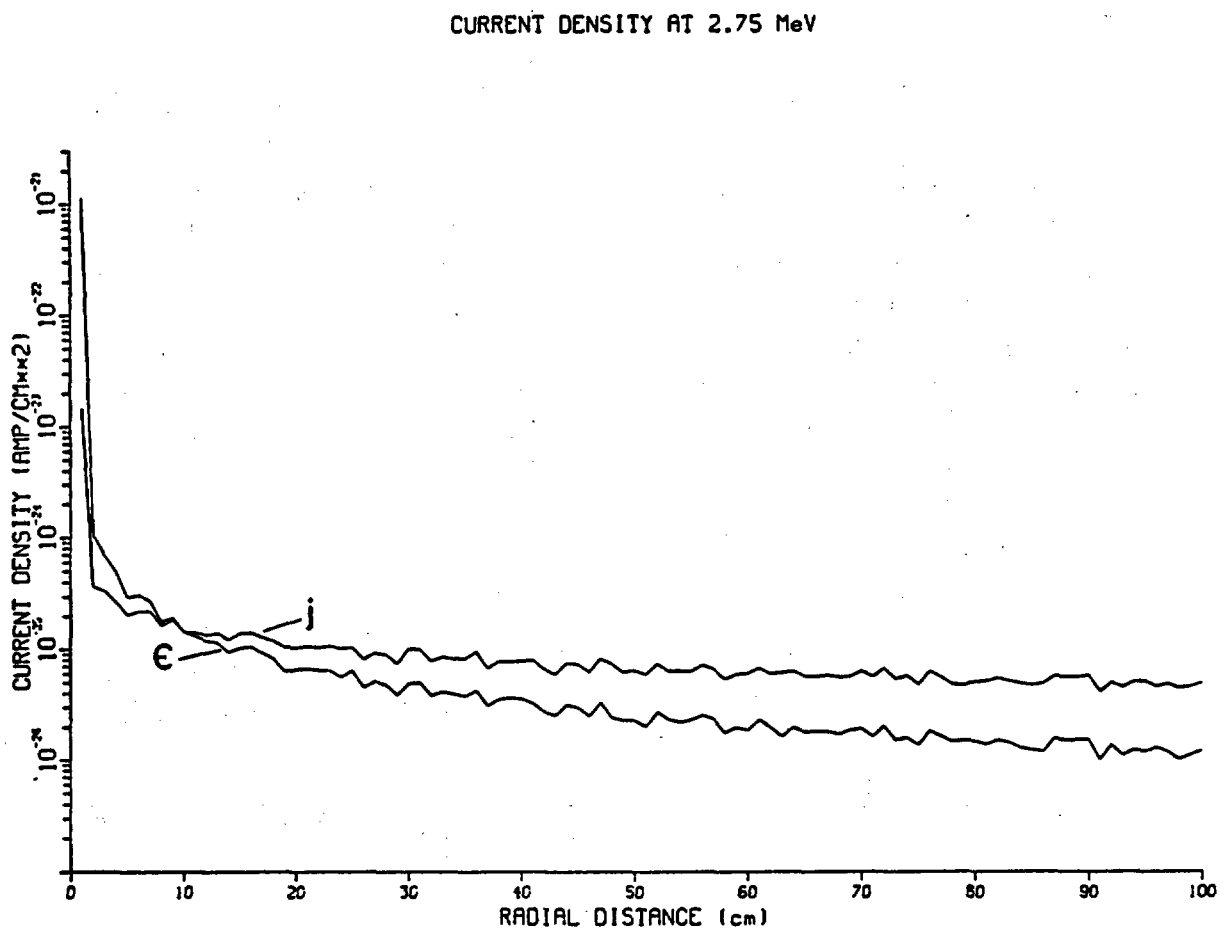

Figure 3.22. Electric current density in air from a 2.75 MeV photon emitted from an infinite line source. Values for e indicate accuracy relative to magnitude of current density.

to the fact that photons (and electrons) travel substantially farther in air than in rock and are, therefore, spread out over a greater distance.

Edge effects of current density near the canister are more pronounced than those observed for current density in the rock mass. Additionally, the falloff in the magnitude of current density versus radial distance is substantially less in air than in the rock mass. Although Figures 3.18 to 3.22 are only for a radial distance out to 100 cm, current density is calculated out to 400 cm through air with a continuing gradual decrease in current density observed.

3.5.3.3 Electric Field Intensity is Air.

A value of 10^{-15} (mhos/cm) for electrical conductivity of air is taken from atmospheric measurements recorded immediately following lightning flashes (Krider and Musser, 1982). The large degree of ionization expected at a HLW canister will affect the electrical conductivity, however the effect upon its value is not determined. Nevertheless, the electric field in air caused by Compton scattered electrons is determined using this value of electrical resistivity for the gas until a better understanding of the effect of ionization on gas electrical conductivity is gained. The intensity of the electric field out to a radial distance of 100 cm is illustrated in Figure 3.23.

3.5.3.4 Ion Drift Velocities in Air.

Ion drift velocity is also illustrated in Figure 3.23 with electric field intensity. Again, a value of 2 cm^2/V-sec is assigned to mobility. As an example, drift velocity is 250 cm/sec at a distance of 10 cm from the canister 300 years after emplacement. If the design period of a HLW canister is 300 years, sizable air spaces at the canister wall may exist at this time. Ion drift velocities as large as 1000 cm/sec are possible at small distances (1-3 cm) from the canister. Forced diffusion can, therefore, provide an important transport link from the canister to the geologic medium if ion density is sufficiently large.

Ion drift velocities and electric fields with an intensity as large as those indicated in Figure 3.23 can only be expected in a region totally devoid of any material other than air. Any material present in the electric field will tend to short circuit the return flow of electrons resulting in a lower effective resistivity and thus lower electric field intensities. One major electron pathway is through the liquid film present on the surfaces of fractures. Fracture surfaces absent of liquid film (such as would be expected proximal to the canister where

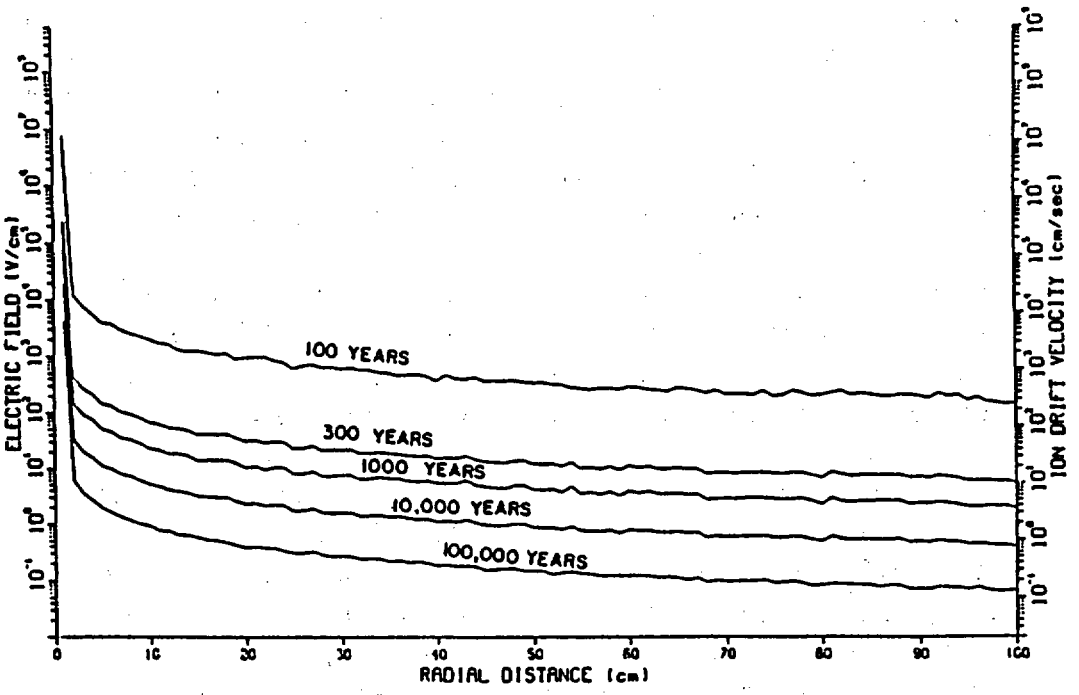

Figure 3.23 Electric field intensity (left axis) and ion drift velocity (right axis) in air at 10^2, 3×10^2, 10^3, 10^4 and 10^5 years versus radial distance from an infinite line source. Resistivity of the air is 10^{15} ohm-cm and mobility is 2 $cm^2/V\text{-}cm$.

temperatures are higher) will not provide pathways with as low a resistivity as fracture surfaces where a liquid film is present. The electrical effect of fractures or fracture surfaces on either the rock mass or air case has not been quantitatively evaluated.

3.5.4 Forced Diffusion Near a HLW Canister

The value of ion density needs to be determined before forced diffusion and the mass flux of radionuclides can be ascertained using Equation (3.1). However, ion density is the most difficult variable in Equation (3.1) to determine. Its value depends on two basic parameters, the density of airborne radionuclides and the fraction of the airborne radionuclides which are ionized. Airborne radionuclide density depends on several factors indirectly (such as temperature, matric potential, degree of fracturing and geochemical composition of the water and the rock mass) and directly on the vapor pressure of the species of interest and their thermodynamic and kinetic properties.

Determination of the fraction of airborne radionuclides which is ionized is another difficult parameter to estimate. It can not be accomplished until the ionization potential of high-level waste and the equilibrium ion density after recombination are determined.

Two limiting cases have been presented which illustrate the importance of ion flux which can be theoretically expected by forced diffusion under different conditions. A more probable scenario to be expected at a HLW repository will be a transitional case which incorporates properties from both extremes. Further analysis is necessary to evaluate a transitional case. Forced diffusion, if important, has potential as a transport mechanism in the zone near the repository. Additionally, the substantial intensity of electric fields in air resulting from Compton currents may contribute to other potentially important but yet unknown coupled processes.

4. AEROSOL TRANSPORT

A possible contributor to radionuclide vapor transport is a mechanism that produces an aerosol in the airspace of a partially saturated fracture. An aerosol originating in rock water would contain any soluble contaminant which could then be transported by diffusion or pressure flow. A physical system near a HLW canister that could bring about aerosol formation is driven by a mechanism referred to as countercurrent or a heat pipe.

The thermal regime at a HLW repository will consist of temperatures at the immediate site rising to 100°-450°C the first 100-200 years after waste emplacement (Wang et al., 1983). During the heating phase, the rock matrix and any saturated or partially-saturated fractures proximal to the repository will dry out. A thermal pulse will extend outward from the source with time. The temperature of the repository will decrease to near the pre-emplacement ambient temperature over a cooling phase lasting up to 10,000 years. When the temperature of the medium surrounding the repository decreases to below 100°C, the rock matrix and fractures will rewet to some degree.

A liquid film of a specified minimum thickness and ample air space overlying the liquid film is required for aerosol production to occur. Therefore, aerosol production and transport are confined to rock fractures and will not occur in the rock matrix. Only individual fractures and fracture systems are of interest in the investigation of aerosol transport.

Heat emanating from the repository will increase the temperature of the water film proximal to the repository and vaporize the liquid water. Water film closer to the repository will become thinner causing a movement of the liquid film toward the repository by larger negative pressures. The force of gravity acting on liquid water film in a vertical fracture located above the HLW repository would enhance flow toward the repository while upward film flow in a vertical fracture located below the repository would be inhibited. Water vaporized near the heat source will diffuse outwardly from the repository, condensing in fractures at a distance where the temperature is lower. The resulting vaporization-condensation and liquid film movement is illustrated in Figure 4.1 and is referred to as countercurrent (Dhir and Catton, 1982) or as a heat pipe (Cotter 1965). The heat pipe is a highly efficient mechanism which dissipates heat away from a heat source. This mechanism has been observed theoretically (Evans, 1982;

Pruess and Wang, 1984; Eaton et al., 1985) and in the laboratory (Gurr et al., 1952; Matthews, 1985).

The countercurrent process enhances the desirability of repository placement in the unsaturated zone because movement of liquid film water toward the repository could detain any radionuclides introduced into the geologic environment by a breached or failed canister.

A possible disadvantage of the above-mentioned setting is the vapor movement of radionuclides away form the repository in the air space of a partially-saturated fracture. Any physical process which contributes to vapor transport of radionuclides in a gaseous phase will contribute to the transport of aerosol.

A bubble created in the liquid film by gas desorption which bursts at the surface of a liquid film has the capability of introducing aerosol particles into the air space of a partially-saturated fracture. A bursting bubble can eject hundreds of droplets away from the surface of the liquid with initial horizontal velocities as high as 800 cm/sec (MacIntyre, 1972). Aerosol droplets vary in size and have a composition similar to the composition of the top few monolayers on the surface layer of the liquid film. Any solute present in the liquid can be ejected into the airspace. This includes heavier molecules such as the transuranic actinides. The physics that govern the inception, growth, movement and bursting of a bubble are discussed in greater detail.

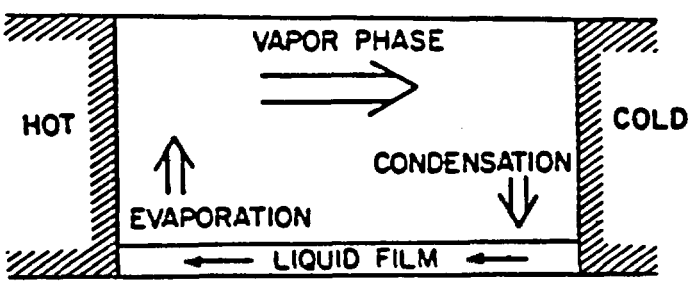

Figure 4.1. Schematic of countercurrent (or heat pipe). Liquid film moves toward heat source in response to gradient in negative pressure and vaporizes. The vapor moves away from heat source in response to pressure or concentration gradient and condenses at lower temperature.

4.1 Nucleation

Bubble nucleation is the process in which molecules cluster together to form the nucleus from which a bubble may grow. Nucleation can be categorized into two basic processes: 1) homogeneous nucleation which occurs in a pure liquid, and 2) bubble inception which occurs on an impurity in a liquid or is caused by radiation acting on the liquid, referred to as heterogeneous nucleation (Apfel, 1971).

4.2 Solubility of Gas in Liquids

The solubility of gas in liquid is important in several aspects of vapor transport of radionuclides. The gas-liquid partition coefficient, K_W, represents the concentration of a gas in moles per gram of the liquid divided by the moles of the gas per cm^3 of the overlying gas phase. The solubility of gas in liquid is also important in the phenomenon that results in the introduction of an aerosol to the airspace of a partially saturated fracture.

The solubility of a gas in liquid is dependent on the prevailing pressure and temperature at the canister. Gas phase pressure also depends on whether the canister remains wet at higher temperatures. Values for gas pressure are calculated by Pruess and Wang (1984) using a numerical model called TOUGH to simulate transport of unsaturated ground water and heat. Although total gas pressures exceed 5 bar for selected cases at early time (less than 20 yrs), the gas pressures asymptotically approach one bar after 50 yrs. The maximum canister surface temperature considered by Pruess and Wang is about 175°C. Because later times are of greater interest in this study, gas pressure is assumed to be one bar. Additionally, the effect of gas pressures greater than one bar on many of the processes is not known.

Temperature, however, will change dramatically both spacially and temporally at a HLW repository. The relationship between temperature and solubility is not a simple function and depends upon the particular gas/liquid system considered. Temperature/solubility relationships also vary differently over different ranges of temperature.

The Clapeyron equation relates temperature to vapor pressure in a system with two phases of a substance in equilibrium (Glasstone, 1946)

$$dP^*/dT = \overline{\Delta H}/T\,\overline{\Delta V} \qquad (4.1)$$

where P^* is vapor pressure and H is enthalpy (the bar denotes per mole).

If the two phases under consideration are liquid and vapor, and if it is assumed that the volume per mole of the vapor phase is much larger than the volume per mole of the liquid phase, it can be stated (for an ideal vapor) that

$$\overline{V} = V_{vapor} = R\ T/P^* \tag{4.2}$$

Substituting (4.2) into (4.1) gives the Clasius-Clapeyron equation

$$dP^*/P^* = \overline{\Delta H}\ /(R\ T^2)\ dT \tag{4.3}$$

Assuming that enthalpy is independent of temperature (which is only valid for small changes in temperature), integration yields

$$\ln(P^*_2/P^*_1) = \overline{\Delta H}/R\ [1/T_1 - 1/T_2] \tag{4.4}$$

Le Chatelier's principle states that if stress is applied to a system at equilibrium, the system adjusts, if possible, to annul the stress. Raising the temperature of a liquid-vapor system has the effect of applying a stress in the form of added heat. The stress can be absorbed by converting some of the liquid to vapor.

The stress can be annulled by another process. The heat of solution is the heat evolved when a constituent dissolves in the solution. The heat of solution in this case equals $\overline{\Delta H}$. If heat is evolved to the surroundings, $\overline{\Delta H}$ is positive. Conversely, if heat is absorbed from the surroundings, $\overline{\Delta H}$ is negative. $\overline{\Delta H}$ for CO_2, SO_2 and O_2 at one bar and moderate temperatures (0-50°C) is negative when the gases are dissolved in water. In fact, most gases have a heat of solution that is negative when dissolved in water (Sienko and Plane, 1965). It follows from Le Chatelier's principle that an increase in temperature will result in a decrease in solubility resulting in gases expelled from the liquid (Glasstone, 1946). The solution is saturated with a gas at the point where the gas is expelled as the temperature is increased.

Solubility of several gases in water has been investigated in detail (Cleaver and Han, 1980; Battino, 1982). Empirically determined values for Henry's constant can be used to determine mole fraction solubility for temperatures in the range of 300 to 600°K (Potter and Clynne, 1978). Henry's constant is defined

(4.5) $$H_{2,1} = \phi_2 P_2 / F_2 x_2$$

Where $H_{2,1}$ is Henry's constant; P_2 the gas pressure; x_2 the mole fraction gas solubility; F_2 the fugacity coefficient; and ϕ_2 the dissolved gas activity coefficient. F_2 is equal to one where Henry's law is valid. Fugacity is close to unity for the gases of interest (nitrogen, oxygen and the noble gases) and ϕ_2 differs little from unity at moderate pressures. At one bar gas pressure, Henry's law states that the mole fraction solubility equals the inverse of Henry's constant. Henry's law also states that for a given gas at constant temperature, the solubility of the gas in the liquid is proportional to the pressure of the gas over the liquid (Brown, 1963).

An empirical relationship relating gas solubility and temperature is determined by Cleaver and Han (1980). Gas solubility data for a given gas are regressed against temperature to obtain the constants of an equation of the form

(4.6) $$\ln X_2 = A_1 + A_2/(T/100) + A_3 \ln(T/100) + A_4 (T/100)$$

A scaling factor of 1/100 is used to make all the parameters of similar magnitude.

Values for the coefficients in Equation (4.6) for krypton, hydrogen, nitrogen and oxygen dissolved in water are listed in Table 4.1. The fourth coefficient is used in only one approximating equation.

- -

Table 4.1 Coefficients for Equation (4.6) to determine the solubility of gases in water (from Cleaver and Han, 1980).

System	A_1	A_2	A_3	A_4
Krypton and water	-61.1802	82.3244	21.5757	
Hydrogen and water	15.2051	-33.3273	-28.9664	5.5265
Nitrogen and water	-55.0165	69.2199	18.7292	
Oxygen and water	-54.0411	69.8961	18.5541	

- -

Values of mole fraction solubility versus temperature are plotted in Figure 4.2 for gases nitrogen and oxygen as an example.

4.3 Gas Desorption

Liquid film on a fracture surface will flow toward a HLW canister according to the physics of a heat pipe and result in an increase in the temperature of the liquid film as it approaches the heat source. Increased temperatures in the liquid film will decrease the solubility of gases that constitute air (basically nitrogen and oxygen) in the liquid.

The liquid film will supersaturate with the gases until the stress imposed on the system in the form of added heat is annulled. Desorption of supersaturated gases and restoration of equilibrium to the system will annul the stress.

Desorption can be accomplished by two distinct mechanisms: 1) quiescent desorption which is the phase transition of dissolved gas at a liquid/gas interface, and 2) bubble desorption which is the nucleation and growth of gas bubbles (Pasiuk-Bronikowski and Rudsinski, 1981). A distinct difference exists between gas bubbles and vapor bubbles. Vapor bubbles occur when a liquid is superheated and the liquid changes phase creating bubbles, while gas bubbles result from gas desorbing out of a liquid.

Gas supersaturation is defined as the bulk gas concentration in excess of the saturation concentration of the gas. An equation of continuity which describes the rate of change of gas supersaturation in a liquid is (Pasiuk-Bronikowski and Rudsinski, 1981)

$$(4.7) \qquad dZ/dt = r_g(Z,t) - F(Z,t)/V(t)$$

where Z is gas supersaturation in liquid, F is the rate of gas desorption, V is the volume of the liquid, and r_g is the rate of gas production by chemical reaction which is assumed here to be negligible. The rate of desorption is the sum of bubble and quiescent rates, or

$$(4.8) \qquad F(Z,t) = F_b(Z,t) + F_q(Z,t)$$

The time dependancy in (4.8) implies a direct dependency of desorption rate on temperature. A known rate of flow of the liquid film and a known thermal regime will permit determination of the saturation concentration at a given time.

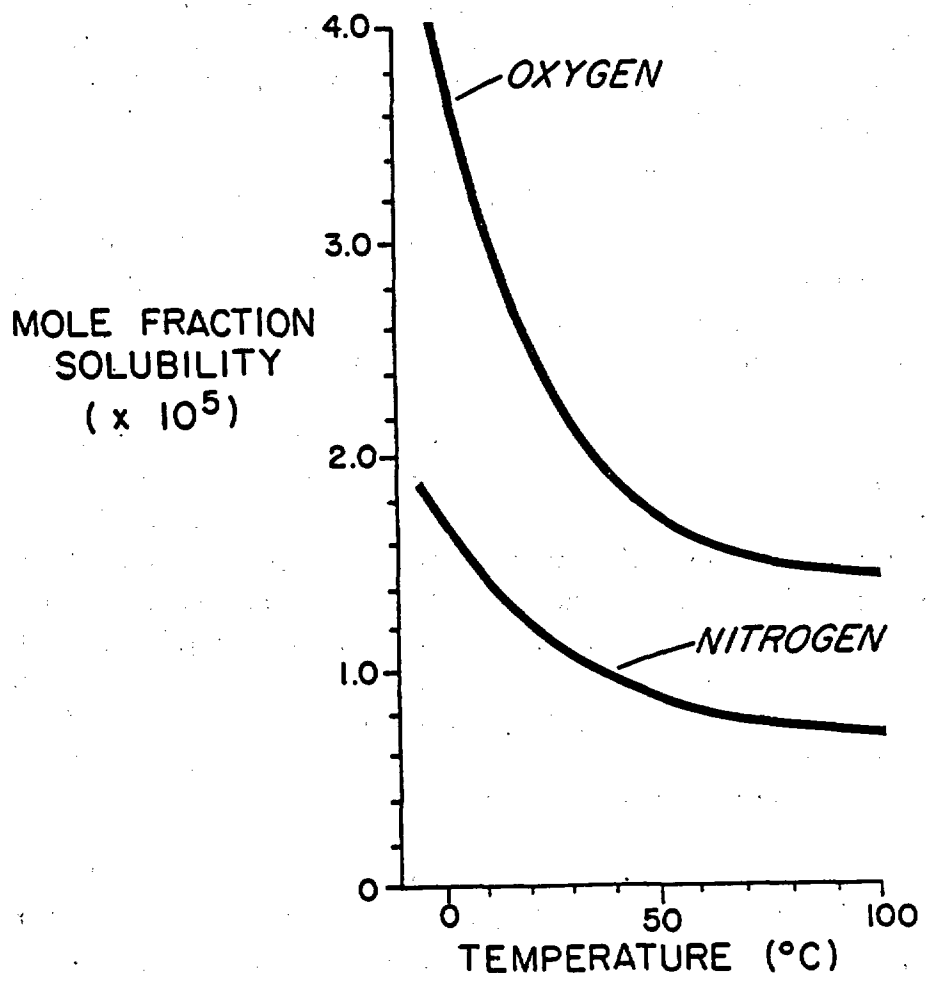

Figure 4.2. Mole fraction solubility of oxygen ans nitrogen in water versus temperature.

The distribution of the amounts of gas desorption between quiescent and bubble desorption is critical to aerosol formation. There will be no aerosol production and therefore no aerosol transport in the absence of bubble desorption.

The ratio of the sum of the partial pressures to the total pressure of the system is defined as the pressure reduction ratio (Weiland et al., 1977). When the pressure of a system is reduced to a level such that the pressure reduction ratio exceeds unity, bubbling has been found to occur. An analogous term to a HLW repository setting would be the temperature increase ratio. As was noted, gas solubility in a liquid is directly related to pressure and inversely related to temperature. The temperature increase ratio is defined as the prevailing system temperature divided by the temperature at which the amount of gas desorbed in the liquid would be at saturation. Desorption by bubbling will occur when the temperature increase ratio exceeds unity by a sufficient degree. This concept has not been verified experimentally.

The inception of bubbling is contingent on several factors in addition to the temperature increase ratio, namely the rate of desorption and the purity of the system. Pressure reduction ratios as high as 3.75 have been achieved without bubbling in a pure system at a sufficiently slow desorption rate (Schweitzer and Szebehely, 1950). A pure system is one in which a minimum of nucleation sites is available. The liquid film on a fracture surface will have particulate matter suspended in the liquid. Asperities on the fracture surface and the suspended particulate matter will supply numerous nucleation sites, therefore, the temperature increase ratio will be considerably closer to unity.

Nucleation sites can also be supplied by the process of radiolysis (Norman and Spiegler, 1963). Radioactive material from a HLW canister is capable of producing an assortment of radiation types. Radiation passing through water creates a thermal spike which expands explosively, thus, producing pressure waves. Surface tension of water breaks the pressure wave into discrete regions of water vapor, hydrogen and oxygen gas. Hydrogen and oxygen gas are therefore produced by the radiolysis of water. The resulting microbubbles can act as nucleation sites in a supersaturated solution.

The type of radiation impinging on water molecules affects the quantity of radiolytic products. Burns and Sims (1981) irradiated water with five different radiation types (^{60}Co gamma, protons and ^{4}He, ^{14}N and ^{20}Ne ions). A significant range in amounts of radiolytic products (OH radical, HO_2 radical, H_2 and H_2O_2) was observed. It appears that the

type of radioactive waste buried in a canister will affect the available number of nucleation sites produced by radiation.

4.4 Diffusion Process and Bubble Growth

The growth of a spherical bubble from a point of inception with a negligible radius occurs by diffusion of gas across the bubble wall from excess gas absorbed in the liquid. Subsequent to nucleation, the dynamics of gas bubble growth are governed by the physical laws of motion. The diffusion of gas from liquid into the bubble obeys Fick's law of diffusion (Equation 2.14) where D is the diffusion of gas in the liquid. The size of the gas bubble and rate of bubble growth are related to pressure in the liquid by equations of viscous flow. Simply stated, the pressure of the gas in the bubble provides the force for bubble growth. The driving force is countered by inertia and viscosity of the fluid and surface tension of the bubble wall.

An analysis of bubble growth requires several assumptions to justify the following mathematical development: 1) a solitary bubble is considered and it is located in a sufficiently large space such that inter-bubble forces can be neglected, 2) the gas bubble is in an incompressible Newtonian fluid with constant viscosity (the concentration of gas to be considered is small enough so that the viscosity of the fluid is unaffected), 3) the gas behaves in an ideal manner, diffuses according to Fick's law and the concentration across the bubble wall abides by Henry's law 4) a state of equilibrium is assumed at the growing surface and 5) the liquid film is assumed to be sufficiently thick for bubbling to occur. The aforementioned assumptions are considered valid at possible repository conditions.

The spherical nature of the problem suggests the use of a spherical coordinate system. A Lagrangian coordinate system is employed with the origin located at the center of the bubble. An angular dependence is therefore avoided.

Fick's second law with a constant diffusion coefficient, D, is written

$$D\nabla^2 c = \partial c / \partial t \qquad (4.9)$$

If the effect of the motion of the liquid relative to the bubble is accounted for, then the material derivative is used (Birkhoff et al., 1958)

(4.10) $$D \nabla^2 c = Dc/Dt$$

In spherical coordinates, Equation 4.10 becomes

(4.11) $$D (1/r^2) \partial c/\partial r (r^2 \partial c/\partial r) = \partial c/\partial t + v \partial c/\partial r$$

where the second term on the right hand side accounts for the relative motion of the liquid and v is the radial velocity of the liquid.

The continuity equation is

(4.12) $$D\rho/Dt = -\nabla \cdot \rho v$$

where ρ is gas density.

Assuming an incompressible fluid, integration of (4.12) yields the relationship

(4.13) $$v r^2 = F(t)$$

where F(t) varies with time only. F(t) is evaluated for the boundary conditions at the surface of the bubble.

Conservation of mass at the bubble surface (r = R) requires that (Scriven, 1959)

(4.14) $$d/dt(4\pi R^3\rho/3) = 4\pi R^2 \rho_l [\dot{R} - v(R,t)]$$

where ρ_l is the liquid density and where the left side of the equation is the change in mass determined using the vapor density inside the bubble. R is the time derivative of the radius at the bubble surface (i.e, r equals R). The right side of Equation (4.14) is the mass flux across the bubble surface where the bracketed term denotes the velocity of the bubble surface, R, less the velocity of the liquid at the bubble surface, v(R,t). If it is assumed that vapor remains invariant with time relative to the rate of growth of the bubble, the following relationship results

(4.15) $$v(R,t) = \dot{R} \rho_r$$

where reduced density is defined

(4.16) $$\rho_r = (\rho_l - \rho)/\rho_l$$

Substituting (4.16) into (4.15) and evaluating at the surface of the bubble yields

$$v(R,t) = \dot{R}\, R^2\, \rho_r / r^2 \tag{4.17}$$

Substitution of (4.17) into (4.11) yields the final form of the equation describing gas diffusion across the surface of the bubble, which is

$$D\,(1/r^2)\,\partial c/\partial r\,(r^2\,\partial c/\partial r) = \partial c/\partial t + R\,\dot{R}^2/r^2\,\partial c/\partial r \tag{4.18}$$

where ρ_r is unity for low gas concentrations.

The remaining boundary conditions required to describe gas concentration are (Barlow and Langlois, 1962)

$$\lim_{r \to \infty} c(r,t) = C_0 \qquad t > 0 \tag{4.19a}$$

$$c(r,0) = C_0 \qquad r > R_0 \tag{4.19b}$$

and

$$c(R + 0,\, t) = K_g(t) \qquad t > 0 \tag{4.19c}$$

where c_0 is the initial gas concentration, R_0 is the initial bubble size and K is a constant. Equation (4.19c) is Henry's law.

4.5 Equations of Viscous Flow

Growth of a gas bubble in liquid will generate a velocity field in the liquid. The resulting velocity field is governed by the Navier-Stokes equation (Landau and Lifshitz, 1959)

$$\rho_\ell Dv/Dt = -\nabla P + \mu' \nabla^2 v \tag{4.20}$$

where the gravity term is neglected and μ' is the viscosity of the liquid. For a homogeneous medium and an incompressible fluid, the continuity equation is expressed as

$$-\nabla \cdot v = 0 \tag{4.21}$$

Following the development of Barlow and Langlois (1962), Equation (4.21) can be written in spherical coordinates as

(4.22) $\partial v/\partial r + 2\, v/r = 0$

Equation (4.20) can be written in spherical coordinates as

(4.23) $\rho_\ell[\partial v/\partial t + v\, \partial v/\partial r] = -\partial P/\partial r + \mu[1/r\,(\partial^2 r\, v/\partial r^2) - 2\, v/r^2]$

Substitution of (4.17) into (4.23) and integrating yields

(4.24) $2\, R\, \dot{R}^2/r + R^2\, \ddot{R} - R^3\dot{R}^2/(2\, r^3) = (P - P_a)/\rho_l$

The velocity field created by bubble growth will result in a stress field which tends to retard the growth of the bubble. The components of the stress field in the liquid are

(4.25a) $S_{rr} = -P - (4\mu' R^2\, \dot{R})/r^3$

(4.25b) $S_{\theta\theta} = S_{\phi\phi} = -P + (2\mu' R^2\, \dot{R})/r^3$

(4.25c) $S_{\theta\phi} = S_{\phi r} = S_{r\theta} = 0$

and for the region within the bubble,

(4.25d) $S_{rr} = S_{\theta\theta} = S_{\phi\phi} = -P_g(t)$

(4.25e) $S_{\theta\phi} = S_{\phi r} = S_{r\theta} = 0$

where P is the pressure at some point outside the bubble and P_g is the pressure of the gas within the bubble. θ and ϕ are the azmuth and declination angles in the spherical coordinate system.

The tangential forces, $S_{\theta\phi}$, $S_{\phi r}$ and $S_{r\theta}$, across the bubble wall must be continuous as indeed they are. The normal force, S_{rr}, has a pressure jump of 2 s/R at the surface of the bubble because of surface tension as stated in the expression

(4.26) $-P - (4\mu' R^2\, \dot{R})/r^3 = -P_g(t) - 2\, s\, /R$

where s is the surface tension of the bubble. Since r equals R at the bubble wall, Equation (4.26) becomes

(4.27) $P = P_g(t) - 2/R\,(s + 2\mu' \dot{R})$

which is an expression defining pressure immediately outside the bubble wall.

To obtain an ordinary differential equation relating the pressure inside the bubble to the growth at the bubble surface, substitute (4.27) into (4.24)

$$(4.28) \qquad 3\dot{R}^2/2 + R\ddot{R} + 2s/(R\rho_1) + 4\mu R/(R\rho_1) = (P_g - P_a)/\rho_1$$

If the gas inside of the bubble is assumed to be ideal, P_g can be defined by the ideal gas law

$$(4.29) \qquad P_g = R\,C\,T/M$$

and substituted into Equation (4.28).

Equation (4.28) relates the size of the bubble to the density of the gas in the bubble relative to the concentration of the gas in the liquid. Equation (4.18) describes the rate of gas diffusion across the bubble wall. Solving these two equations at the appropriate boundary conditions (4.19a-c) defines the dynamics of a gas bubble.

Gas bubbles tend to rise in a liquid because of buoyancy forces. Bubbles existing in the liquid film will be small enough so that surface tension will tend to keep the bubbles spherical. Theoretical drag, D_r, on the bubble is (Birkhoff, 1960)

$$(4.30) \qquad D_r = 6\pi r v \mu(2\mu' + 3\mu)/(3\mu' + 3\mu)$$

where μ' is the viscosity of the liquid. If $\mu' >> \mu$, Equation (4.30) reduces to

$$(4.31) \qquad D_r = 4\pi r v\,\mu'$$

However, experimentally the bubble behaves as

$$(4.32) \qquad D_r = 6\pi r v \mu'$$

which is Stokes equation of buoyancy. The apparent paradox may be attributed to the bubble behaving as if it was rigid. The rigidity may be caused by a monomolecular layer of impurities on the bubble interface which causes the interface to be resistant to deformation (Bond, 1927).

4.6 Aerosol Phenomenon

The rupture of a bubble at the surface of the ocean is the principle mechanism of particulate transfer from sea to air (MacIntyre, 1972). The same mechanism can introduce aerosol droplets into the air space of a partially-saturated fracture. A bubble at the air-liquid film interface will burst as a result of evaporation in a millisecond or less ejecting droplets into the airspace above the liquid film. The top several monolayers of liquid of which the bubble cap is composed can be of different composition than liquid film as a whole.

One possible cause of compositional differences are concentration gradients which form in the liquid film. The addition of a solute to the liquid film causes a difference in the resulting surface activity (McBain and Davies, 1927; and Bloch and Luecke, 1972). A solute that lowers the surface activity will diffuse toward the liquid-air interface (Taylor and Glasstone, 1931). Organic molecules are an example of this. Inorganic molecules increase surface activity and tend to diffuse away from the liquid-air interface. The top one or several monolayers at the surface of the liquid film can, therefore, be more concentrated with solutes that lower the surface tension of the liquid than the average concentration of the liquid.

The significance of higher concentration surface monolayers arises when a gas bubble bursts at the liquid-air interface. At the moment before a bubble bursts, the bubble wall interfacing with the airspace of the fracture is composed of the top one or several monolayers of the liquid film. Bubble wall fragments ejected into the airspace contain a higher concentration of the solute than a volume average of the liquid film. The amount of solute contained within aerosol droplets is increased by this phenomenon. Solutes of interest include radionuclide species such as some of the fission products and the transuranic actinides.

Fractionation of chemical species in the top monolayers can also cause a differentiation in solution composition (Komabayasi, 1962; Bloch et al., 1966). Fractionation may occur in response to the species atomic weights or according to an undetermined mechanism.

The phenomenon of a bubble bursting at the surface of the liquid film, therefore, provides a vehicle to eject hundreds of aerosol droplets of various sizes into the airspace of the fracture provided the proper physical conditions exist at a HLW site necessary for the bubble phenomenon to occur. Larger aerosol droplets (diameter $> 10^{-6}$ cm) will fall back into the liquid film because of gravity. Smaller droplets,

however, will remain suspended in the airspace at least momentarily. The production of aerosol droplets will increase as the liquid film flows toward the HLW repository because of added heat and reduced solubility of gas in the liquid fill. A concentration gradient of droplets in the airspace will occur. Diffusion will transport the aerosol from a region of high concentration (near the HLW repository) to a region of lower concentration (away from the HLW repository). Aerosol droplets will remain suspended in the airspace until either diffusion results in their reabsorption into the liquid film or until the droplets reach a fully saturated section in the fracture and are then reabsorbed.

The mean life time, $\bar{t}$, of a particle between two neutrally charged walls is (Fuchs, 1964)

$$\bar{t} = b^2/12\ D \qquad (4.33)$$

where b is the aperture between the walls and D is the diffusion coefficient. Thus, in a one micrometer wide fracture, the mean life time of a particle is about 2.8×10^{-9} sec where the diffusion coefficient has an assumed value of 0.3 cm^2/sec. A bubble fragment ejected at 800 cm/sec can travel an average of 2.2×10^{-6} cm before resorbing onto the liquid film on the fracture surface. Similarly, the mean life of a particle in a fracture with aperture of 1 mm is 2.8×10^{-3} sec during which time a particle can travel 2.2 cm.

The liquid film on fracture surfaces, however, can provide likely pathways for the return flow of electrons traveling in response to Compton scattered electrons. Fracture surfaces will not be electrically neutral and the above expression (Equation 4.33) will not be valid for ionized aerosol particles. A particle with a negative charge will repel, to some degree, reabsorption onto the fracture surfaces and will possibly travel further while airborne. However, a positively charged ion will be attracted to a fracture surface and sorbed.

4.7 Analysis of Aerosol Formation at Repository Conditions

The prospect of aerosol formation at expected conditions at a HLW repository located in unsaturated fractured rock as proposed in this work has been analysed by Smith et al., (1985). They conclude that gas bubbles and aerosol formation will never occur at any foreseen repository conditions. The arguments they used are based on 1) the expected physical conditions in fractured rock at a HLW repository and 2) an analytic diffusion model for supersaturation of air in water. The major points of their analysis are discussed in this section.

Ogard et al. (1983) measured fracture apertures of 57 to 252 μm for natural fractures located in six core samples of tuff. The maximum thickness on the surface of a partially saturated fracture with this aperture is approximately 100 μm. Day (1964) used a diffusion cloud chamber which forced compressed air through a column of water to optically measure ejected droplets. It was determined that no aerosol particles are ejected by gas bubbles that have a radius less than 100 μm. Thus, the liquid film on a fracture surface should be a minimum of 100 μm thick and fracture apertures must be of an order of magnitude of at least several hundred μm to provide viable conditions for bubble formation.

Placement of a repository shaft and canister boreholes and the heat emanating from high level waste will create a disturbed zone enveloping a repository site. The effect of the disturbance on the natural fracture system is not entirely understood. It is conceivable that fracture apertures can be altered (reduced or enlarged) by thermal, chemical, hydrologic or mechanical forces. Additionally, the six core samples tested by Ogard et al. do not adequately characterize the entire zone of canister placement for a HLW repository. The possibility of fracture apertures greater than 250 μm cannot be totally dismissed.

Secondly, Smith et al. (1985) developed an analytic model to examine the variation in supersaturation of gas in water for various values of selected parameters used to define a repository site. A minimum level of 2% supersaturation was deemed necessary for bubble formation (Hsu and Grahm, 1976). The equilibrium solubility of air in the liquid film was assumed to decay exponentially with a decay constant, t_d, of 100 years. This assumption translates to a 62.3% change in solubility in 100 years.

Fick's second law is the governing equation used to calculate the concentration of gas in the liquid film

$$D_{AB}\, \partial^2 c / \partial x^2 = \partial c / \partial t \qquad (4.34)$$

where the boundary and initial conditions are

$$c(x,0) = c_0 \qquad (4.35a)$$

$$\partial c(0,t) / \partial x = 0 \qquad (4.35b)$$

and

(4.35c) $c(L,t) = (c_0-c_f) \exp(-t/t_d) + c_f$

where c_0 is the initial gas concentration, c_f is the final gas concentration in the liquid and t_d is an exponetial decay time constant.

Smith et al. solve Fick's second equation for the prescribed conditions by first converting the equation into non-dimensional form, applying a finite Fourier transform, inverting and finally expressing the answer in terms of the degree of supersaturation as a function of the dimensionless variables plus the exponent of time divided by the time constant.

It is not explicitly stated if air solubility in liquid is determined at a fixed location along the fracture or at a point in the liquid as it moves toward the heat source in response to the dynamics on a heat pipe. By assuming a decay constant of 100 years, Smith et al. suggest they are examining the decrease in solubility of gas in liquid at a fixed location. The decrease in solubility would occur over a time frame of an order of magnitude of 100 years in their analysis.

This analysis, however, does not represent the decrease in gas solubility of the liquid film during its movement toward the heat source. As an example, if sufficiently rapid desorption of gas in the liquid film occurs in a time of an order of magnitude less than about ten minutes, then the time decay constant would be about seven orders of magnitude less than the 100 year decay constant used in the analysis by Smith et al. Liquid film velocities would have to be about 2 cm/min for an assumed temperature gradient of 5°C/cm. Liquid film velocities as large as 2 cm/min are expected near a HLW canister during the operation of a heat pipe in regions proximal to the source of heat. Temperature gradients in this section of the heat, pipe, however, are very small and the required rate of gas desorption will not occur. Large liquid film velocities may be experienced in vertical fractures above a HLW canister at extreme conditions. The phenomenon of bubble formation and hence aerosol formation, however, should not exist under expected conditions.

Processes other than bubble formation, however, may furnish a mechanism for aerosol formation on fracture surfaces. One possible mechanism is the rupture of thin liquid films. The properties of thin films are different from those of the bulk phase (Sheludko, 1966). Thin films (i.e. 50-500 Å) can rupture and although the mechanisms of rupturing are not entirely understood, aerosol droplets may be ejected into the airspace of a partially saturated fracture during this process.

Thin film rupturing and other unidentified physical processes can provide a mechanism of aerosol formation. Because of the potential importance of aerosol transport (i.e. movement as vapor of actinides and other non-volatile contaminants) further analysis of aerosol formation is required.

A critical parameter affecting the potential for bubble formation in fractured media, however, is fracture aperture. Fractures with an aperture less than 250 μm are incapable of providing the needed space required for gas bubble formation under any possible conditions.

5. FREE CONVECTION

A potential transport mechanism of gas through non-isothermal fractured rock at large field scale is convective flow. The driving force of convective flow at a HLW repository is caused by the temperature gradient. Convective gas flow results from thermally induced density differences or buoyancy in the gas.

Representing convective gas flow mathematically is a complicated endeavor but can be made managable by invoking several standard assumptions. Foremost is Boussinesq's approximation which states that fluid density variations are negligible except in buoyancy (Lapwood, 1948). Another assumption is that the thermal characteristics of the medium are considered constant and independent of temperature. Density is assumed to vary linearly with temperature.

The equations of balance of mass, momentum and energy which govern convective flow can be expressed in dimensionless terms as follows (Witherspoon et al., 1977)

$$\partial V_i / \partial X_i = 0 \tag{5.1}$$

$$Pr\ \partial V_i/\partial z + V_i = Ra^{1/2}\ \Delta_{i3} - \partial p_D/\partial\ X_i \tag{5.2}$$

and

$$H\ \partial e/\partial t^* = Ra^{1/2}\ V_i\ \partial e/\partial X_i + Ra^{1/2}\ V_i\ \Delta_{i3} + \partial^2 e/\partial X^2_i \tag{5.3}$$

where the dimensionless groups are defined

Thermal diffusivity

$$\alpha = x_{eff}/(\rho_o\ c_v) \tag{5.4}$$

Rayleigh number

$$Ra = k\ \rho_o^2\ g\ \beta\ \Delta T\ c_v\ D_s/(\mu\ x_{eff}) \tag{5.5}$$

Prandtl number

$$Pr = k\ \alpha\ \rho_o/(\mu\ D^2) \tag{5.6}$$

Heat capacity ratio

(5.7) $H = (\rho\ c_v)_{eff}/(\rho_o c_v)$

Aspect ratios

(5.8) $D_1 = a_1/D_s;\ \ D_2 = a_2/D_s$

The dimensionless variables are similarly defined

dimensionless velocity

(5.9) $V_i = D_s\ v_i/(\alpha\ Ra^{1/2})$

dimensionless temperature

(5.10) $\theta = T/\Delta T$

dimensionless pressure

(5.11) $p_D = k\ p/(\mu\ \alpha\ Ra^{1/2})$

dimensionless time

(5.12) $t^* = t\ \alpha/D^2_s$

dimensionless distance

(5.13) $X_i = x_i/D_s$

The variables used in equations (5.4) to (5.13) are defined

a = width
c_v = heat capacity at constant volume
D_s = depth from heat source to surface
g = acceleration of gravity
k = intrinsic permeability
t = time
T = temperature
v = Darcian velocity
β = coefficient of volumetric thermal expansion
Δ_{ij} = Kronecker delta
x_{eff} = effective thermal conductivity
μ = viscosity

ρ = density
P = porosity

Effective thermal conductivity for one-phase flow is determined using the expression

(5.14) $$x_{eff} = x_{gas} + (1 - P) x_{rock}$$

The variable of interest in investigating convective flow is the Rayleigh number. The Rayleigh number is the ratio of buoyancy to viscous retardation and when sufficiently large for a given system, is a strong indicator that convective flow will occur.

A HLW repository in unsaturated fractured rock may be as large as 1 x 2 km in lateral extent at a depth of 300m. The fractured rock mass overlying the repository can be considered either an equivalent porous medium or a consolidated rock mass with distinct fracture sets or zones. An evaluation of each approach can be made using dimensionless Rayleigh numbers.

Lateral spacing of canisters along the plane of the repository is assumed to be small enough relative to the magnitude of the repository depth (300 m) that the lower boundary can be considered to be of uniform temperature. Thus, edge effects and a non-uniform heat source are not considered.

Convection is classified as free, forced or a mixture of the two. The difference between forced and free convection is that an external hydraulic force is the driving force of forced convection. Free convection is driven by a contrast in gas or fluid density (referred to as buoyancy). Free convection is assumed even though gas leaves the system at ground level. An equal amount of gas is introduced into the system at the lower sections of the convective cells but is not introduced by external hydraulic forces.

Lapwood (1948) calculates the minimum Rayleigh number necessary for free convective flow to occur in several idealized models in a homogeneous porous medium. This minimum Rayleigh number is referred to as the critical Rayleigh number, Ra_{cr}. If the Rayleigh number of a system exceeds the critical Rayleigh number, a thermal disturbance in the system can theoretically induce convective flow, otherwise, the disturbance will die out.

The first case investigated by Lapwood considers a closed system with an impervious, conducting boundary above and a permeable layer below. The critical Rayleigh number is determined $4\pi^2$ upon solving the governing equations. The second case to be considers a system with a conducting impervious layer below the system and a conducting layer of water as the upper boundary. The critical Rayleigh number for the second case is evaluated as 27.1. These two values for the critical Rayleigh number are believed to represent the limiting cases of expected boundary conditions pertinent to convective gas flow in a homogeneous medium.

The rock mass overlying a HLW repository can be treated as an homogeneous equivalent porous medium, a layered equivalent porous medium or as a consolidated medium with discrete fractures zones as illustrated in Figure 5.1. The propensity for convective gas flow to occur in each scenario is investigated.

A first approximation of convective gas flow is made by treating the overlying rock mass as an homogeneous equivalent porous medium. Conservatively, the rock mass is assumed dry, thus, the air intrinsic permeability of the rock mass equals the intrinsic permeability. The Rayleigh number is calculated for a range of reasonable scenarios at a HLW repository. A list of values for the variables needed to determine the Rayleigh number is presented in Table 5.1. The variables are assumed to be spacially and temporally constant.

The values assumed for most variables are reasonable for a wide variety of physical settings and have only minor changes in value over the entire range of possible HLW repository settings. Two major exceptions are the temperature difference between ground level and a repository at a depth of 300 m depth and, most importantly, the intrinsic air permeability of the rock mass overlying the repository. The difference in temperatures between the repository and ground level can be less than 100°C to as much as 400°C. Intrinsic permeability can range from 10^{-11} to 10^{-14} cm^2 (Wang et al., 1983). The limits of the Rayleigh number for these values is 3.2×10^{-5} for a temperature difference of 100°C and intrinsic permeability of 10^{-14} cm^2 to 0.13 when the temperature difference is 400°C and the intrinsic permeability is 10^{-11} cm^2. The largest conceivable Rayleigh number of 0.13 is significantly less than the critical Rayleigh number required for free convection to occur.

The rock mass above the HLW repository is treated as a layered porous medium when making a second approximation of convective gas flow. A stratum of welded tuff will usually underlie a layer of nonwelded tuff

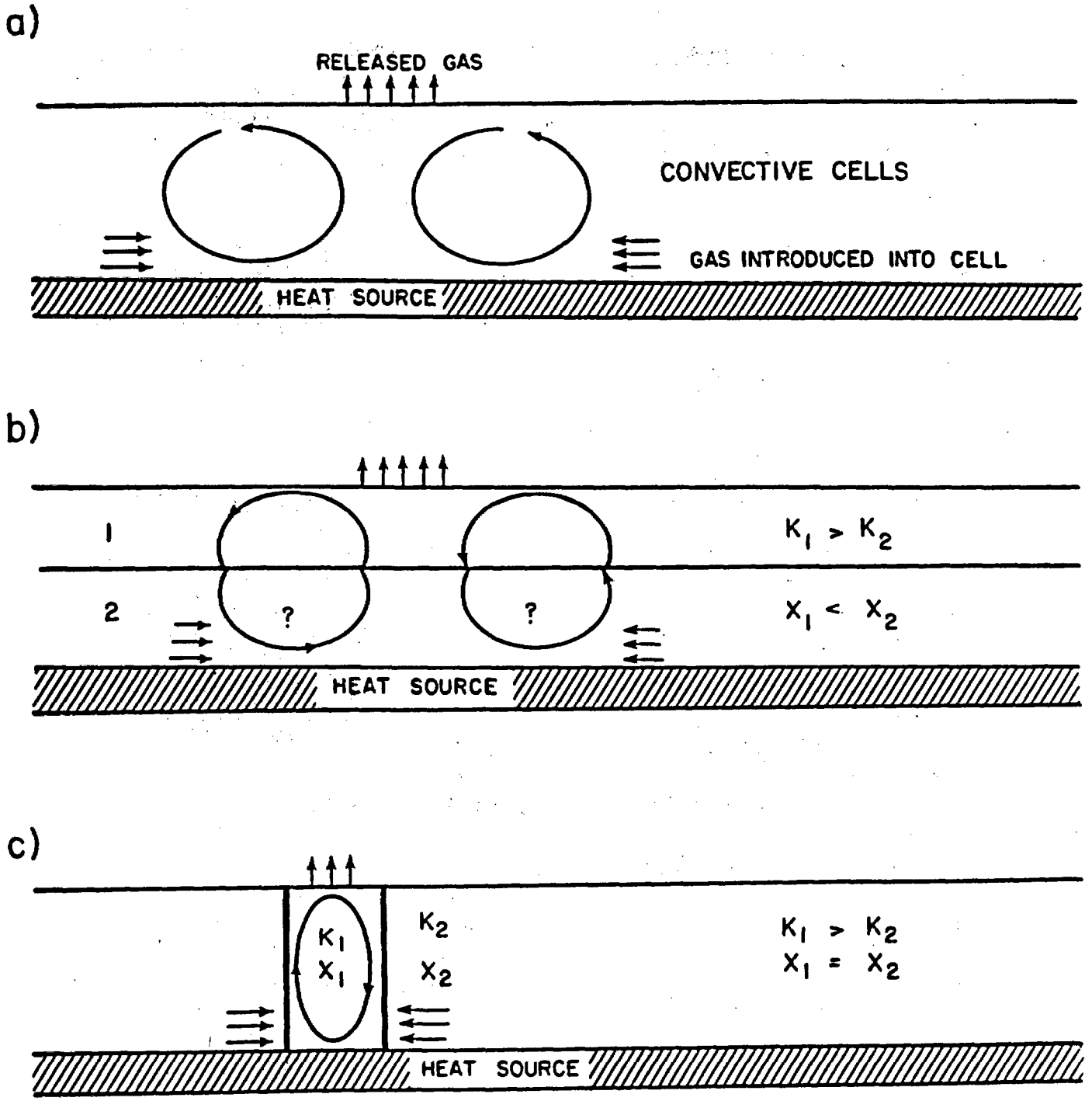

Figure 5.1. Three idealized cases of free convection flow: a) homogeneous equivalent porous medium; b) layered equivalent porous medium and c) zone of fractures or piped flow model. Arrows denote direction of gas flow. k is intrinsic permeability and x is thermal conductivity.

Table 5.1. A list of values assigned to the variables needed to determine the Rayleigh number (from Wang et al., 1983).

k	$= 10^{-11}$ to 10^{-14} cm^2
ρ_o	$= 0.0012$ g/cm^3
g	$= 980$ cm/sec^2
β	$= 2.7 \times 10^{-3}$ to 3.7×10^{-3} $°C^{-1}$
ΔT	$= 100$ -400°C
D	$= 30{,}000$ cm
μ	$= 2 \times 10^{-4}$ g/cm-sec
c_v	$= 0.16$ cal/°C-g
x_{eff}	$= 3.24 \times 10^{-3}$ cal/cm-sec-°C (at 10% porosity)
x_{air}	$= 6.3 \times 10^{-5}$ cal/cm-sec-°C
$x_{welded\ tuff}$	$= 3.24 \times 10^{-3}$ cal/cm-sec-°C
$x_{nonwelded\ tuff}$	$= 1.444 \times 10^{-3}$ cal/cm-sec-°C

as a consequence of the cooling history of volcanic flows. The physical properties of welded tuff can vary significantly from those of a nonwelded tuff. Therefore, modeling the rock mass as a two layer system of layers with different properties instead of a uniform block may better represent the actual system.

Convective gas flow in layered porous media exhibits anisotropic properties as compared to isotropic behavior through a homogeneous medium. The Rayleigh number representing a layered porous medium has to account for the anisotropic behavior. The Rayleigh number for a layered system is defined in terms of effective vertical intrinsic permeability and thermal conductivity by the expression (McKibben and Tyvand, 1982)

$$(5.15) \qquad Ra^L = k_v \rho_0^2 g \beta \Delta T D_s c_v/(\mu x_v)$$

where the average vertical intrinsic permeability and thermal conductivity for n layers are given by

$$(5.16) \qquad k_v = (\sum_i^n r_i/k_i)^{-1}$$

and

$$(5.17) \qquad x_v = (\sum_i^n r_i/x_i)^{-1}$$

The variable r_i is the ratio of the thickness of the i^{th} layer, D_i, to the total thickness, D_s.

The critical Rayleigh number for the multilayer system is defined relative to the critical Rayleigh number of a single layer system. The expression relating the two is

$$(5.18) \qquad Ra^L_{cr} = [r + (1 - r)/\beta_p]/[r + (1 - r)/\lambda_p]\, Ra_{cr}$$

where r is the thickness ratio of the lower layer to overall thickness and where λ_p and β_p are measures of proportionality between the properties of intrinsic permeability and thermal conductivity of the two layers (i.e., $k_2 = \lambda_p K_1$ and $x_2 = \beta_p x_1$) which are determined as follows

$$(5.19) \qquad k_h/k_1 = r + (1 - r)\lambda_p$$

and

$$x_h/x_1 = r + (1 - r)\,\beta_p \tag{5.20}$$

The effective horizontal intrinsic permeability and thermal conductivity are calculated by

$$k_h = \sum_{i}^{n} r_i\, k_i \tag{5.21}$$

and

$$x_h = \sum_{i}^{n} r_i\, x_i \tag{5.22}$$

Typical values of intrinsic air permeability for welded and nonwelded tuff are 10^{-13} and 10^{-12} cm^2, respectively (Wang et al., 1983). For an assumed nonwelded tuff thickness of 100 m and a welded tuff thickness of 200 m, the effective intrinsic permeability has a value of 4×10^{-13} cm^2 horizontally and 1.43×10^{-13} cm^2 in the vertical direction.

Effective values of thermal conductivity were also calculated. Typical values of thermal conductivity for welded tuff (3.6×10^{-3} cal/cm-sec-°C) and nonwelded tuff (1.44×10^{-3} cal/cm-sec-°C)(Wang et al., 1983) are volume averaged with air ($\beta = 6.3 \times 10^{-5}$ cal/cm-sec-°C). It is not known if values for thermal conductivity given by Wang et al. (1983) are volume averaged, therefore, to be conservative, x_{eff} is volume averaged in this investigation. Air porosity values used in this calculation are 0.10 for welded tuff and 0.35 for nonwelded tuff. Effective vertical and horizontal thermal conductivity are determined using Equations (5.17) and (5.22) to yield values of 1.81×10^{-3} and 2.48×10^{-3} cal/cm-sec-°C, respectively.

Layer proportionality constants are calculated using Equation (5.16) and (5.21). The constant β_p equals 0.3 and λ_p equals 4.0. The critical Rayleigh number for the aforementioned layered tuff is 1.23 times the critical Rayleigh number of a single layered system or 48.6. Thus, according to the two layered analysis, the Rayleigh number of the rock mass above a HLW repository must exceed 48.6 before free convection will occur.

The Rayleigh number for the two layered system described above using parameter values listed in Table 5.1 and the effective vertical values for intrinsic permeability and thermal conductivity is 2.8×10^{-6}, a value substantially less than the critical Rayleigh number.

The flow of gas through fractured rock can also be analysed for the case when gas flow occurs through a series of high permeability fracture zones separated by zones of low gas permeability. A piped flow model is one which has zones of high and low permeability. The potential of piped or channel flow through high gas permeability zones has been evaluated by Donaldson (1970) for a hot-water geothermal system. If all other variables are held constant, Ra_{cr} is solely a function of the aspect ratio, S_R, of the high permeability column (width/height) and is defined by the expression

$$(5.23) \qquad Ra_{CR} = \pi^2(m^2 + S^2_R)^2/(m^2S^2_R)$$

where m is the largest integer less than

$$(5.24) \qquad 1 + [-1/2 + 1/2(1 + 4S^2_R)^{1/2}]$$

In virtually all areas of interest concerning large field scale convection at a HLW repository site, m equals unity and Ra_{cr} reduces to

$$(5.25) \qquad Ra_{cr} = \pi^2(1 + S^2_R)^2/S^2_R$$

Ra_{cr} has been evaluated for several different values of the aspect ratio. An aspect ratio of 10/300 portrays a vertical flow channel 10 m wide and 300 m high. This corresponds to a Ra_{cr} value of about 8900. Similarly, flow channels of widths 50 m, 100 m and 300 m equate with values of 374, 105, and 39.4, respectively for Ra_{cr}. The value for Ra_{cr} conveniently degenerates to $4\pi^2$ (39.4) when the aspect ratio is unity which is the value for the critical Rayleigh number given by Lapwood for free convection in a porous medium.

Flow channels and low gas permeability zones require the system to exist under the conditions of higher Rayleigh numbers in order to have convective flow than would be necessary for a system with uniformly distributed flow paths (i.e., an equivalent porous medium). The occurance of narrow zones of high gas permeability rather than large zones of uniform moderate permeability can be impediments to the formation convection cells at a HLW repository.

Free convective flow of gas in the rock mass above the repository has been analyzed for three simplified scenarios. The conservative case has been assumed where possible, however, the assumptions of neglecting edge effects and treating the heat source as uniform are not conservative assumptions. Nonetheless, because of the low magnitude of the computed Rayleigh numbers for the three cases, convective flow of gas above a HLW

repository is not expected for scenarios with conditions similar to those investigated. Since actual HLW repository settings are expected to have conditions similar to the three case studies, free convection is not believed to be a potential contributor to the transport of radionuclides as vapor at large-field scale.

6. THERMAL DIFFUSION AND THERMOPHORESIS

Thermal diffusion and thermophoresis are the movement of vapor in response to a thermal gradient. Thermophoresis is the result of gas molecules (with variable mean velocities) impinging on larger size particles from opposite sides (Fuchs, 1960). Thermal diffusion usually refers to thermally induced movement of gas molecules, however, it is has been applied to the analysis of movement of larger particles (as large as micrometer size particles) through angstrom size gas molecules (McDaniel and Mason, 1973). Although the two expressions refer to the same physical process for at least some size scales, thermal diffusion is based on rigorous kinetic theory while thermophoresis is defined by determining the net momentum imparted onto a particle by molecular collisions.

The effect of thermal diffusion or thermophoresis is generally small, however, significant quantities can be moved when the thermal gradient is steep and conditions are favorable. One major condition necessary for either thermal diffusion or thermophoresis to be significant is that gas molecules and airborne particles are of widely varied sizes. Particles among other particles of similar size will not respond (by moving) to a thermal gradient whereas large particles among substantially smaller sized particles can respond at the same conditions. It is possible that radionuclide transport by thermal diffusion or thermophoresis is significant in zones near the a HLW canister.

Thermal diffusion is examined using rigorous kinetic theory by Hirschfelder et al., (1954). A brief description of their first approximation of the thermal diffusion coefficient is presented here. Next, the theory of thermophoresis from Fuchs (1960) based on conservation of momentum is summarized. An assessment of particle or gas molecule movement is then performed using the analysis of Fuchs.

The flux, j_t, resulting from thermal diffusion can be stated

$$(6.1) \qquad j_t = - D_a^t \nabla \ln T$$

where D_a^t is the thermal diffusion coefficient. The driving force is the gradient of the natural log of temperature and not the gradient of temperature, thus sufficiently large differences in temperature must be present for the driving force to be appreciable.

The thermal diffusion coefficient is a difficult parameter to determine and is usually defined in terms of the thermal diffusion ratio k_t. The relationship between these two is expressed

$$(6.2) \quad D_A^t = (n^2/\rho)\, M_A\, M_B\, D_{AB}\, k_t$$

The thermal diffusion ratio is related to two other commonly used parameters, the thermal diffusion factor α_t and the Sorret coefficient C_{Sorret}, by the following expressions (Bird et al., 1960)

$$(6.3) \quad k_t = \alpha_t\, x_A\, x_B$$

where x_i is the mole fraction of gas i and

$$(6.4) \quad k_t = C_{Sorret}\, x_A\, x_B\, T$$

One other important property pertaining to thermal diffusion coefficient is defined

$$(6.5) \quad \sum_i D_i^t = 0$$

The significance of which is that as one gas flows from a cooler region to a warmer region, the other gas will move in the opposite direction in a binary system.

The thermal diffusion ratio is also a difficult parameter to ascertain. A first approximation of k_t (Hirschfelder et al., 1954) based on rigorous kinetic theory is expressed

$$(6.6) \quad k_t = [x_A x_B/(6\lambda_{AB})]\,[(S^{(A)}x_A - S^{(B)}x_B)/(X_\lambda + Y_\lambda)](6c^* - 5)$$

where

$$(6.7) \quad S^{(A)} = (M_A\, M_B)\lambda_{AB}/(2M_B\lambda_A) - 15(M_B - M_A)/(8a^*M_A) - 1$$

$$(6.8) \quad S^{(B)} = (M_B\, M_A)\lambda_{AB}/(2M_A\lambda_B) - 15(M_A - M_B)/(8a^*M_B) - 1$$

$$(6.9) \quad \lambda_A = (1.9891\times10^{-4})(T/M)^{1/2}/[\, C^2\Omega_{AB}^{(2,2)}T^*]$$

$$(6.10) \quad \lambda_{AB} = (1.9891\times10^{-4})[T(M_A + M_B)/2M_AM_B]^{1/2}/[\, d_{AB}^2\Omega_{AB}^{(2,2)}T^*]$$

$$(6.11) \quad a^* = \Omega_{AB}^{(2,2)}/\Omega_{AB}^{(1,1)}$$

(6.12) $b^* = [5\Omega_{AB}(1,2) - 4\Omega_{AB}(1,3)]/\Omega_{AB}(1,1)$

(6.13) $c^* = \Omega_{AB}(1,2)/\Omega_{AB}(1,1)$

(6.14) $X_\lambda = x_A^2/\lambda_A + 2x_Ax_B/\lambda_{AB}$

(6.15) $Y_\lambda = x_A^2U^{(1)}/\lambda_A + 2x_Ax_BU^{(y)}/\lambda_{AB} + x_B^2U^{(2)}/\lambda_B$

(6.16) $U^{(1)} = 4a^*/15 - [12b^*/5 + 1]M_A/12M_B + (M_A - M_B)^2/2M_AM_B$

(6.17) $U^{(2)} = 4a^*/15 - [12b^*/5 + 1]M_B/12M_A + (M_B - M_A)^2/2M_AM_B$

(6.18) $U^{(y)} = 4a^*[(M_A+M_B)^2/4M_AM_B]\lambda_{AB}/(15\lambda_A\lambda_B - (12b^*/5 + 1)/12$

$$- (5/32a^*)(12b^*/5 - 5)(M_A - M_B)^2/M_AM_B$$

The variables defined in Equations (6.9) and (6.10) are thermal conductivities of the respective gases. T^* is dimensionless temperature and equals KT/e_{AB}.

The collision integrals used in Equations (6.9) to (6.13) are from a general form of the collision integral defined in Equation (2.19). The general form is (Hirschfelder et al., 1954)

(6.19) $$\Omega_{AB}(l,s) = (2\pi\ KT/\mu_{AB})^{1/2}\int_0^\infty\int_0^\infty \exp(-\ V_{AB}^2)\ \ V_{AB}^{(2s+3)} \cos(1 - \cos X)b\ db\ dV_{AB}$$

The various choices of l and s allow calculation of the first approximation of different transport coefficients (that is, viscosity, diffusion coefficient, thermal diffusion ratio, etc.) using Chapman-Enskog theory. The remaining variables used in Equations (6.7) to (6.19) are defined in Chapter 2.

The behavior of particles in the presence of a thermal gradient varies with the temperature of the system. There is an inversion in the sign of the thermal diffusion ratio when the quantity from Equation (6.6) $(6c^* - 5)$ passes through zero. If $(6c^* - 5)$ is positive, then k_t is positive when $M_A > M_B$, likewise, k_t is negative for $M_A < M_B$. Thus, particles change their direction when $(6c^* - 5)$ and hence k_t change signs.

If the gas molecule or aerosol particle of interest is substantially heavier than the parent gas (air), significantly larger values of the thermal diffusion ratio are possible (McDaniel and Mason, 1973). It is this condition that may give rise to potential radionuclide transport in the presence of large thermal gradients. The thermal diffusion ratio for movement of heavy gas molecules or airborne particles can be determined using a simplified version of Equation (6.6). This formula is written (Hirschfelder et al., 1954)

$$(6.20) \quad k_t = 15(2a^* + 5)(6c^* - 5)(M_A - M_B)/$$

$$[2a^*(16a^* - 12b^* + 55)(M_A - M_B)]x_A x_B$$

Equation (6.20) is not yet evaluated for possible thermal diffusion of heavier radionuclide gas molecules or aerosol particles expected near a HLW canister.

As was stated earlier, thermophoresis is the result of gas molecules impinging on airborne particles from opposite sides with different mean velocities. The difference in mean velocities is a consequence of an imposed thermal gradient.

Fuchs (1964) presents an analysis of the importance of thermophoresis relative to the resistance of a gas from molecular and hydrodynamic particle motion. For molecules of radius less than the mean free path ($r \gg \lambda$) the net force resulting from a difference in momentum caused by the thermal gradient is defined

$$(6.21) \quad F_T = -32\, r^2\, X_a\, T/15\, \bar{v}$$

where X_a is the translational part of the thermal conductivity of the gas which equals Kn/m.

Equation (6.21) can be approximated by the expression

$$(6.22) \quad F_T = 4\, r^2\, \Delta T\, \lambda\, P/T$$

However, a more complicated physical process occurs when $r \gg \lambda$. The force resulting from a thermal gradient is referred to as photophoresis and is determined for spherical particles by the expression

$$(6.23) \quad F_T = 3\, \pi\, n^2\, r\, R\, \Delta T/p\, M$$

where R is the gas constant.

Forces caused by a thermal gradient are countered by resistance forces on molecules and particles. Molecular resistance occurs when $r \ll \lambda$ and hydrodynamic resistance occurs when $r \gg \lambda$. Resistance at atmospheric pressure (with $\lambda = 6 \times 10^{-6}$ cm) is, therefore, a result of molecular forces for molecules with radius less than about 10^{-6} cm. Molecular resistance for the case when the mass of the particle is sufficiently greater than the mass of the gas molecules is stated by

$$(6.24) \qquad F_M = - (4/3) \pi (\beta_o) n m \bar{v} r^2 V_p$$

where n and m are the concentration and mass of gas molecules and $\bar{v}$ is their mean velocity.

Molecular resistance of particles with radii greater than the free mean path is calculated using Stokes equation

$$(6.25) \qquad F_M = - 6 \pi n r V_p$$

Velocity of the particle caused by thermophoresis, V_p, for the case when $r \ll \lambda$ is determined by

$$(6.26) \qquad V_p = - 3 \lambda \bar{v} \Delta T/[8(1 + \pi f/8)T]$$

where f is the fraction of gas molecules reflected diffusely by the particle.

Likewise, the particle velocity for $r \gg \lambda$ is

$$(6.27) \qquad V_p = - [3 X_a \Delta T]/[2(2 X_a + X_i)\rho T]$$

where subscript a denotes the larger molecules or particles and i denotes the smaller parent gas molecules.

In general, gas molecules or particles with radii exceeding 10^{-6} cm will not remain airborne because the force of gravity will attract them downward until they sorb onto a surface. Thus, Equation (6.22) is used to determine the thermophoresis force which is countered by molecular resistance. This analysis is calculated at 500°K since elevated temperatures at a HLW canister should average about this temperature for an extended time period. The thermal gradient is assumed to have the extreme value of 100°K/cm and pressure is assumed to be atmospheric (10^6 dynes/cm^2). The force generated by thermophoresis is calculated as -4.8×10^{-12} dynes/molecule.

Molecular resistance requires additional information for determination. Particle velocity is determined for the case $r << \lambda$ using Equation (6.25) and is found to equal 1.9×10^{-2} cm/sec. When reflection is diffuse ($\beta_o = 1$), gas density is 2.4×10^{19} molecules/cm^3 and the mass of a molecule of air is about 5×10^{-23} g, then molecular resistance is determined to be -5.9×10^{-12} dynes/molecule.

Based on the above discused theory and assumed parameter values, this analysis indicates that the force upon a molecule created by thermal diffusion is approximately equal to molecular resistance. A thermal gradient of 100°K/cm, therefore, is not sufficient to cause movement of particles by thermophoresis under these conditions.

An exception to this scenario occurs when the fracture walls are not electrically neutral and particles which are negatively ionized are repelled from surfaces. Negatively charged particles with diameter greater than 10^{-6} cm can remain airborne and since the force caused by thermophoresis increases with particle size, some movement of larger particles away from the heat source (HLW canister) may result from thermophoresis. Equation (6.5), however, suggests that a return flow of gas molecules results from particle movement induced by a thermal gradient perhaps nullifying any net mass transport.

The magnitude of mass flux of radionuclides caused by thermophoresis can not be ascertained until gas density and the size distribution of the airborne radionuclides (either as gas molecules or as aerosol particles) are known. Additionally, the preliminary results from evaluating the importance of thermophoresis should be verified by calculating the first approximation of thermal diffusion for the region where thermal diffusion and thermophoresis overlap--that of large particles or molecules moving through substantially smaller molecules--and comparing the results produced by each approach.

7. DISCUSSION AND SUMMARY

The objective of this study has been to identify and examine potential mechanisms of radionuclide transport as vapor at a HLW repository located in unsaturated fractured rock. The transport mechanisms and processes of interest have been investigated at a zone near the repository and at a larger distance. In general, transport mechanisms near the repository are influenced by the nature of the high-level waste and design of the waste package while at larger distances transport mechanisms are influenced by the geologic medium.

Transport mechanisms or processes potentially important at large distances include ordinary diffusion, viscous flow and free convection. Ordinary diffusion includes any diffusion process driven by a concentration gradient. These are self and binary diffusion, Knudsen flow and surface diffusion. Pressure flow and slip flow comprise viscous flow. The driving force of viscous flow is the total gas pressure gradient.

A parameter useful in the examination of ordinary diffusion and viscous flow is the Knudsen number, Kn--the ratio of the mean free path length of a gas molecule to the aperture of the pore space. Greater flow of gas is observed by Knudsen flow and slip flow than the flow of gas predicted by self diffusion and pressure flow, respectively, when the Knudsen number is large, that is, $Kn > 1$. The mean free path length of a gas molecule in air at atmospheric pressure is about 6×10^{-6} cm. Thus, Knudsen flow and slip flow are important when the apertures of pores are less than about 6×10^{-6} cm. An order of magnitude increase in mass flow in a welded tuff has been observed over the flow predicted by pressure flow (Reda, 1985). This increase is attributed to either Knudsen flow, slip flow or surface diffusion. Therefore, these transport mechanisms must be considered when investigating gas flow through welded tuff.

Free convection is the movement of a fluid (or gas) in response to a difference in density. As a large scale transport mechanism, free convective flow may be possible in fractured rock overlying a HLW repository. A HLW repository of sufficiently large lateral extent can create an artifical high temperature layer causing a density contrast in the gas which permeates the interconnected air space of the rock. The density contrast in the gas can result in free convection cells. The Rayleigh number, which is a dimensionless parameter measuring the ratio of buoyancy forces relative to viscous resistance, is a useful indicator as to whether convection cells will occur. Free convection will result

from a thermal disturbance when the Rayleigh number representing the system exceeds a critical threshold (usually $4\pi^2$).

Three idealized scenarios representing the rock mass overlying a HLW repository are investigated as to their propensity for the formation of free convection cells: 1) a homogeneous equivalent porous medium 2) a two layer system with each layer treated as a homogeneous porous medium and 3) vertical zones of high fracture density and hence higher permeability separated by zones of lower permeability. The Rayleigh number representing each scenario was calculated based on reasonable and conservative rock and gas properties and in each case the Rayleigh number was significantly less than the critical Rayleigh number of $4\pi^2$ (all Rayleigh numbers were at least two orders of magnitude less than the critical Rayleigh number).

The individual cases investigated were not conservative because the heat source at the HLW repository was assumed uniform and edge effects were not considered. Further analysis is required to insure that this preliminary conclusion is also valid for the conservative case where a non-uniform heat source and edge effects are considered.

Transport mechanisms important near a repository include ordinary diffusion, viscous flow plus several mechanisms whose driving forces arise from the non-isothermal, radioactive nature of high-level waste. These mechanisms include forced diffusion of ionized vapor particles, aerosol transport, thermal diffusion and thermophoresis.

An additional driving force near the repositroy is one resulting from an electric field. Ionized particles will move in response to an electric field if the intensity of the electric field is sufficiently large and the particles are relatively mobile.

Gamma ray emission by high-level waste can create an electric field by Compton scattering. Gamma rays of a specific range in energy (0.03 to 10.0 MeV) result in Compton scattering upon collision with particles located along their pathway. A photon of lower energy and an electron are scattered during the collision. The collision causes a preferential outward movement of electrons resulting in a charge displacement. A return flow of electrons results to counter this displacement thus inducing an electric field. The resulting electric field can cause movement of any ionized mobile particle. This particle or gas molecule movement is referred to as forced diffusion.

Two limiting cases were investigated for their potential of forced diffusion: 1) a HLW canister located in a rock mass and 2) a HLW canister located in air. The two cases are thought to approximate the range of conditions at a HLW canister.

The effect of partially saturated fractures on the electric field in the rock mass case is neglected even though the importance of ion movement through the fractures is examined. Significantly large air spaces may occur near the surface of a HLW canister as a resul of several different effects (i.e., large fractures, open boreholes, canister cladding failure, etc.) hence, the justification for the second case.

Ion density measurements are dependent upon the physical and geochemical properties of the waste, rock mass and rock water and are not yet known. The importance of ion flux caused by forced diffusion can not be assessed until this quantity is determined. Ion drift velocities in air, however, can be predicted for both cases with assumed values for ion mobility. Electric field intensity and ion drift velocities do not exceed about 10^{-6} V/cm and 2×10^{-6} cm/sec in unsaturated fractures superimposed onto the rock mass in the first case. The electric field intensity in air, however, is as large as 50 V/cm and the ion drift velocity is 100 cm/sec within 10 cm of the canister surface 300 years after emplacement.

A more realistic scenario needs to be analysed to better simulate actual repository conditions. This scenario would include minor air spaces proximal to the waste package with nearby rock surfaces capable of providing electron pathways that could partially short-circuit the electric field. Forced diffusion as a mechanism of transport can not yet be dismissed based on the results predicted by this investigation.

Radionuclide transport as an aerosol is a potentially important mechanism near a repository. Radionuclides in high-level waste with a significant vapor phase include ^{3}H, ^{14}C, ^{85}Kr and ^{129}I. Only these radionuclides are expected as gases. Aerosol particles, however, can contain any soluble radionuclide present in the solution from whence the aerosol is produced. The formation of a heat pipe proximal to a HLW canister can provide an opportunity for aerosol production. The liquid film on a fracture surface moves toward the source of heat (waste canister) in response to differences in matric potential and surface forces, is vaporized at higher temperatures then moves away from the heat source until it condenses at lower temperatures. The decrease in gas solubiltiy in the liquid film as temperature rises in the moving

liquid may cause bubbling which in turn introduces aerosol droplets into the airspace overlying the liquid film.

Aerosol generation, however, requires specific conditions to be present at the canister. Sufficiently thick liquid film thicknesses in conjunction with sufficiently large air spaces must be available for bubble growth and rupturing to occur. Fractures of less than several hundred micrometers are too narrow for the formation of bubbles and thus can not provide a setting for aerosol production. Additionally, temperature increase in the liquid film must occur rapidly so that gas desorption will result in bubbling rather than quiescently gas desorption.

In the situation where bubbling occurs and an aerosol is produced, the airborne particles will move in response to any driving force acting on the airspace. Typical driving forces include pressure and concentration gradients. Other driving forces, however, may be present. For example, ionized aerosol particles will respond to an external electric field resulting from Compton scattering or any other cause.

Airborne ionized particles will repel any similarly charged surfaces and move toward an area of opposite charge. The return flow of electrons which move in response to forced diffusion will seek the path of least resistance, one probable pathway being the liquid film on fracture surfaces, thereby negatively charging fracture surfaces. The significance of this process is that negatively particles will, on the average, remain airborne longer and thus travel farther than positively or neutrally charged particles in the presence of forced diffusion. Positively charged particles will move quickly to the negatively charged surfaces and resorb without traveling a significant distance. In this respect, the electric field may aid the containment of contaminants.

High temperatures and related thermal gradients can occur at waste canisters during decay of high-level waste, thus, creating significant thermal gradients. Movement of gas molecules or particles in response to a thermal gradient is another potential transport mechanism near a repository. The transport mechanism resulting from thermal gradients is generally referred to as thermal diffusion when gas molecules are of concern and as thermophoresis when larger sized particles are of interest. Although different theoretical arguments are used to explain each mechanism, the resulting movement from either is not significant unless widely varying sized molecules or particles are present.

The force caused by thermophoresis was calculated for a particle near a HLW canister. Only particles with radii less than 10^{-6} cm were considered because larger particles would respond to the force of gravity and move downward until sorbing onto a surface or a liquid film. If an extreme thermal gradient of 100°C/cm is assumed, this force is calculated to be the same order of magnitude as the counter force caused by molecular resistance. However, negatively charged surfaces will suspend negatively charged particles in an airspace as was previously mentioned. The force of repulsion can overcome the force of gravity and in this case larger particles can remain airborne and move in response to thermal gradients (the larger particles move away from the source of heat). The force from thermophoresis is directly proportional to particle size, thus an order of magnitude increase in the diameter of a particle increases the thermophoresis force by an order of magnitude which would then exceed the force of resistance for the abovementioned case. Mass flux from this case or any other case by thermophoresis has not been estimated because particle and gas molecule densities and size distributions are not known at this time.

Several radionuclide transport mechanisms and processes have been individually introduced and investigated. Additional transport mechanisms however, may exist which do not fit into any of the earlier mentioned categories. These additional transport mechanisms or processes include any other process or coupled process not yet discussed which may occur at possible repository conditions. Furthermore, the significance of an individual transport mechanism may be augmented by forces other than the major driving force of the transport mechanism.

A chart with the four major gradients (head, concentration, temperature and electric potential) and fluxes (water, elements in solution, heat and electric current) aids in illustrating additional possible transport mechanisms (Figure 7.1, from de Marsily, 1985). Also included in Figure 7.1 are off diagonal entries referred to as phenomenological coefficients. These are the proportionality constants relating the gradients to the different fluxes.

The intensity of the electric field was predicted during investigation of forced diffusion. Until ion density is determined, the flux of airborne ions resulting from diffusion caused by an electric field can not be established. It is predicted, however, that the intensity of a Compton current induced electric field can be 10^2 V/cm or larger in an air environment immediately proximal to a HLW canister at times up to 1000 years.

Fluxes of \ Gradients of	Head	Concentration	Temperature	Electric potential
Water	DARCY	Chemical osmosis	Thermal osmosis	Electro osmosis
Elements in solution	Ultrafiltration	FICK	Soret (Thermal Diffusion Thermophoresis)	Electro-phoresis (Forced Diffusion)
Heat	Thermal filtration	Dufour	FOURIER	Peltier
Electric current	Rouss	Sedimention current	Seabeck or Thompson	OHM

Figure 7.1. Chart of major gradients and fluxes with off diagonal phenomenological coefficients (from de Marsilly, 1985).

An electric field intensity of this magnitude is large enough to warrant investigation of other transport mechanisms fueled by electric potential gradients. An example is electrophoresis--electrical field induced movement of ionized particles suspended in a fluid. Electrophoresis could occur in the liquid film on a fracture surface. This mechanism is analogous to forced diffusion of ionized particles suspended in air. A prediction of the intensity of a Compton current induced electric field in the liquid film on a fracture surface was not determined in this study. The scenario is complicated because any additional pathway for returning electrons (such as liquid films or fracture surfaces) short-circuits the electric current and reduces the intensity of the electric field by an undetermined amount. Since the electric field intensity for this case is unknown, the magnitude of electrophoresis can not be predicted. Electrophoresis if important, however, will occur near a repository because Compton scattering occurs only near a repository.

Surface diffusion may also be affected by gradients other than concentration. In general, the importance of surface diffusion becomes appreciable when gas sorbed on a solid surface is limited to a few layers. The driving force of surface diffusion is a gradient in concentration of the sorbed gas. However, the driving force of particles or molecules along the surface can be augmented or impeded by the presence of other gradients. Gradients in temperature or electric potential need to be coupled with surface diffusion to ascertain the complete significance of the surface flow of contaminants.

Near a repository vapor transport mechanisms and processes, either individually or coupled with other transport mechanisms, can provide a significant means of transport from a failed canister to the geologic medium and possibly as far as the zone of higher saturation enveloping the canister or repository region (Figure 7.2). From the point where vapor transport processes which are important near a repository cease significance, other transport mechanisms--both in the vapor phase or in liquid phase--can transport contaminants outward to the accessable environment. Although the distance at which vapor transport near a repository is significant may be as short as several centimeters, mass flux by vapor transport could be an important--if not the most important--means of transport across this gap during specific periods of time after cansiter emplacement. Any investigation of transport mechanisms and processes near a repository will necessarily be engineering design dependent.

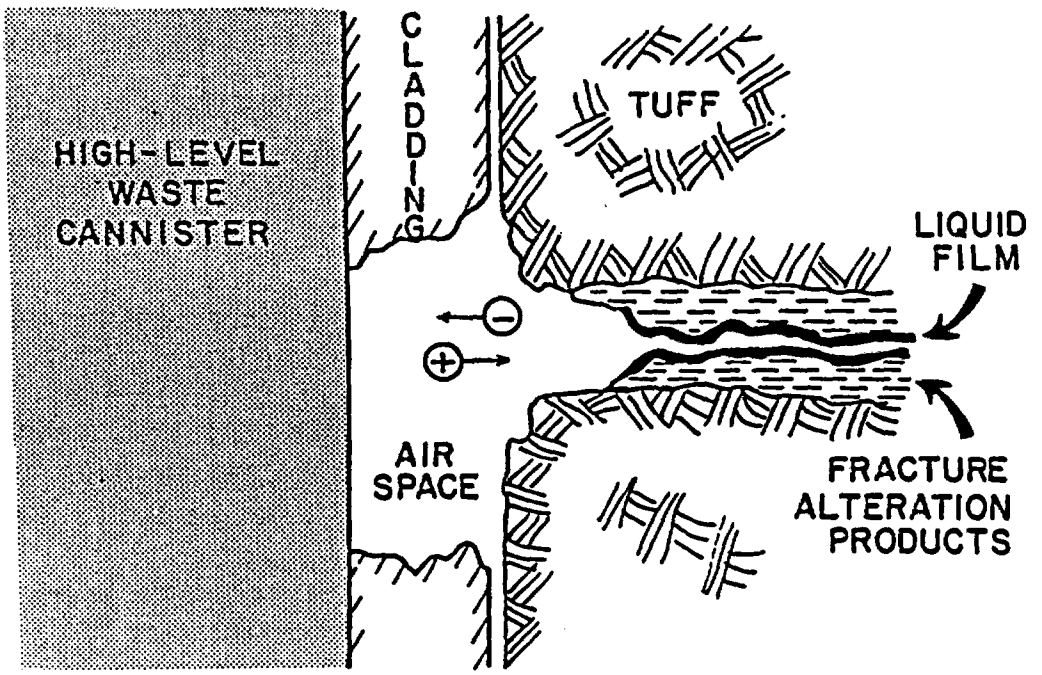

Figure 7.2. Near-field transport of radionuclides as vapor in air space proximal to HLW canister. Vapor transport may provide integral transport link to geologic medium.

Radionuclide transport by ordinary diffusion and viscous flow are also potentially important at large distances. Characterization of the geologic medium and adequate gas flow modelling is necessary to ascertain the importance of radionuclide transport as vapor at this scale.

The issues brought forth and discussed in this study are believed to be important factors that must be addressed in the assessment of the specific engineering design (vapor transport near a repository) and site selection (vapor transport a larger distance) of a potential HLW repository.

REFERENCES

Apfel, R.E., "A Novel Technique for Measuring the Strength of Liquids," Journal of the Acoustic Society of America, Vol. 49, No. 1, p145-155, 1971.

Barlow, E.J. and W.E. Langlois, "Diffusion of Gas from a Liquid into an Expanding Bubble," IBM Journal July, p329-337, 1962.

Battino, R., Solubility Data Series--Nitrogen and Air, Vol. 10, Pergamon Press, New York, 1982.

Berman A. S. and W. S. Maegley, "Internal Rareified Gas Flows with Backscattering," The Physics of Fluids, Vol. 15, No. 5, May, 1972.

Bird, R.B., W.E Stewart, and E.N. Lightfoot, Transport Phenomena, John Wiley and Sons, New York, 780p, 1960.

Birkoff, G., Hydrodynamics: A Study in Logic, Fact; and Similitude, Princeton University Press, 1960.

Birkoff G., R.S. Margulies, and W. A. Horning, "Spherical Bubble Growth," Physics of Fluids, Vol. 1, No. 3, 1958.

Bloch, M.R., D. Kaplan, V. Kertes, and J. Schnerb, "Ion Separation in Bursting Air Bubbles--Irregular Ion Ratios," Native, Vol. 209, 1966.

Bloch, M.R. and W.L. Lueke, "Geochemistry of Ocean Water Bubble Spray," Journal of Geophysical Research, Vol. 77,No. 27, 1972.

Brown, T.L., General Chemistry, Merrill Publishing Co., Columbus, Ohio, 1968.

Bond, W.N., "Bubbles and Drops and Stoke's Law," Philosophy Magazine, Vol. 7, No. 4, p889-898, 1927.

Burns, W.G. and H.E. Sims, "Effect of Radiation Type in Water Radiolysis," Journal of Chemistry Society--Faraday Transactions, Vol. 77, p2803-13, 1981.

Carman, P.C., Flow of Gases through Porous Media, Academic Press, N.Y., 182p, 1956.

Carslaw, H.S., and J.C. Jaeger, Conduction of Heat in Solids, Clarendon Press, Oxford, 1959.

Chapman, S. and T.G. Cowling, The Mathematical Theory of Non-Uniforform Gases, Cambridge, New York, 1970.

Cleaver, H.L. and C.H. Han, Thermodynamics of Aqueous Systems with Industrial Application, ed. S. A. Newman, ACS Symposium Series 133, American Chemical Society, Wash. D.C., p513-536, 1980.

Code of Federal Regulations, Title 40 Part 191, Environmental Standards for the Management and Disposal of Spent Nuclear Fuel, High Level and Transuranic Radioactive Waste, Working Draft 4, Environmental Protection Agency, Wash. D.C., 1984.

Cotter, T.P., "Theory of Heat Pipes," LA-3246-MS, 1965.

CRC Handbook of Chemistry and Physics, 1974, 54th ed., CRC Press.

Dacey, J.R., "Gas Adsorption," Industrial and Engineering Chemistry, Vol. 57, No. 6, 1965.

Day, J.A., "Production of Droplets and Salt Nuclei by the Bursting of Air-Bubble Films," Quarterly Journal of the Royal Meteorlogical Society, Vol. 90, No. 72, 1964.

deBoer, J.H., The Dynamic Character of Adsorption, Oxford, N.Y., 240p, 1968.

DeMarcus, W.C., "Knudsen Flow Through a Channel with Rough Walls," K-1435, 1959.

de Marsily, G., "An Overview of Coupled Processes with Emphasis on Geohydrology," International Symposium on Coupled Processes Affecting the Performance of a Nuclear Waste Repository, Lawrence Berkeley Laboratory, 1985.

Dhir, V.K., and I. Canton, "Boiling in a Porous Bed," Applied Scientific Research, Vol. 38. No. 1, p69-76, 1982.

Dietrich, R.V., and others, 1982, AGI Data Sheets: Amer. Geol. Inst.

Donaldson, L.G., "The Simulation of Geothermal Systems with a Simple Convection Model," Geothermics, Special Issue 2, 1970.

Eaton, R.R., N.E. Bixler and D.C. Reda, "Coupled Hydrothermal Flows of Liquid and Vapor in Welded Tuff: Numerical Modeling of Proposed Experiment," International Symposium on Coupled Processes Affecting the Performance of a Nuclear Waste Repository, Lawrence Berkeley Laboratory, 1985.

Evans, D.D., Unsaturated Flow and Transport Through Fractures Rock-Related to High-Level Waste Repositories, NUREG/CR-3206, March, 1982.

Fernandez, J.A. and M.D. Freshley, Repository Sealing Concepts for the Nevada Nuclear Waste Storage Investigations Project, SAND83-1778, 1984.

Filippone, W.L., Course Notes on Computational Methods in Engineering Science, University of Arizona, 1986.

Filippone, W.L., S. Woolf and R. Lavigne, "Particle Transport Calculations with the Method of Streaming Rays," Nuclear Science Engineering, Vol. 11, p119, 1980.

Freeze, R.A., and J.A. Cherry, Groundwater, Prentice-Hall, Englewood Cliffs, N.J., 1979.

Fuchs, N.A., The Mechanics of Aerosols, MacMillan, New York, 1964.

Geankoplis, C.J., Mass Transport Phenomena, Ohio State University Bookstores, Columbus, Ohio, 1972.

Glasstone, S., Physical Chemsitry, van Nostrand Co., New York, 1946.

Goldstein, H., Fundamental Aspects of Ractor Schielding, Addison-Wesley, 1959.

Gregg, S.J., The Surface Chemistry of Solids, Reinhold, New York, 393p, 1961.

Gurr, C.G., T.J. Marshall, J.T. Hutton, "Movement of Water in Soil Due to Temperature Gradient", Soil Science, Vol 74, p335-345, 1952.

Hagashi, K., H. Ito and J. Oisho, "Surface Diffusion Phenomena in Gaseous Diffusion, (I)," Journal of the atomic Energy Society of Japan, Vol. 5, No. 10, 1963.

Hamilton, C.J., N.D. Holden, V.H. Pierce, and M.W. Robertson, HTGR Fuel Compostion and Fuel Element Block Flow, General Atomic Co., GA-A-13886, Vol. 1, 1976.

Hiby, J.W. and M. Pahl, "Der Einfluss von Zweierstossen auf die Molekulare Gasstromung," Z. Naturforschg, Vol. 7a, p524-533, 1952.

Hill, T.L., "Surface Diffusion and Thermal Transpiration in Fine Tubes and Pores," Journal of Chemical Physics, Vol. 25, No. 4, 1956.

Hirschfelder, J.O., R.B. Bird and E.L. Spotz, "The Transport of Gases and Gaseous Mixtures," Chemical Reviews, Vol. 44, p205-231, 1941.

Hirschfelder, J.O., C.F. Curtis and R.B. Bird, Molecular Theory of Gases and Liquids, John Wiley and Sons, New York, 1219p, 1954.

Hsu, Y.Y. and R.W. Graham, Transport Processes in Boiling and Two-Phase Flow, McGraw-Hill, New York, 1976.

Kaplan, I., Nuclear Physics, Addison-Wesley, 1955.

Knudsen, M.C., Kinetic Theory of Gases, John Wiley and Sons, N.Y., 64p, 1950.

Kennard, E. H., Kinetic Theory of Gases McGraw-Hill, New York, 1938.

Komabayasi, M., "Enrichment of Inorganic Ions with Increasing Atomic Weight in Aerosol, Rainwater and Snow in Comparison with Sea Water," Journal of Meteorlogical Society of Japan, Vol. 40, No. 1, 1962.

Krider, E.P. and J.A. Musser, "Maxwell Currents Under Thunderstorms," Journal of Geophysical Research-O A, Vol. 87, No. C13, p1171, 1982.

Lamarsh, J.R., Introduction to Nuclear Reactor Theory, Addison-Wesley, Reading, Mass., 1966.

Landau, L.P. and Lifshitz, E.M., Fluid Mechanics, Pergamin Press, New York, 1959.

Lapwood, E.R., "Convection of a Fluid in a Porous Medium," Proceedings of Cambridge Philosophical Society, Vol. 44, 1948.

Lassettre, E.N., "The Influence of Specular Reflection on the Permeability of Porous Media," K-1258, 1956.

Loeb, L.B., Kinetic Theory of Gases, McGraw-Hill, New York, 555p, 1927.

MacIntyre, F., "Flow Patterns inBreaking Bubbles," Journal of Geophysical Research, Vol. 72, No. 27, 1972.

Marshall, T.J., "The Diffusion of Gases Through Porous Media," Journal of Soil Science, Vol. 10, p1959, 1959.

Massignon, D., "Gaseous Diffusion," in Uranium Enrichment, ed. by S. Villani, Springer-Verlag, New York, 1979.

Matthews, D.W., Thermally Induced Countercurrent Flow in Unsaturated Rock, M. S. Thesis, University of Arizona, 1986.

McBain, J.W. and G.P. Davies, "An Experimental Test of the Gibb's Adsorption Theorem," Journal of the American Chemical Society, Vol. 49, p2230-2257, 1927.

McDaniel E.W., and E.A. Mason, The Mobility and Diffusion of Ions in Gases, John Wiley, New York, 1973.

McKibben, R. and P.A. Tyvand, "AnisotropicModelling of Thermal Convection in Multilayered Porous Media," Journal of Fluid Mechanics, Vol. 118, 1983.

Meyers, D.M., Gamma Ray Dosimetry Using Compton Scattered Electrons, M.S. Thesis, Univ. of Arizona, 1970.

Millington, R.J., "Gas Diffusion in Porous Media," Science, p100-102, 1959.

Neuman, S.P., Course Notes on Subsurface Fluid Dynamics, University of Arizona, 1981.

Norman, A. and P. Spiegler, "Radiation Nucleation of Bubbles in Water," Nuclear Science and Engineering, Vol. 16, p213-217, 1963.

Ogard, A.E., K. Wolfsberg and D.T. Vaniman, "Research and Development Related to the Nevada Nuclear Waste Storage Investigations, April 1 - June 30, 1983," Los Alamos National Laboratory, LA-9846-PR, 1983.

Pasiuk-Bronikowski, W. and K.J. Rudzinski, "Gas Desorption from Liquids," Chemical Engineering Science, Vol. 36, p1153-1159, 1981.

Pollard, W.G. and R.D. Present, "On Gaseous Self-diffusion in Long Capillary Tubes," Physical Review, Vol. 73, No. 7, p762-774, 1948.

Potter, R.W. and M.A. Clynne, "The Solubility of the Noble Gases He, Ne, Ar, Kr, and Xe in Water up to the Critical Point," Journal of Solubility Chemistry, Vol. 7, No. 11, p837-844, 1978.

Present, R.D., Kinetic Theory of Gases, McGraw-Hill, New York, 280p, 1958.

Pruess, K., Y.W. Tsang and J.S.Y. Wang, "Modeling of Strongly Heat-Driven Flow in Partially Saturated Fractured Porous Media," Proceedings of the International Association of Hydrogeologists 17th Congress, Tucson, Arizona, 1985.

Pruess, K., J.S.Y. Wang, "TOUGH - A Numerical Model for Nonisothermal Flow to Study Waste Canister Heating Effects," Material Research Society Symposium Proceedings, Vol. 26, 1984.

Reda, D.C., "Slip-Flow Experiments in Welded Tuff," International Symposium on Coupled Processes Affecting the Performance of a Nuclear Waste Repository, Lawrence Berkely Laboratory, 1985.

Roseboom, E.H., "Disposal of High-level Waste Above the Water Table in Arid Regions," Geological Survey Circular 903, 1983.

Schweitzer, P.H. and V.G. Szebehely, "Gas Evolution in Liquids and Cavitation", Journal of Applied Physics, Vol. 21, p1218-1224, 1950.

Scriven, L.E., "On the Dynamics of Phase Growth," Chemical Engineering Sciience, Vol. 10, No.1/2, p1-13, 1959.

Sienko, M.J. and R.A. Plane, Chemistry, McGraw-Hill, New York, 1966.

Slattery, J.C., and R.B. Bird, "Calculation of the Diffusion Coefficient of Dilute Gases and the Self-diffusion of Dense Gases," AIChE J., Vol. 4, No. 2, p137-142, 1958.

Sheludko, A., Colloid Chemistry, Elsevier, New York, 1966.

Smith, D.M., C.D. Updegraff and E.J. Bonano, "A Preliminary Assessment of Radionuclide Vapor Phase Transport in Unsaturated Tuff," SAND DE-AC04-76DP00789, 1985.

Spinks, J.W.T. and R.J. Woods, An Introduction to Radiation Chemistry, WileyInterscience, New York, 1976.

Sutherland, S.H. and D.E. Bennett, Defense High-Level and Spent Fuel Characterization for Geologic Waste Repositories, SAND79-0172, 1979.

Taylor, H.S. and S. Glasstone, Treatise on Physical Chemistry, Vol 2, van Nostrand, New York, 1951.

Telford, W.M., L.P. Geldart, R.E. Sheriff and D.A. Keys, Applied Geophysics, Cambridge Press, New York, 1976.

Wang, J.S., D.C. Mangold, R.K. Spencer, and C.F. Tsang, Thermal Impact of Waste Emplacement and Surface Cooling Associated with Geologic Disposal of Nuclear Waste, Lawrence Berkeley Lab., NUREG/CR-2910, 1983.

Weber, S., "The Connection Between the Laminar Flow of Pure Gases Through Tubes and the self-Diffusion Coefficient," AERE-Trans 946, 1963.

Weeks, E.P., D.E. Earp and G.M. Thompson, "Use of Atmospheric Fluorocarbons F-11 and F-12 to Determine the Diffusion Parameters of the Unsaturated Zone in the Southern High Planes of Texas," Water Resources Research, Vol. 18, No. 5, 1982.

Weiland, RH., L.T. Thuy and A. N. Liveris, "Transistion from Bubbling to Quiscient Desorption of Dissolved Gas," Industrial Engineering and Chemistry Fundmentals, Vol. 16, No. 3, p332-335, 1977.

Winograd, I.J., "Radioactive Waste Disposal in Thick Unsaturated Zones," Science, Vol. 212, No. 4502, 1981.

Witherspoon, P.A., S.P. Neuman, M.L. Sorey and M.J. Lippmann, "Modeling Geothermal Systems," Il Fenomeno Geotermico E Sue Applicazioni, Atti dei Convegni Linsei, Rome, March, 1975.

Wilke, C.R., "A Viscosity Equation for Gas Mixtures," Journal of Chemical Physics, Vol. 18, No. 4, 1950.

Wollenberg, H.A., J.S.Y. Wang and G. Korbin, "An Appraisal of Nuclear Wate Isolation in the Vadose Zone in Arid and Semi-Arid Regions," NUREG/CR-3158 LBL-15010, 1983.

Woolf, S., W.L. Filippone, B.D. Ganapol, and J.C. Garth, "Electron Transport Calculational Methods for a Plane Source Embedded in an Infinite Medium," to appear in Nuclear Science Engineering, January, 1986,

APPENDIX A

```
      PROGRAM COMPMC(INPUT,OUTPUT,TAPE5=INPUT,TAPE6=OUTPUT)

C       THIS PROGRAM DETERMINES COMPTON CURRENT BY MONTE CARLO
C       SIMULATION OF GAMMA RAYS

C   M = NUMBER OF ENERGIES OF GAMMA PARTICLES
C   N = NUMBER OF PARTICLES
C   L = NUMBER OF BINS
C   E = ENERGY OF INCIDENT GAMMA RAYS
C    BIN(I,1) = DISTANCE TO BIN
C    BIN(I,2) = TOTAL OUTWARD CURRENT IN BIN
C    PHI = AZMUTH ANGLE (X-Z PLANE)
C    THETA = ANGLE OFF OF Y-AXIS
C    GMEW = ADSORPTION COEFFICIENT
C    NMAX = NUMBER OF COLLISIONS PER GAMMA RAY
C    DIST = DISTANCE OF PHOTON TO POINT OF COLLISION
C    DENSE = DENSITY OF SCATTERER (G/CM**3)
C    THEEL = ELECTRON ANGLE OFF OF Z-AXIS
C    PHIEL = ELECTRON AZMUTH ANGLE
C    ELENR = ELECTRON ENERGY
C    OM_   = UNIT VECTORS IN LOCAL SYSTEM
C    OM_PR = UNIT VECTORS IN GLOBAL SYSTEM
C    S_    = PHOTON VECTORS IN GLOBAL SYSTEM
C    R_    = COMPOSITE VECTORS TO COLLISION LOCATION
C    SCATN = NUMBER OF SCATTERERS/UNIT VOL (Δ/BARNS**3/2)


      PARAMETER(PI=3.141592654,PI2=6.283185308,SCATN=1.631E-3)
      PARAMETER(N=200000,COUL=1.6E-19,RESIST=1.0E6,DENSE=1.225E-3)
      CHARACTER GNAME(5)*5
      DIMENSION BIN(400,4)

      M=1
      NMAX=400
      ENEMIN=0.03
      L=400

C INITIALIZE THE COMPARTMENTS

      BIN(1,1)=1.0
      BIN(1,2)=0
      BIN(1,3)=0
```

```
      BIN(1,4)=0
      DO 5 I=2,L
      BIN(I,2)=0
      BIN(I,3)=0
      BIN(I,4)=0
 5    BIN(I,1)=BIN(I-1,1)+1.0

C J-LOOP IS FOR EACH GAMMA ENERGY

      DO 10 J=1,M
C     READ(5,*)ENER(J),GNAME(J)

C     E=ENER(J)

C I-LOOP IS FOR EACH MONTE CARLO PARTICLE

      DO 60 IONE=1,N/10
      DO 60 ITWO=1,10
      I=10*(IONE-1)+ITWO
      E=2.75

C DETERMINE INITIAL ANGLES OF GAMMA RAY

      THETA=ACOS(RANF()*2-1)
      PHI=RANF()*2*PI

C DETERMINE COLLISION PHOTON DISTANCE BY MONTE CARLO

      GMEW=SIG(E)*SCATN

      DIST=-LOG(RANF())/GMEW

C DETERMINE VECTOR COMPONENTS OF PHOTON VECTOR

      OMX=0
      OMY=COS(THETA)
      OMZ=SIN(THETA)

C DETERMINE INITIAL R-VECTOR

      RY=OMY*DIST

C JJ-LOOP COUNTS NUMBER OF COLLISIONS PER GAMMA RAY
```

```
      DO 50 JJ=1,NMAX

C DETERMINE COLLISION AZMUTH ANGLE OF PHOTON

      PHINEW=RANF()*PI2

C DETERMINE ANGLE OFF OF RADIAL AXIS OF PHOTON

      NSTOP=1
 40   THETEST=ACOS(RANF()*2-1)

C REJECTION TEST

      TEST=0.1194*RANF()
      IF(NSTOP.GT.200) STOP 1
      IF(TEST.LE.SIGT(E,THETEST)) THEN
      THENEW=THETEST
      ELSE
      NSTOP=NSTOP+1
      GO TO 40
      END IF

C DETERMINE LOCAL VECTOR COMPONENTS OF PHOTON VECTOR

      C1=COS(THENEW)
      C2=COS(THETA)
      C3=COS(PHINEW)
      C4=COS(PHI)
      S1=SIN(THENEW)
      S2=SIN(THETA)
      S3=SIN(PHINEW)
      S4=SIN(PHI)

C EXPRESS NEW PHOTON VECTOR SYSTEM IN TERMS OF OLD SYSTEM

      OMXPR=C1*S2*C4+S1*S3*C2*C4-S1*C3*S4
      OMYPR=C1*C2-S1*S3*S2
      OMZPR=S1*C3*C4+C1*S2*S4+S1*S3*C2*C4

C DETERMINE COLLISION PHOTON ENERGY

      EPRIME=E/(1+E*(1-COS(THENEW)))

C DETERMINE ABSORPTION COEFFICIENT FOR A GIVEN  OF COLLISION PHOTON ENERGY
```

```
      GMEW=SIG(EPRIME)*SCATN

C DETERMINE DISTANCE OF TRAVEL OF SCATTERED PHOTON

      RNEW=-LOG(RANF())/GMEW

C EXPRESS PHOTON DISTANCE IN GLOBAL VECTORS

      SX=OMXPR*RNEW
      SY=OMYPR*RNEW

C DETERMINE THE ENERGY OF A COMPTON ELECTRON

      ELENR=E-EPRIME

C UPDATE PHOTON ENERGY

      E=EPRIME

C UPDATE PHOTON ANGLES

      VECT=(OMXPR*OMXPR+OMZPR*OMZPR)**0.5
      THETA=ATAN(VECT/OMYPR)
      PHI=ATAN(OMZPR/OMXPR)

C DETERMINE THETA AND PHI FOR THE ELECTRON IN LOCAL UNITS

      PHIEL=PHINEW+PI
      THEEL=ATAN((1/(1+E/0.511))*(1/TAN(THENEW/2)))

C DETERMINE LOCAL COMPONENTS OF ELECTRON VECTOR

      C1=COS(THEEL)
      C3=COS(PHIEL)
      S1=SIN(THEEL)
      S3=SIN(PHIEL)

C EXPRESS NEW PHOTON VECTOR SYSTEM IN TERMS OF OLD SYSTEM

      OMXPR=C1*S2*C4+S1*S3*C2*C4-S1*C3*S4
      OMYPR=C1*C2-S1*S3*S2
      OMZPR=S1*C3*C4+C1*S2*S4+S1*S3*C2*C4
```

```
C UPDATE ELECTRON ANGLES IN TERMS OF GLOBAL SYSTEM

      VECTEL=(OMXPR*OMXPR+OMZPR*OMZPR)**0.5
      THELPR=ATAN(VECTEL/OMYPR)
      PHELPR=ATAN(OMZPR/OMXPR)

C DETERMINE RANGE OF COMPTON ELECTRON IN SCATTERER

      RANGEL=DETRANG(ELENR)/DENSE

C DETERMINE Y-COMPONENT OF ELECTRON VECTOR

      RAELVT=COS(THELPR)*RANGEL

C DETERMINE CURRENT DENSITY

      CURENT=RAELVT*COUL*GMEW

C CALCULATE THE SQUARE OF THE RADIAL CURRENT VECTOR

      CURSQ=CURENT*CURENT

C PUT COLLISION INTO BIN AT DISTANCE OF IMPACT
C L = NUMBER OF BINS
C ADD Y-COMPONENT OF CURRENT TO BIN

      DO 30 K=1,L
      IF(RY.GT.BIN(K,1)) THEN
      ELSE
      BIN(K,2)=BIN(K,2)+1.0
      BIN(K,3)=BIN(K,3)+CURENT
      BIN(K,4)=BIN(K,4)+CURSQ
      GO TO 35
      END IF
30    CONTINUE
35    CONTINUE

C DETERMINE NEW R-VECTOR

      RX=SX
      RY=((RY+SY)*(RY+SY)+(RX*RX))**0.5

C DETERMINE IF PHOTON ENERGY IS SUFFICIENT TO CAUSE ANOTHER COLLISION
```

```
      IF(EPRIME.LT.ENEMIN) GO TO 60

   50 CONTINUE

   60 CONTINUE

   10 CONTINUE

      WRITE(6,650)
  650 FORMAT(10X,'DISTANCE',15X,'Δ OF COLLISIONS',10X,'CURRENT',
     1 T80,'ELECTRIC FIELD',T100,'EPSILON',/,12X,'CM',T58,'AMP/CM**2',
     2 T83,'VOLT/CM',//)

      DO 70 I=1,L
      CURR=BIN(I,3)/(BIN(I,1)*PI2*N)
      STDEV=(ABS(BIN(I,4)/N-(BIN(I,3)/N)**2)/(BIN(I,1)*PI2))**0.5
      EPSILON=1.282*STDEV/N**0.5
      WRITE(6,660)I,BIN(I,1),BIN(I,2)/(BIN(I,1)*PI2*N),
     1 CURR,CURR*RESIST,EPSILON
  660 FORMAT(1X,I4,F10.2,10X,2E20.5,T70,E20.5,T90,E20.5)

   70 CONTINUE

      STOP

      END
      FUNCTION SIG(E)

C DETERMINE TOTAL CROSS SECTION PER ELECTRON IN THOMPSON UNITS

      C1=(1+E)/E**3
      C2=2*E*(1+E)/(1+2*E)
      C3=LOG(1+2*E)
      C4=LOG(1+2*E)/(2*E)
      C5=(1+3*E)/(1+2*E)**2
      SIG=(0.75)*(C1*(C2-C3)+C4-C5)

      RETURN

      END

      FUNCTION SIGT(E,TEST)

      C1=1/(1+E*(1-COS(TEST)))
```

```
      C2=0.059683
      C3=1/C1
      C4=SIN(TEST)**2
      SIGT=C2*(C1**2)*(C3+C1-C4)

      RETURN

      END


      FUNCTION DETRANG(E)

C  FUNCTION DETERMINES THE EFFECTIVE RANGE OF COLLISION ELECTRONS
C  BASED ON RESULTS OF BILL FILIPPONE'S PROGRAM--SR  WHICH SOLVES
C  THE SPENCER LEWIS EQUATION NUMERICALLY

      IF(E.LT.0.01) THEN
         DETRANG=(E/0.01)*1.05E-4
         ELSE IF(E.LT.0.1) THEN
         DETRANG=-5.3942784E-5+(1.1277976E-2)*E+(4.5761904E-1)*E*E
         ELSE IF(E.LT.0.8) THEN
         DETRANG=-7.29460672E-3+(1.1018352E-1)*E+(8.7394431E-2)*E*E
         ELSE
         DETRANG=-6.234667E-2+(2.31789E-1)*E+(1.4291623E-2)*E*E

      END IF

      RETURN

      END
```

NRC FORM 335 (7 77) U.S. NUCLEAR REGULATORY COMMISSION

BIBLIOGRAPHIC DATA SHEET

1. REPORT NUMBER (Assigned by DDC)
NUREG/CR-4654

4. TITLE AND SUBTITLE (Add Volume No., if appropriate)
Radionuclide Transport as Vapor Through Unsaturated Fractured Rock

2. (Leave blank)

3. RECIPIENT'S ACCESSION NO.

7. AUTHOR(S)
Ronald T. Green and Daniel D. Evans

5. DATE REPORT COMPLETED
MONTH September YEAR 1986

9. PERFORMING ORGANIZATION NAME AND MAILING ADDRESS (Include Zip Code)
Department of Hydrology & Water Resources
University of Arizona
Tucson, AZ 85721

DATE REPORT ISSUED
MONTH July YEAR 1987

6. (Leave blank)

8. (Leave blank)

12. SPONSORING ORGANIZATION NAME AND MAILING ADDRESS (Include Zip Code)
Division of Engineering
Office of Nuclear Regulatory Research
U.S. Nuclear Regulatory Commission
Washington, D.C. 20555

10. PROJECT/TASK/WORK UNIT NO.

11. CONTRACT NO.
NRC-04-81-224
FIN B7291

13. TYPE OF REPORT
Technical Report

PERIOD COVERED (Inclusive dates)
1983-1986

15. SUPPLEMENTARY NOTES

14. (Leave blank)

16. ABSTRACT (200 words or less)

The objective of this study is to identify and examine potential mechanisms of radionuclide transport as vapor at a high-level radioactive waste repository located in unsaturated fractured rock. Transport mechanisms and processes have been investigated near the repository and at larger distances. Transport mechanisms potentially important at larger distances include ordinary diffusion, viscous flow and free convection. Ordinary diffusion includes self and binary diffusion, Knudsen flow and surface diffusion. Pressure flow and slip flow comprise viscous flow. Free convective flow results from a gas density contrast. Transport mechanisms or processes dominant near the repository include ordinary diffusion, viscous flow plus several mechanisms whose driving forces arise from the non-isothermal, radioactive nature of high-level waste. The additional mechanisms include forced diffusion, aerosol transport, thermal diffusion and thermophoresis. Near a repository vapor transport mechanisms and processes can provide a significant means of transport from a failed canister to the geologic medium from which other processes can transport radionuclides to the accessible environment. These issues are believed to be important factors that must be addressed in the assessment of specific engineering designs and site selection of any proposed HLW repository.

17. KEY WORDS AND DOCUMENT ANALYSIS

17a DESCRIPTORS

contaminant transport
vapor transport
unsaturated zone..
fractured rock
radionuclides

17b. IDENTIFIERS/OPEN-ENDED TERMS

18. AVAILABILITY STATEMENT
Unlimited

19 SECURITY CLASS (This report)
Unclassified

21 NO OF PAGES

20 SECURITY CLASS (This page)
Unclassified

22 PRICE
S

NRC FORM 335 (7 77)

*U.S. GOVERNMENT PRINTING OFFICE:1987-181-682:60163

UNITED STATES
NUCLEAR REGULATORY COMMISSION
WASHINGTON, D.C. 20555